

Generation of genetic and epigenetic variation during  
cellular senescence and early tumorigenesis in a human  
and nonhuman primate lung fibroblast model

Dissertation

zur Erlangung des Grades

Doktor der Naturwissenschaften

am Fachbereich Biologie

der Johannes Gutenberg-Universität Mainz

**Valentina Woronzow**

geboren am 14.02.1995 in Bălți, Republik Moldau

Mainz, 2023

---

Dekan: Prof. Dr. Eckhard Thines

1.Berichterstatter: Prof. Dr. Hans Zischler

2.Berichterstatter: Prof. Dr. Thomas Hankeln

Tag der mündlichen Prüfung: 18.03.2024

---

# Table of contents

<b>Zusammenfassung .....</b>	<b>1</b>
<b>Abstract.....</b>	<b>2</b>
<b>Abbreviations .....</b>	<b>3</b>
<b>1 Introduction.....</b>	<b>6</b>
1.1 Implications of mammalian aging.....	6
1.2 Cellular senescence as a hallmark of aging.....	7
1.3 Induction and features of cellular senescence.....	7
1.4 Biomarkers of cellular senescence and their limitations.....	10
1.5 Tetraploidy as a cancer precursor model .....	11
1.6 Focus and strategies of this thesis .....	12
<b>2 Material and methods.....</b>	<b>15</b>
2.1 Material .....	15
2.1.1 Cell culture .....	15
2.1.2 Extraction methods.....	16
2.1.2.1 RNA .....	16
2.1.2.2 DNA.....	16
2.1.3 Synthesis methods .....	17
2.1.3.1 Poly(A) tailing of miRNA inhibited RNA samples.....	17
2.1.3.2 Reverse transcription .....	17
2.1.4 Quantification and detection methods .....	17
2.2.4.1 Senescence-associated $\beta$ -galactosidase assay (SA-beta gal) .....	17
2.2.4.2 DNA & RNA measurement via Qubit.....	18
2.2.4.3 RT-qPCR .....	18
2.2 Methods.....	19
2.2.1 Cell culture .....	19

---

2.2.1.1 Thawing cells .....	19
2.2.1.2 Subcultivation .....	19
2.2.1.3 Harvesting cells.....	20
2.2.1.4 miRNA inhibition .....	21
2.2.2 Extraction methods .....	22
2.2.2.1 RNA .....	22
2.2.2.2 DNA.....	22
2.2.3 Synthesis methods .....	22
2.2.3.1 Poly(A) tailing of miRNA inhibited RNA samples.....	22
2.2.3.2 Reverse transcription .....	23
2.2.4 Quantification and detection methods .....	23
2.2.4.1 Senescence-associated beta galactosidase assay.....	23
2.2.4.2 DNA & RNA measurement via Qubit.....	23
2.2.4.3 RT-qPCR .....	23
2.2.5 Next generation sequencing .....	24
2.2.5.1 Small RNA sequencing.....	24
2.2.5.2 Transcriptome sequencing.....	24
2.2.6 Bioinformatical analysis.....	24
2.2.6.1 Small RNA data analysis .....	24
2.2.6.2 RNA sequencing data analysis .....	25
<b>3 sncRNA and transcriptomic profiles in senescent and tetraploid lung fibroblasts</b> .....	<b>26</b>
3.1 Results.....	26
3.1.1 Small non-coding RNA: an overview .....	26
3.1.2 Differentially expressed miRNAs .....	30
3.1.3 Senescence-associated miRNA in common marmosets.....	33
3.1.4 Senescence-associated miRNA inhibition.....	35

---

3.1.5 Transcriptomics in senescent and tetraploid IMR-90 cells .....	37
3.2 Discussion .....	41
3.2.1 Small RNA sequencing in senescent and tetraploid lung fibroblasts.....	41
3.2.2 miRNAs in the context of cellular senescence and early tumorigenesis.....	42
3.2.3 miRNA in the context of primate cellular senescence .....	46
3.2.4 miR-29a-3p as a biomarker for cellular senescence.....	47
3.2.5 Implications of transcriptomics in senescent and tetraploid cells .....	50
3.2.6 Conclusions of small RNA and transcriptomic analysis in the context of cellular senescence .....	51
<b>4 Generation of somatic de novo structural variation as a hallmark of cellular senescence in human lung fibroblasts .....</b>	<b>53</b>
4.1 Abstract .....	53
4.2 Introduction .....	54
4.3 Material and Methods .....	56
4.3.1 Sample preparation: cell culture and SA- $\beta$ -Gal activity.....	56
4.3.2 DNA isolation.....	57
4.3.3 RNA isolation.....	57
4.3.4 RNA-Sequencing.....	57
4.3.5 Differential Expression Analysis.....	57
4.3.6 Local BLAST+ of transcriptomic data .....	57
4.3.7 Representational difference analysis (RDA) of SVAs .....	58
4.3.8 Genomic target sites and Gene Ontology analysis of SVA integrations.....	58
4.3.9 Human Whole Genome Sequencing (hWGS).....	58
4.3.10 AluScan-PCR and Next Generation Sequencing .....	59
4.3.11 Bioinformatical scanning of <i>de novo numts</i> .....	59
4.3.12 Genomic target sites and Gene Ontology analysis of <i>de novo numts</i> .....	60
4.4 Results .....	61

---

4.4.1 RNA abundance of SVAs and genes critically influencing chromatin remodeling in proliferative and senescent IMR-90 cells.....	61
4.4.2 Active <i>de novo</i> SVA retrotransposition in cellular senescent IMR-90 cells ..	63
4.4.3 Genomic target sites of <i>de novo</i> SVA integrations .....	65
4.4.4 SVA integrations localize in close proximity to genes associated with mitosis and cell proliferation.....	66
4.4.5 Cytosolic mtDNA accumulation in cellular senescent IMR-90 cells.....	66
4.4.6 Cellular senescence drives <i>de novo</i> nuclear integration events of mtDNA....	67
4.4.7 mtDNA mobility and <i>numts</i> .....	68
4.4.8 Mitochondrial quality control and somatic interorganellar transfer.....	69
4.4.9 Target sites of <i>de novo numts</i> in senescent IMR-90 cells and Gene Ontology .....	71
4.5 Discussion .....	72
4.6 Author Contributions .....	78
4.7 Conflict of Interest .....	78
4.8 Funding .....	78
4.9 Acknowledgments.....	78
4.10 Tables.....	79
<b>5 Conclusion of the present thesis .....</b>	<b>81</b>
<b>References.....</b>	<b>83</b>
<b>Supplement.....</b>	<b>105</b>
<b>Danksagung .....</b>	<b>119</b>
<b>Eidesstattliche Versicherung .....</b>	<b>120</b>
<b>Lebenslauf.....</b>	<b>121</b>

## Zusammenfassung

Zelluläre Seneszenz bildet einen grundlegenden Faktor für chronische Erkrankungen und funktionale Einbußen im Alterungsprozess. Sobald eine finite Anzahl an Zellteilungen überschritten wird, unterliegen seneszente Zellen einem permanenten Proliferationsstopp, bleiben jedoch weiterhin metabolisch aktiv. Ihre Anreicherung in Geweben stellt eine erhebliche Herausforderung für Organismen dar. In der vorliegenden Arbeit werden zwei Ansätze implementiert, um Seneszenz in einem Lungenfibroblasten-Modell auf genetischer und epigenetischer Ebene zu untersuchen. Zusätzlich werden tetraploidie-induzierte Zellen als ein frühes Tumorgenesemodell einbezogen. Profile von nicht-kodierenden, kleinen RNAs und Transkriptomdaten werden mittels NGS und anschließender bioinformatischer Auswertung in proliferierenden, seneszenten und tetraploiden IMR-90 Zellen analysiert. In den Profilen der seneszenten und tetraploiden Daten ergeben sich Ähnlichkeiten jeweils überexprimierter miRNAs, die eng mit Tumorbildung und Inflammation verknüpft sind. Daraus lassen sich Zusammenhänge zwischen übermäßiger Zellproliferation, aberranter Replikation und induzierter Seneszenz herstellen. Die in seneszenten Zellen signifikant hochregulierte miR-29a-3p bildet ein bisher unbeschriebenes Potenzial als Seneszenzmarker in menschlichen Lungenfibroblasten ab. Die experimentelle Inhibierung von miR-29a-3p in proliferierenden Zellen führt jedoch zur Akkumulation von Stressreaktionen und dem Auftreten von seneszenz-assoziierten Expressionsmustern. Folglich hat die Inhibierung nachteilige Auswirkungen, was mit dem antagonistischen Pleiotropie-Modell der Alterung erklärt werden kann. Epigenetische Veränderungen, einschließlich des Verlusts von repressivem konstitutivem Heterochromatin, führen zu L1-Derepression, ein Phänomen, das mit Seneszenz in Verbindung gebracht wird. Strukturelle Variationen in alternden Genomen können durch *de novo* Retrotransposition von SVAs sowie *de novo* Insertion von zytosolisch akkumulierter mtDNA (*Numts*) in das Genom verursacht werden. Ein kinetischer Anreicherungsansatz in Kombination mit NGS wird verwendet, um *de novo* SVA-Insertionen in seneszenten Genomen zu detektieren. Darüber hinaus werden die Genome von proliferierenden und seneszenten IMR-90-Zellen durch WGS und anschließender bioinformatischer Auswertung verglichen. Meine Arbeit gibt starke Hinweise auf *de novo* SVA- und *Numts*-Integrationen in seneszenten IMR-90-Zellen. Diese strukturellen Unterschiede können Auswirkungen auf die Mechanismen der zellulären Seneszenz in menschlichen Lungenfibroblasten haben.

## Abstract

Cellular senescence has garnered greater attention as a fundamental contributor to chronic illness and functional decline in aging. Once they exceed a finite number of cell divisions, senescent cells undergo permanent growth arrest while still being metabolically active. By accumulation they pose significant challenges to the organism. The present work provides two approaches to investigate senescence in a human lung fibroblast model both genetically and epigenetically while incorporating induced tetraploidy as an early tumorigenesis model. First, I compared small non-coding RNA and transcriptomic changes in proliferating, senescent, and tetraploid IMR-90 cells by conducting sncRNA sequencing, transcriptomic NGS and a subsequent bioinformatical analysis. Overall, both senescent and tetraploid IMR-90 cells exhibit amplified miRNA profiles that are pertinent to cancer progression and inflammation, as demonstrated through miRNA ontology analysis. This provides a unique opportunity to investigate the relationship between cell proliferation arrest, excessive cell proliferation, and aberrant replication. Of particular interest is hsa-miR-29a-3p, which displays significant upregulation in senescent IMR-90 cells, suggesting its yet to be described potential as a reliable senescence marker in human fibroblasts. The hypothesis that decreasing miR-29a-3p levels may increase longevity has some merit. However, inhibiting miR-29a-3p in proliferating cells led to the accumulation of stress responses and the appearance of senescence-related patterns, as evidenced by the observed biomarkers. Consequently, the inhibition had adverse outcomes, indicating an association with the antagonistic pleiotropy model of aging. Epigenetic alterations, including loss of repressive constitutive heterochromatin, may result in LINE-1 derepression, a phenomenon often connected with senescence. In addition to epigenetic changes, structural variations in aging genomes can be caused by *de novo* retrotranspositions of transposable elements like SVAs, as well as *de novo* insertions of accumulated mitochondrial DNA into nuclear DNA. A kinetic enrichment approach was utilized to detect the nuclear flanks of *de novo* SVA insertions in senescent genomes. The technique was coupled with deep sequencing. Furthermore, the genomes of proliferating and senescent IMR-90 cells were compared through deep sequencing or by enriching nuclear DNA with AluScan technology. Evidence was uncovered for *de novo* SVA and *numts* integrations in senescent IMR-90 cells using both methods. I hypothesize that the structural disparities have an impact on the mechanisms associated with cellular senescence in human lung fibroblasts.



## Abbreviations

AP	antagonistic pleiotropy
ATP	adenosine triphosphate
BLAST	basic local alignment search tool
cDNA	complementary DNA
circRNA	circular RNA
Cja	<i>Callithrix jacchus</i>
DAMP	damage-associated molecular pattern
DSB	double strand break
FWD	forward
G1 phase	growth 1 phase
GOI	gene of interest
Hsa	<i>Homo sapiens</i>
hWGS	human whole genome sequencing
kb	kilo base
LINE	long interspersed nuclear element
lncRNA	long non-coding RNA
LTR	long terminal repeat
MIO	miRNA of interest
miRNA	micro RNA

---

MOMP	mitochondrial outer membrane permeabilization
mRNA	messenger RNA
mtDNA	mitochondrial DNA
nDNA	nuclear DNA
NGS	next generation sequencing
NHEJ	non-homologous end joining
<i>Numts</i>	nuclear mitochondrial DNA
OXPHOS	oxidative phosphorylation
PDL	population doubling level
Prolif	proliferating
RDA	representational difference analysis
REV	reverse
ROS	reactive oxygen species
RPM	reads per million
rRNA	ribosomal RNA
RT-qPCR	real time quantitative polymerase chain reaction
SASP	senescence-associated secretory phenotype
Sa- $\beta$ -Gal	senescence-associated $\beta$ -galactosidase assay
Sen	senescent
SINE	short interspersed nuclear element

siRNA	small interfering RNA
sncRNA	small non-coding RNA
snoRNA	small nucleolar RNA
SVA	SINE-Alu-VNTR
TE	transposable element
Tetra	tetraploid
tRF	tRNA derived fragments
tRNA	transfer RNA
TSS	transcription start site
untransf.	untransfected
UTR	untranslated region
VNTR	variable number of tandem repeats
WT	wildtype
X-Gal	5-Brom-4-chlor-3-indoxyl- $\beta$ -D-galactopyranosid
YsRNA	YRNA-derived small RNA

# 1 Introduction

## 1.1 Implications of mammalian aging

The underlying mechanisms of human aging form a vital field in today's medical research. The characteristics of aging, which are reflected in cellular processes and involved genes conserved in evolution, form the basis of hypotheses such as the "disposable soma theory" first formulated by Tom Kirkwood in 1977. The theory regards the soma as a "disposable envelope" of transgenerationally relevant germline cells (Kirkwood, 1977). One aspect of this theory encloses that metazoans do not age without a true germline. First experimental evidence for this theory was published almost 30 years after its conception. Berman and Kenyon (2006) were able to show that germ cell loss extends the life span of *C.elegans*. In the context of evolutionary biology, it is enigmatic why natural selection does not become effective for a *per se* maladaptive trait, continuously reducing the number of individuals with corresponding aging phenotypes over evolutionary time periods. This noticeably represents a paradox that received a seminal answer with George C. Williams' hypothesis of antagonistic pleiotropy (AP) - suggesting at least two antagonistic effects of a gene depending on the reproductive status. Williams (1957) proposed that natural selection - in the sense of differential reproduction - enriches genes in subsequent generations that promote reproductive success but may disregard their negative effects on longevity after reproduction is accomplished. The AP-theory can be extended to regulatory compartments such as miRNAs that may hold beneficial and detrimental functions alike, impacting mRNA expression and therefore a multitude of cellular pathways in the context of somatic aging (Liu et al., 2012). López-Otín et al. (2013; 2023) reviewed nine significant hallmarks of mammalian aging, grouped into three categories with functional interconnections: 1. *Primary hallmarks*: genomic instability, telomere attrition, epigenetic alterations, and loss of proteostasis; 2. *Antagonistic hallmarks*: deregulated nutrient-sensing, mitochondrial dysfunction, cellular senescence; 3. *Integrative hallmarks*: stem cell exhaustion, altered intercellular communication.

## 1.2 Cellular senescence as a hallmark of aging

Cellular senescence, broadly studied and well implemented in aging research, – as well as a hallmark of cancer and overall indicator of health in organisms - is characterized by a permanent termination of cell proliferation. Accumulation of senescent cells has been observed in several somatic tissues undergoing aging (Baker et al., 2008; Wang et al., 2009). In 1961, Hayflick and Moorhead described a finite amount of cell divisions (approx. 40-60 population doublings) in cultured human fibroblasts, describing the phenomenon of replicative senescence for the first time (Hayflick & Moorhead, 1961). The observed replication arrest in the G1/G0 phase of the cell cycle was induced by telomere shortening and thus activation of the DNA damage response (DDR). Telomeres – tandem repetitive DNA sections located at the end of chromosomes - serve as a protection against DNA degradation and interchromosomal translocation. Each time chromatids replicate, these regions shorten due to incomplete replication (Blasco, 2005) and – after reaching a critical length – the possibility for chromosomal translocation increases. As a protective mechanism, the tumor suppressor p53 is activated and the affected cell enters telomere-induced senescence (De Lange, 2005). Fusion of two telomeres has been observed in various tumor cells (Hastie & Allshire, 1989). Telomere-induced senescence thus protects against the formation of deteriorating cells (Feldser & Greider, 2007), but acts on the other hand – with progression of the senescence-associated phenotype - as a "pro-aging" factor (Collado et al., 2007). In addition to telomere shortening and DNA damage, various factors can trigger cellular senescence as a protective organismal mechanism including oncogene activation, oxidative stress, and inflammation.

## 1.3 Induction and features of cellular senescence

Induction of cellular senescence is linked to a variety of different signaling pathways, such as the p53 and ATM cascades and repression of the tumor suppressor gene *INK4/ARF* (Collado et al., 2007; Faget et al., 2019). Primarily, senescence and subsequent cellular degradation and elimination by the immune system serve as a protective mechanism against tumorigenesis. However, once the regenerative capacity of affected tissues is exhausted, tumor suppressors are broadly described as aging-promoters in the context of cellular senescence (López-Otín et al., 2013). Depending on the initial trigger

set, senescence is distinguished between the *acute variant* – linked to the activation of the senescence-associated secretory phenotype (SASP) when the cell shows defective properties such as DNA damage and the *chronic variant* – which results from subthreshold, cumulative stress (Sturmlechner et al., 2017). The SASP serves as a marker system for the innate immune system to clear senescent cells through the secretion of a variety of immunomodulating chemokines, cytokines, and matrix remodeling factors. The process of immuno-clearance is dependent on the signaling of secreted marker proteins and proper reception during the preneoplastic phase of tumor formation (Childs et al., 2014). While representing a vital asset in this process, excessive or uncontrolled SASP excretion can act as a tumor progressor and negatively affect the structural and functional properties of tissues when a chronic inflammation response occurs. The recruitment of lymphocytes and leukocytes in the process of immuno-clearance serves to remove the senescent or inflammatory cells and preserve the tissue's structure. Once defects within the inflammatory pathways occur, the accumulation of immune cells may result in active tissue damage (Franceschi et al., 2007, Salminen et al., 2011). The chronic variant of cellular senescence is not characterized by an active SASP excretion and thus affected cells are only inefficiently targeted and removed and tend to accumulate in the affected tissues (Sturmlechner et al., 2017). Distinguishing both variants is significant when investigating and categorizing biomarkers of aging, chronic inflammation, and cancer.

In contrast to cellular senescence - in which cells cease proliferation due to several stimuli but remain a functional part of the tissue - apoptosis is marked by programmed cell death. In the presence of severe cellular damage, or as a fatal consequence of late senescence, apoptosis can remove affected cells to maintain tissue homeostasis (Baar et al., 2017). Apoptosis occurs without the activation of the inflammatory pathways, thus reducing inflammatory-induced tissue damage (Salminen et al., 2011). Initiation of apoptosis is linked to mitotic pathways via reactive oxygen species (ROS), as investigated in tumor cells (Jafri et al., 2019). In accordance with the disruption of apoptosis by the accumulation of mitochondrial DNA (mtDNA) damage due to DNA polymerase  $\gamma$  dysfunction, an acceleration of the aging phenotype has been observed (Kujoth et al., 2005). Accumulation of mtDNA damage is strongly linked to mutations that cause genomic instability, which is a known hallmark of aging and thus cellular senescence. The mitochondrial genome consists of approx. 16 kb of circular DNA, encoding tRNAs, rRNAs and mito-specific proteins that are primarily active in the oxidative

phosphorylation (OXPHOS). During ATP synthesis of the cellular respiration process, ROS are produced as a byproduct and - depending on the extent – might be actively involved in the cause of mtDNA and nuclear DNA damage and thus participate in the erosion of genomic integrity (Argüelles et al., 2019; Srinivas et al., 2019).

Another aspect decisively influencing initiation and activity of senescence is the change in epigenetic modification patterns of the genome. These modifications include DNA methylation, histone modification, chromatin modulation and the associated changes in transcriptional activity. The latter may be influenced by miRNAs and other non-coding, regulatory RNA such as lncRNAs and circRNAs (Ghafouri-Fard et al., 2022). Highly complex molecular mechanisms underlie DNA methylation patterns, their assembly and maintenance. Several studies describe the link between global hypomethylation and age progression (Liu et al., 2003; Xia et al., 2017). However, Maegawa et al. (2010) describe individual sites within tumor suppressor genes and chromatin restructuring factors that are hypermethylated with age, suggesting an overall redistribution of hyper- and hypomethylation for specific sites within the aging genome. Assessment of DNA methylation is an essential tool in aging research. In fact, Steve Horvath (2013) established an epigenetic clock, which estimates biological age in healthy and cancerous tissues such as cell lines, applying a set of 353 CpGs. Since then, epigenetic age has gained more attention and thus additional mathematical clocks were created. Kabacik et al. (2022) further investigated whether the epigenetic clocks can be applied to the hallmarks of aging. Strikingly, the Horvath clock does not measure cellular senescence, as the increased patterns in epigenetic markers of replicative senescent cells are irrevocably linked to progressing biological age and not causal to the irreversible cell proliferation arrest. Further, histone modifications are observed within the process of aging and cellular senescence. Depending on the histone type, methylation and acetylation – as well as demethylation and deacetylation - are viable markers of the aging process (Han & Brunet, 2012; Peleg et al., 2016). Additionally, the overall structure of chromatin is used as an age determination marker, as loss and a general redistribution of heterochromatin can be measured in senescent tissue (Shaban & Gasser, 2023). These changes in chromatin structure are accompanied by decreased levels of chromatin remodeling factors such as heterochromatin protein 1 $\alpha$  (Pegoraro & Misteli, 2009). In the process of cellular senescence, many genetic and epigenetic mechanisms are simultaneously activated and deactivated, affecting one another. The above-mentioned

factors influence the expression patterns of a cell and its' progression within the cell cycle, reaction to inflammation and intrinsic as well as extrinsic damages.

#### **1.4 Biomarkers of cellular senescence and their limitations**

Detection of senescence biomarkers is essential for the proper investigation in aging and cancer studies. Up to this point, research on cellular senescence has relied on a combination of multiple biomarkers for verification. For one, cellular senescent cells undergo morphological changes. The cells appear enlarged and flattened, with an altered cytoplasm-to-nucleus ratio. In cell culture practices, the assessment of the *population doubling level* (PDL) is an important tool, as the moment of stagnating cell growth is identified by taking cell density, cell seeding number and harvesting number into account, thus enabling accurate preparation for further assays such as the senescence-associated  $\beta$ -galactosidase assay (Sa- $\beta$ -Gal; Dimri et al., 1995). The endogenous  $\beta$ -galactosidase is accumulated in senescent cells and can thus be identified and distinguished from proliferating cells by applying the cytochemical assay. The assay is known to be one of the most used detection methods for replicative senescent cells. However, Yang and Hu (2005) elucidated important weaknesses such as the reliance on nutrient availability, cell confluency and reactive environment which may drive results of false positives. With the progression of the tumor suppressor pathways controlled by p53, expression of the cyclin-dependent kinase inhibitors p16 and p21 increases (Stein et al., 1999). Measuring the expression levels of both proteins proved to be sufficient and is well established in senescence research, although limitations may occur as they are not identifiable in all senescent cell types and may moreover be accumulated in some tumorous tissues as well (Witkiewicz et al., 2011). A crucial part of the detection of acute senescence is the excretion of several cytokines, proteases, chemokines, and growth factors, belonging to the senescence-associated secretory phenotype (SASP). Depending on the investigated tissues and triggers of senescence initiation, the SASP may vary broadly. However, a subset of markers is commonly used as solid molecular tags, including the multifunctional proinflammatory cytokine IL-6 which can be identified both on transcript and protein level. Interestingly, the presence of IL-6 and other components of the SASP are not exclusively dependent on p16-mediated senescence, adding to the difficulty of solid senescence detection (Coppe et al., 2011). Due to the complexity of the SASP, Basisty et al. (2020) established a proteome database to further categorize the markers by



senescence induction and include several tissues. Heterogenous senescence phenotype and diverse initial triggers which may result in different molecular profiles render the definition of universal biomarkers challenging. Therefore, the investigation of novel markers to add to the broad picture of senescence is a necessity and should be continuously included in aging and cancer studies.

### **1.5 Tetraploidy as a cancer precursor model**

As senescence and cancer may be viewed as two sides of the same coin, disclosing similarities and dissimilarities in molecular patterns to determine functional properties in both is critical for determining functional properties in both. Most malignant tumors are characterized by an aneuploid karyotype (Storchova & Kuffer, 2008). According to a study conducted by Zasadil et al. (2013) with appliance of the Mitelman database (Mitelman et al., 2010), 26 % of tumors have a near-polyploid (marked by exhibiting  $\geq 58$  chromosomes per cell) chromosome set – with 11 % of solid tumors showing near-tetraploid and above chromosome numbers in the data sets. More strikingly, further bioinformatical analyses indicate that a significant proportion of cells in solid tumor tissues– with estimates ranging from 40 % (Lim & Ganem, 2014) to  $\geq 60$  % (Tanaka et al., 2018) – are tetraploid. Cells with double DNA content or two nuclei, i.e., tetraploid (4n) cells, arise from defective or absent cytokinesis after genome replication. Cells with four homologous sets of chromosomes are often considered a natural physiological state in humans, e.g., in hepatocytes, cardiomyocytes and cells of hematopoiesis. While most tetraploid cells stop dividing, single cells remain capable of dividing. Whole genome duplication alters cell metabolism and increases cell volume. Strikingly, tetraploid cells exhibit high chromosomal instability and signs of replication stress at the gene expression level. Chromosome instability resulting from tetraploidy subsequently promotes oncogenesis. Tetraploidy is thus causally related to the development of preneoplasia and the pathogenesis and somatic evolution of tumors (Storchova & Kuffer 2008). Various mechanisms cause the development of tetraploid cells such as cell fusion (e.g., caused by viral infection), endoreduplication (e.g., caused by defective DNA repair), mitotic “slippage” or defective cytokinesis (Davoli & de Lange, 2011). The timing of chromosome segregation is regulated by the spindle assembly checkpoint, i.e., with interference of the spindle apparatus by inhibition, tetraploidy can be induced *in vitro*. The method involves the treatment of the cells with colcemid, which is a less toxic

colchicine derivate. At this stage of the cell cycle, a tetraploid set of chromosomes is present in the cell. Thus, chromosomes are arrested in metaphase by colcemid treatment and remain tetraploid (Rieder & Palazzo, 1992). Tetraploidy is a balanced state with respect to gene dosage effects, but the consequences, such as loss of whole chromosomes or reciprocal translocations, may alter this balance. Taken together, with its' importance in the formation of malignant tumors and straight-forward induction protocol of diploid cells, tetraploid cells are experimentally suitable as a cancer precursor model.

## 1.6 Focus and strategies of this thesis

With its' multifactorial, complex mechanisms, cellular senescence is a key player in recent aging and cancer research. The present work has been separated in two research directions dealing with epigenetic and genetic changes during cellular senescence. The former is intensively worked on for the phenomenon of DNA methylation and histone modifications. For my part, I concentrated on non-coding RNAs. To shed more light on regulatory pathways triggered by non-coding RNA – more precisely miRNAs -, changes in transcriptomic patterns related to aging phenotypes were examined.

Epigenetic “mutations” and changes frequently involve the mobilization of transposable elements (Heard & Martienssen, 2014). In this regard, it is often described that autonomous mobile DNA - e.g., LINE sequences that parasite our genomes by copy-paste mechanisms - are more abundantly transcribed during cellular senescence. To see if the activity can be used in trans by non-autonomous SINEs to be mobilized and reintegrated into the genome, I have checked the senescence-dependency of patterns in genomic variations entailing active retrotransposition of so-called SINE-Alu-VNTRs (SVAs).

Another form of mobile DNA hinges to the integrity of mitochondria. The latter is a key trigger of SASP induction and was recently shown to be linked to the permeabilization of the mitochondrial outer membrane (MOMP, Victorelli et al., 2023). In consequence and in the context of cellular senescence, mitochondrial DNA is released into the cytosol representing a possible source of so-called nuclear mitochondrial DNA (*numt*) insertions. For each project described, the primary model organism of this thesis includes proliferating, fetal human lung fibroblasts (IMR-90 cells) that are passaged in cell culture until natural replicative senescence is achieved.

In the first chapter of this thesis (*chapter 3: sncRNA and transcriptomic profiles in senescent and tetraploid lung fibroblasts*), proliferating and senescent IMR-90 cells are cultured, the population doubling level and Sa- $\beta$ -Gal activity are assessed to mark the initiated replicative senescence and finally total RNA is extracted of both sample sets (n=2). Additionally, total RNA of tetraploid IMR-90 cells is included as a comparative cancer precursor model and the three samples (n=2) are then next generation sequenced to obtain small non-coding RNA profiles and transcriptomic data. The proliferating (2n) data serves as the control for the obtained profiles of tetraploid (4n) and senescent IMR-90 cells. The tetraploid and senescent data are subsequently checked for senescence- and cell cycle-associated patterns in the expression levels of small non-coding RNA and transcriptomics, using a variety of bioinformatical approaches such as genomic mapping, annotation, and differential expression analysis. Moreover, to elucidate cellular senescence in the context of primate variation, a non-human primate model – i.e., proliferating and senescent adult lung fibroblasts of *Callithrix jacchus* – is checked for small non-coding RNA patterns and compared to the human model applied in this thesis. With the knowledge obtained by the small non-coding RNA data analysis, potential candidates for senescence-associated markers are chosen and inhibition of such – i.e., miRNAs -is experimentally performed on proliferating IMR-90 cells to gain more insight on the impact of senescence-associated miRNAs regarding cellular integrity and cell cycle hallmarks.

The second topic of this thesis (*chapter 4: generation of somatic de novo structural variation as a hallmark of cellular senescence in human lung fibroblasts*) was submitted to *Frontiers in Cell and Developmental Biology, Epigenomics and Epigenetics* and is currently in the peer review process. The aim is to gain further insights into the possible structural variance occurring in the genomes of cellular senescent IMR-90 cells and thus investigate *de novo* retrotransposition of SVAs and somatic insertions of *numts*. For the detection of *de novo* SVA integrations, a subtractive and kinetic enrichment technique using proliferating cell DNA as a driver and senescent genomes as a tester is applied, followed by deep sequencing, a method that I co-developed together with colleagues in our laboratory and co-authored (see Möhner et al., 2023). The experimental setup is followed by a customized bioinformatical pipeline as established therein. Furthermore, the identification of *de novo numts* is performed by implementing a comparative method. Total DNA of proliferating and senescent IMR-90 cells is whole genome sequenced and

– additionally - a strategy of specifically enriching nuclear sequences applying an AluScan PCR with primers anchored in Alu-SINEs as described by Mei et al. (2011) combined with NGS-sequencing is added. The resulting data of both experimental approaches are then bioinformatically scanned for sequences perfectly fitting both mtDNA and flanking nuclear DNA. Several bioinformatical filtering steps are included in this data evaluation process. Thus, the identification of possible *de novo numts* is performed.

The combination of these two topics allows me to draw conclusions on the machinery of cellular senescence with emphasis on cell cycle regulators and tumorigenesis in the context of small non-coding RNA and transcriptomics - and lastly genomic variation occurring by the often epigenetically controlled activation of mobile elements such as SVAs and *numts*, possibly causally relevant in the context of cellular senescence and decaying mitochondrial integrity.

## 2 Material and methods

### 2.1 Material

#### 2.1.1 Cell culture

##### Primary cells

- Adult common marmoset lung fibroblasts (*Callithrix jacchus*; *Supplementary Figure 3*), provided by Henk Niphuis and Ernst Verschoor of the Biomedical Primate Research Centre, Rijswijk

##### Established cell lines

- IMR-90 cells, human fetal lung fibroblasts, provided by AG Moosmann, Institute of Pathobiochemistry, University Medical Center of the Johannes Gutenberg-University Mainz

##### Modified cell lines

- Tetraploid IMR-90 cells (*Supplementary Figure 2*). Tetraploidy induction was performed on IMR-90 cells (see above: *established cell lines*) by Carina Daubermann in our laboratory (AG Zischler, Institute of Organismal and Evolutionary Biology, Johannes Gutenberg-University Mainz)

##### Disposables and devices

- Incubator (37 °C, 5 % CO<sub>2</sub>; Integra Biosciences)
- Incubator (37 °C)
- Julabo® Water Bath (Merck)
- Hettich Rotina 38R Centrifuge (Merck)
- Hettich Rotina 22R Centrifuge (Merck)
- Primo Vert Microscope (Zeiss)
- Microbiological safety workbench (Clean Air by Baker)
- Automatic pipetting aid (Heathrow Scientific)
- ErgoOneCanal pipettes (Starlab)

- Fuchs-Rosenthal cell counting chamber (ThermoFisher Scientific)
- Nunc non-treated T25/T75 EasyFlask (ThermoFisher Scientific)
- Nunc 6-well multidish (ThermoFisher Scientific)
- Nunc 24-well multidish (ThermoFisher Scientific)

### Chemicals and Reagents

- *Dulbecco's modified eagle's medium* 1x GlutaMAX™ Medium (DMEM) (ThermoFisher Scientific; 41966029)
- Opti-MEM™ I Reduced Serum Medium (ThermoFisher Scientific; 11058021)
- Fetal bovine serum (FBS) (ThermoFisher Scientific; 16000044)
- *Recovery Cell Culture Freezing Medium* (ThermoFisher Scientific; 12648010)
- Phosphate Buffered Saline Solution (PBS, 10X; ThermoFisher Scientific; 70013032)
- Trypsin-EDTA (0.05 %), phenol red (ThermoFisher Scientific; 25300054)
- Lipofectamine™ RNAiMAX Transfection Reagent (ThermoFisher Scientific; 13778075)
- miRNA inhibitor: 5 nmol IDT® *negative control*:  
5'-mG/ZEN/mCmG mUmAmU mUmAmU mAmGmC mCmGmA mUmUmA  
mAmCmG/3ZEN/ -3'
- miRNA inhibitor: 5 nmol IDT® *hsa-miR-29a-3p*:  
5' -mU/ZEN/mAmA mCmCmG mAmUmU mUmCmA mGmAmU mGmGmU  
mGmCmU /3ZEN/ -3'
- 70 % EtOH

## **2.1.2 Extraction methods**

### **2.1.2.1 RNA**

- *Quick*-RNA Miniprep Kit (Zymo Research; R1055)
- 99,9 % EtOH

### **2.1.2.2 DNA**

- *QIAamp* DNA Mini Kit (Qiagen; 51306)

### 2.1.3 Synthesis methods

#### 2.1.3.1 Poly(A) tailing of miRNA inhibited RNA samples

- *E. coli* Poly(A) Polymerase (NEB; M0276)
- RNA samples treated with miRNA inhibitor

#### 2.1.3.2 Reverse transcription

- Biozym cDNA synthesis kit (Biozym; 331470)
- 10  $\mu$ M *miRTQ*: Oligonucleotide for Poly(A) tailed RNA samples:  
CGAATTCTAGAGCTCGAGGCAGGCGACATGGCTGGCTAGTTAAGCTT  
GGTACCGAGCTCGGATCCACTAGTCCTTTTTTTTTTTTTTTTTTTTTTTTTTTT  
TVN
- 25  $\mu$ M Hexamer oligonucleotides for RT-qPCR Agingmarker RNA samples
- 10  $\mu$ M Oligo (dT) for RT-qPCR Agingmarker RNA samples

### 2.1.4 Quantification and detection methods

#### 2.2.4.1 Senescence-associated $\beta$ -galactosidase assay (SA-beta gal)

- 3.7 % formaldehyde in 1X PBS
- 1X PBS
- 70 % glycerol

#### Staining solution

- 4 ml Citric acid/Na<sub>2</sub>HPO<sub>4</sub> Buffer (pH 6)
- 100  $\mu$ l 200 mg/ml X-Gal (thermoscientific; R0404) in DMF  
(Cell Signaling Technology; 12767S)
- 1 ml 100 mM K<sub>3</sub>[Fe(CN)<sub>6</sub>] (III)
- 1 ml 100 mM K<sub>3</sub>[Fe(CN)<sub>6</sub>] x 3 H<sub>2</sub>O (II)
- 40  $\mu$ l 1 M MgCl<sub>2</sub> X 6 H<sub>2</sub>O
- 600  $\mu$ l 5 M NaCl
- 13.26 ml H<sub>2</sub>O<sub>VE</sub>

### 2.2.4.2 DNA & RNA measurement via Qubit

- Qubit™ RNA Broad Range (BR) Assay Kit (ThermoFisher Scientific; Q10210)
- Qubit™ 1X dsDNA High Sensitivity (HS) Assay Kit (ThermoFisher Scientific; Q33230)

### 2.2.4.3 RT-qPCR

- qPCR Qiagen Rotorgene Q
- SYBR Green Mix (Qiagen, 204056)

### Oligonucleotides

<i>miRNA</i>	<i>Sequence 5'-3'</i>	<i>Information</i>
<b>Hsa-miR-29a-3p</b>	TAGCACCATCTGAAATCGGTTA	FWD Primer for hsa-miR-29a-3p (inhibition)
<b>Hsa-let-7a</b>	TGAGGTAGTAGGTTGTATAG	FWD Primer for hsa-let-7a (control)
<b>RTQ-UNI</b>	CGAATTCTAGAGCTCGAGGCAGG	REV Primer for miRNA sequences
<i>Gene of Interest</i>	<i>Sequence 5'-3'</i>	<i>Information</i>
<b>COL1A3</b>	GATTCCCTGGACCTAAAGGTGC	FWD Primer for miR-29a-3p target gene
	AGCCTCTCCATCTTTGCCAGCA	REV Primer for miR-29a-3p target gene
<b>SIRT1</b>	TAGACACGCTGGAACAGGTTGC	FWD Primer
	CTCCTCGTACAGCTTCACAGTC	REV Primer
<b>LMNB1</b>	GAGAGCAACATGATGCCCAAGTG	FWD primer
	GTTCTTCCCTGGCACTGTTGAC	REV Primer
<b>BETA ACTIN</b>	CGAGCACAGAGCCTCGCCTTT	FWD Primer
	CATGCCACCATCACGCCCTGG	REV Primer



## 2.2 Methods

### 2.2.1 Cell culture

All steps were performed under sterile conditions in a ventilated workbench. Prior to the standard procedures, the workbench was irradiated for 10-15 minutes with UV light and surfaces, disposables and pipettes were sterilized with 70 % EtOH.

#### 2.2.1.1 Thawing cells

Frozen cell vials were thawed in a water bath (37 °C) for 1-2 minutes. Thawed cells were transferred to 15 ml centrifuge tubes and resuspended in warm 10 ml DMEM medium. The centrifugation step was performed at 200 x g for five minutes at room temperature. After carefully aspirating the excess medium, 5 ml of DMEM medium was added to the cell pellet and thoroughly resuspended. The cell suspension was transferred to a T75 or T25 flask and placed in an incubator until further processing (37 °C, 5 % CO<sub>2</sub>).

#### 2.2.1.2 Subcultivation

With a cell density of 70-80 %, adherent cells can be passaged to the desired ratio. DMEM medium was removed from the flasks and the cells were rinsed with 1-2 ml 1X PBS. PBS was then removed, and 1-2 ml Trypsin was applied to the cells. The suspension was incubated at 37 °C, 5 % CO<sub>2</sub> for at least five minutes to ensure full detachment of adherent cells. To inhibit the digestion, DMEM medium was added to the suspension (5 ml for 1 ml trypsin, 8 ml for 2 ml trypsin), thoroughly resuspended and, depending on the chosen ratio, transferred to new T25/T75 flasks containing 5 ml/10 ml DMEM medium. The cell number was assessed with every passaging to calculate the population doubling level (PDL), which served as an additional indicator for cellular senescence. The initial cell number was assessed right after the trypsin inhibition with DMEM medium (pre-splitting), as well as the cell number after creating new cell suspensions (post-splitting, 1:2 – 1:5 ratio). Of each cell suspension (pre-splitting and post-splitting), 15 µl were applied to a Fuchs-Rosenthal-counting chamber (Figure 1). Cell numbers in five of the 16 quadrants were counted, added and multiplied by 1000 to gain the cell number per one milliliter (ml).

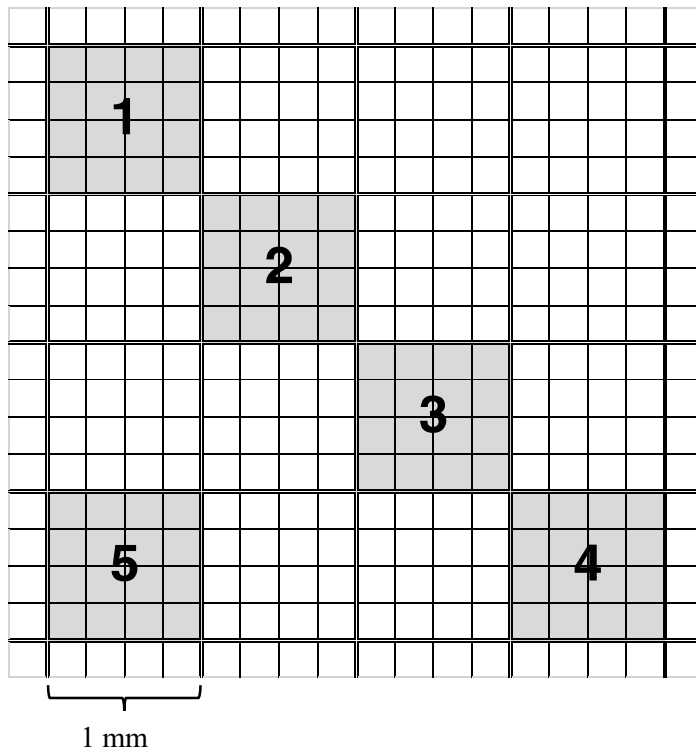


**Figure 1** – Fuchs-Rosenthal-counting chamber scheme

Cell subcultivation was repeated until cells enter the desired PDL. For PDL calculation, the following formula is applied:

$$PDL = n + \left( \frac{\log (A) - \log (B)}{\log (2)} \right)$$

*n* Initial PDL of the cells

*A* cells per ml, pre-splitting

*B* cells per ml, post-splitting of the previous cell passaging

As soon as the cells enter the desired PDL and confluency, they are harvested for further treatments.

### 2.2.1.3 Harvesting cells

For further analyses, cells were harvested at the desired PDL and/or 70-80 % confluency by performing a washing step with 1X PBS, ensuring cell detachment with trypsin (T25 flask: 1 ml, T75 flask: 2 ml) and resuspension in DMEM (5 ml, 8 ml) medium. After counting the cells in the suspension, cells were centrifuged at 500 x g and room

temperature for 5 minutes, the supernatant was discarded and the cell pellet resuspended in 1X PBS, centrifuged at 500 x g, room temperature for 5 minutes and the supernatant discarded in an additional washing step.

For RNA isolation, the cell pellet was put on ice after harvesting, resuspended in RNA Lysis Buffer and stored at -80 °C or immediately processed according to the manufacturer's protocol.

For DNA isolation, the cell pellet ( $\leq 5$  million cells) was resuspended in 200  $\mu$ l 1X PBS and stored at -20 °C or further processed according to chapter 2.2.2.2.

To cryopreserve cells, the washed cell pellet was resuspended in freezing medium, containing 1-2 million cells per 1 ml medium and stored at -80 °C.

#### 2.2.1.4 miRNA inhibition

Proliferating IMR-90 cells were harvested according to 2.2.1.3 and transferred to a 24-well plate, containing 50.000 cells per well (Table 1). Cells were incubated for 24-48 hours until the desired confluency is reached ( $\geq 70$  %) prior to the treatment.

*Table 1 – transfection scheme for anti-miRNA inhibition, including wells for negative control, untransfected cells and mock transfected cells.*

miRNA Inhibitor	hsa-miR-29a-3p		negative control		no transfection	
miRNA Inhibitor/RNAiMax	5 pmol ( $\approx 10$ nM) / 1.5 $\mu$ L (end conc./vol.)					
mock	1	2	3	4	5	6
mock	7	8	9	10	11	12
untransf.	13	14	15	16	17	18
untransf.	19	20	21	22	23	24

On the day of the transfection, DMEM medium was removed, and cells were washed using 500  $\mu$ l of 1X PBS per each well. For the miRNA inhibitor (hsa-miR-29a-3p), such as the negative control, 1  $\mu$ l of miRNA (10  $\mu$ M) was resuspended with 50  $\mu$ l Opti-MEM medium per well. 3  $\mu$ l of the Lipofectamine RNAiMAX Reagent were diluted with 50  $\mu$ l

Opti-MEM. Depending on the sample quantity, master mixes with a 10 % surplus were created for the RNAiMAX dilution, the miRNA inhibitor dilution, and the negative control dilution. Each diluted miRNA was added to the diluted Lipofectamine RNAiMAX Reagent in a 1:1 ratio and incubated for five minutes at room temperature. 50  $\mu$ l of the resulting miRNA-lipid complex was applied to each well containing 500  $\mu$ l DMEM medium. Cells were incubated for 48 hours at 37 °C, 5 % CO<sub>2</sub> before visualization and analysis were performed. After 48 hours, the transfected cells were harvested according to 2.2.1.3 and further processed for total RNA isolation. Four wells of miRNA inhibitor-transfected cells were further plated and harvested after seven days to investigate the inhibition effect in comparison to the freshly transfected cells.

## **2.2.2 Extraction methods**

### **2.2.2.1 RNA**

Total RNA was isolated from harvested cells according to the manufacturer's protocol (*Quick-RNA Miniprep Kit*, Zymo Research). A modification of the protocol was applied for small RNA enrichment by adding two volumes of 100 % ethanol to the flow-through of step 2 before transferring the samples to the Zymo-Spin™ IICG Column1 (green). Samples were eluted in 50  $\mu$ l RNase-free ddH<sub>2</sub>O and stored at -80 °C.

### **2.2.2.2 DNA**

Genomic DNA was isolated from harvested cells according to the manufacturer's protocol (*QIAamp DNA Mini Kit*, Qiagen). Harvested cell pellets were resuspended in 200  $\mu$ l 1X PBS, containing up to 5 x 10<sup>6</sup> cells per sample. Prior to the DNA isolation, an additional step of RNA digestion was included. 5  $\mu$ l RNase A (20 mg/ml) were added to each sample and incubated for 20 minutes at 37 °C. For enzyme inactivation, 20  $\mu$ l Proteinase K and 200  $\mu$ l AL Buffer were added and incubated for 10 minutes at 56 °C. The following steps were performed according to the manufacturer's protocol.

## **2.2.3 Synthesis methods**

### **2.2.3.1 Poly(A) tailing of miRNA inhibited RNA samples**

500 ng of extracted RNA were used as input for Poly(A) tailing according to the manufacturer's protocol (*E. coli Poly(A) Polymerase*, NEB). After the synthesis, the

samples (20 µl) were then mixed with 2:1 EtOH and then transferred to Quick RNA ZymoResearch columns. RNA samples were eluted in 50 µl RNase free H<sub>2</sub>O.

### **2.2.3.2 Reverse transcription**

500 ng of Poly(A) tailed RNA was used as input for the miRNA specific reverse transcription and additionally 500 ng of total RNA for standard reverse transcription using random hexamer and Oligo(dT) oligonucleotides. Reverse transcription with MmuL reverse transcriptase was performed according to the manufacturer's protocol (cDNA synthesis kit, Biozym). All oligonucleotides are provided in the material list.

## **2.2.4 Quantification and detection methods**

### **2.2.4.1 Senescence-associated beta galactosidase assay**

Cells were harvested and transferred to a 6-well plate, containing 50.000 cells per well. After one to three days, depending on the cell density, DMEM medium was removed, and cells were washed twice with 1X PBS. All reagents used in this assay were freshly prepared prior to usage. To fixate cells, 2 ml of 3,7 % formaldehyde was applied to each well and incubated for 5 minutes at room temperature, followed by two additional washing steps with 1X PBS. 2 ml of the staining solution were applied to each well and incubated at 37 °C (without CO<sub>2</sub>) over night. From each well, 3-4 pictures were taken of the light microscopic imagery (100x). For each sample, blue stained and stainless cells were counted and the percentage of blue stained cells in total per sample was evaluated. For storage at 4 °C, staining solution was removed, and 70 % glycerol applied to each well. The 6-well was then sealed with parafilm.

### **2.2.4.2 DNA & RNA measurement via Qubit**

To estimate DNA and RNA quantity in the studied samples, measurements were performed by using the dsDNA Assay Kit for DNA and the RNA Broad Range Assay Kit for RNA samples according to the manufacturer's protocol (ThermoFisher Scientific).

### **2.2.4.3 RT-qPCR**

Quantification of human miRNA (miR29a-3p, let-7a) and specific genes of interest (Oligonucleotides provided in material list) was performed utilizing real time quantitative polymerase chain reaction (RT-qPCR) according to the manufacturer's protocol (SYBR

Green Mix, Qiagen). The “70-64 touchdown with melt” program was applied from the manufacturer’s software. The quantification and melting curves were analyzed, and target gene/miRNA expression was recorded for each group according to the  $2^{-\Delta\Delta CT}$  method.

## **2.2.5 Next generation sequencing**

### **2.2.5.1 Small RNA sequencing**

Quantities of  $\geq 1 \mu\text{g}$  total RNA of proliferating diploid, proliferating tetraploid and senescent diploid IMR-90 cells (n=2), as well as proliferating and senescent (n=1) primary lung fibroblasts of an adult common marmoset were 50 single-end small RNA sequenced, resulting in raw data s FASTQ files provided by BGI Group (Hong Kong) using the DNBSEQ™ sequencing platform.

### **2.2.5.2 Transcriptome sequencing**

2  $\mu\text{g}$  total RNA of proliferating diploid, proliferating tetraploid, and senescent diploid IMR-90 cells (n=2) were 150 paired-end mRNA sequenced, resulting in raw data as FASTQ files provided by Novogene Co., Ltd. using the Illumina NovaSeq 6000 platform.

## **2.2.6 Bioinformatical analysis**

### **2.2.6.1 Small RNA data analysis**

For small RNA profiling, raw FASTQ files of diploid proliferating, tetraploid proliferating and diploid senescent IMR-90 cells were analyzed by applying the sRNAtoolbox routine (Aparicio-Puerta et al., 2019). Total small RNA sequences were mapped to the human genome (hg38) with Bowtie2 and mapped features were annotated using sRNAbench. Differentially expressed miRNAs in senescent and tetraploid IMR-90 cells were estimated and depicted using sRNAde.

Additionally, total small RNA profiles of the IMR-90 batches such as the proliferating and senescent common marmoset small RNA sequencing data were annotated applying Unitas (Gebert et al., 2017; Chan et al., 2009; Quast et al., 2013; Rosenkranz, 2016; Yates et al., 2016; Kozomara & Griffiths-Jones, 2014).

To gain more insight on functional properties of differentially expressed miRNAs ( $p$ -value  $\leq 0.05$ ) in senescent and tetraploid IMR-90 small RNA sequencing data, miRNA enrichment ontology using miEAA 2.1 was applied (Aparicio-Puerta et al., 2023).

#### **2.2.6.2 RNA sequencing data analysis**

The provided transcriptomic data of proliferating, tetraploid and senescent IMR-90 cells were analyzed by firstly quantifying transcript expression into read count files using Salmon (Patro et al., 2017), then transforming the generated transcript-level abundancies to gene-level estimates utilizing tximport (Soneson et al., 2015) and finally performing differential expression analysis using DESeq2 (Love et al., 2014). Transcriptome data (hg38) was obtained from Ensembl (Martin et al., 2023). Fold changes and p-values were checked for genes of interest as obtained and compared between tetraploid and senescent IMR-90 cell transcriptomic data. For the visualization of differentially expressed genes, volcano plots were created using VolcanoR (Goedhart & Luijsterburg, 2020).

## 3 sncRNA and transcriptomic profiles in senescent and tetraploid lung fibroblasts

### 3.1 Results

#### 3.1.1 Small non-coding RNA: an overview

For the assessment of possible senescence and cancer precursor-associated patterns, small non-coding RNA sequencing data of diploid proliferating, tetraploid proliferating (Supplementary Figure 2) and diploid senescent (Supplementary Figure 1) IMR-90 cells were generated by BGI. For the proliferating IMR-90 cells, 25,607,547 (first replicate: *IMR-90\_Prolif\_1*) and 23,769,239 (second replicate: *IMR-90\_Prolif\_2*) clean reads were counted. The senescent data sets included 29,804,305 (first replicate: *IMR-90\_Sen\_1*) and 22,446,258 (second replicate: *IMR-90\_Sen\_2*) clean reads. For the tetraploid data, 21,870,936 (first replicate: *IMR-90\_Tetra\_1*) and 25,276,786 (second replicate: *IMR-90\_Tetra\_2*) clean reads were generated (Supplementary Table 1). To obtain annotations, the sRNAtoolbox routine was applied to the clean reads. Total small RNA sequences were mapped to the human genome (hg38) and features were annotated using sRNAbench. Differentially expressed miRNAs in senescent and tetraploid IMR-90 cells were estimated and depicted using sRNAde. Overall small RNA annotation has additionally been generated by applying Unitas to compare the output and get a broad perspective on the specific subtype distributions (Supplementary Table 2-4). By comparing the replicates within the three sample batches, several small RNA classes differ in overall quantity for proliferating (Figure 2), senescent (Figure 3) and tetraploid (Figure 4) IMR-90 cells. The most abundant RNA class throughout all samples is miRNA, with most reads ranging from 20 to 25 nt in size, with peaks around 22 and 23 nt. The distribution and annotation of miRNAs are overall consistent in the replicates, whereas other classes such as tRNA fragments and yRNA are highly heterogenous in their abundancy (Supplementary Table 2-4). The tetraploid samples (Figure 4) show a limited variety of small RNA classes in comparison to the diploid proliferating and senescent samples. The main annotated RNA classes contain lncRNA, miRNA, snoRNA and additionally tRNA for one of the replicates.



### 3 snRNA and transcriptomic profiles in senescent and tetraploid lung fibroblasts

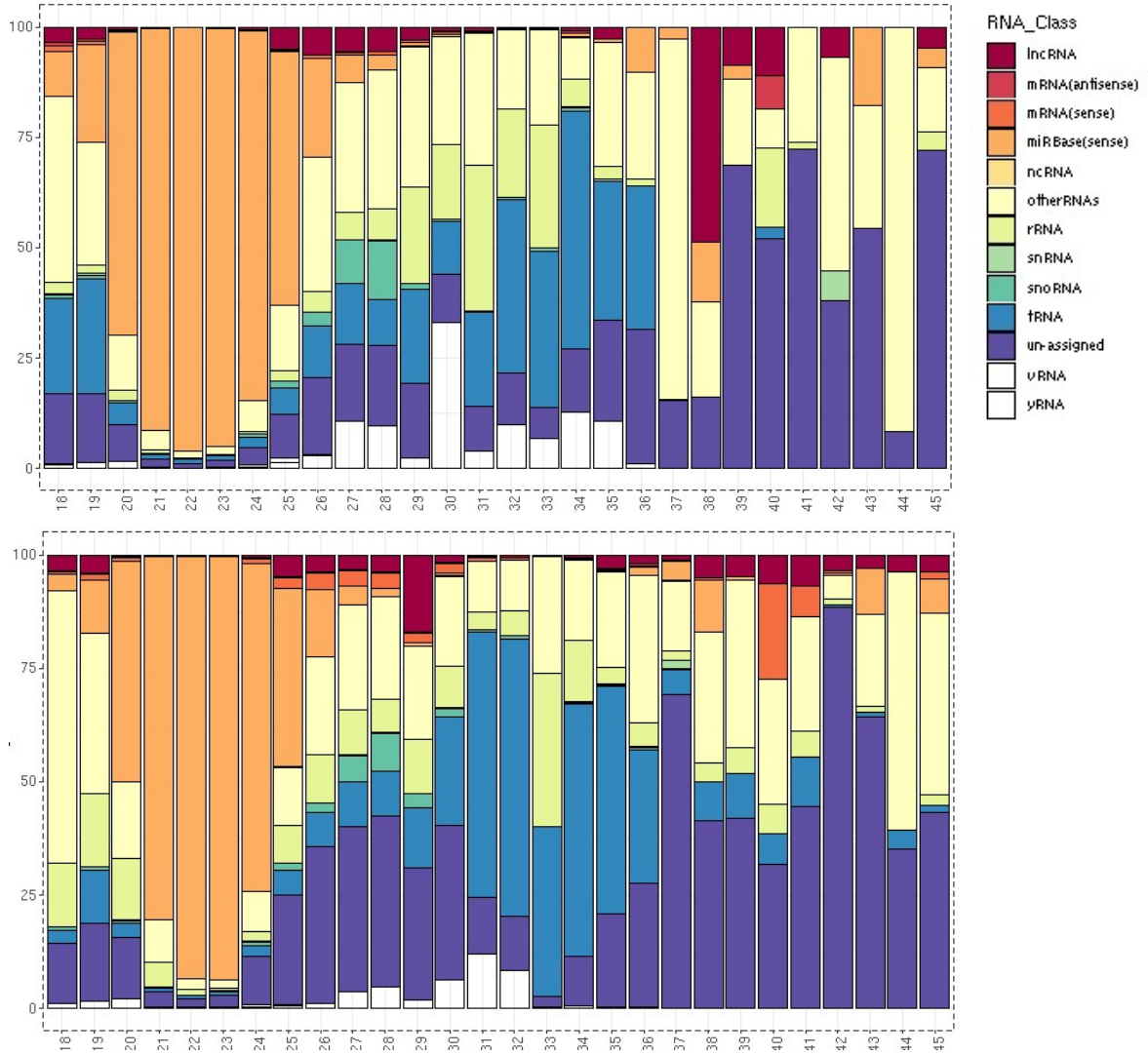


**Figure 2** - sRNA-Bench annotation of small non-coding RNA in proliferating, diploid IMR-90 cells ( $n=2$ ). Top and bottom diagram depicting each replicate). X-axis: read length [nt], y-axis: percentage of RNA classes per read length.

### 3 snRNA and transcriptomic profiles in senescent and tetraploid lung fibroblasts

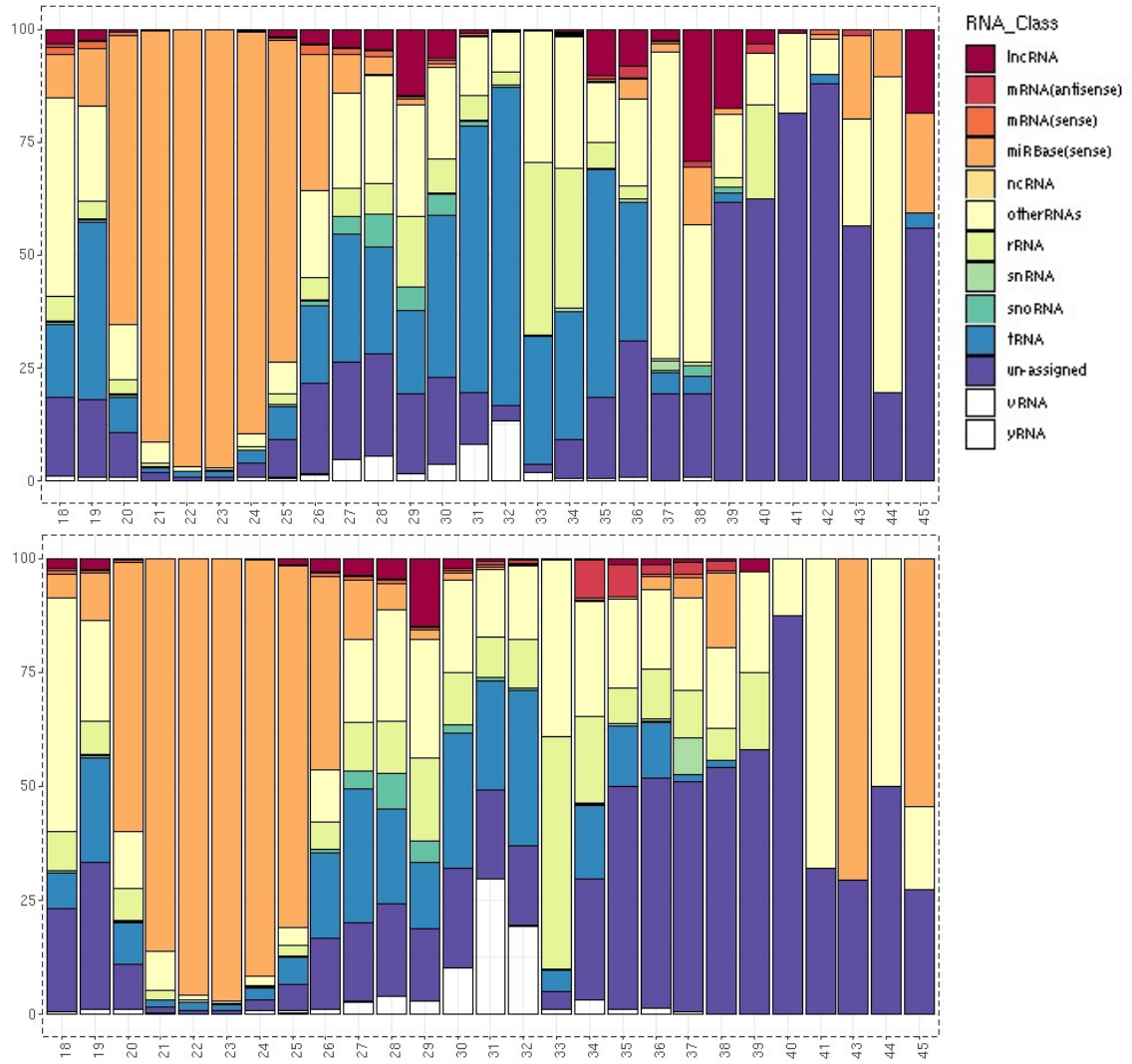


**Figure 3** - sRNABench annotation of small non-coding RNA in senescent, diploid IMR-90 cells ( $n=2$ . Top and bottom diagram depicting each replicate). X-axis: read length [nt], y-axis: percentage of RNA classes per read length.

### 3 snRNA and transcriptomic profiles in senescent and tetraploid lung fibroblasts

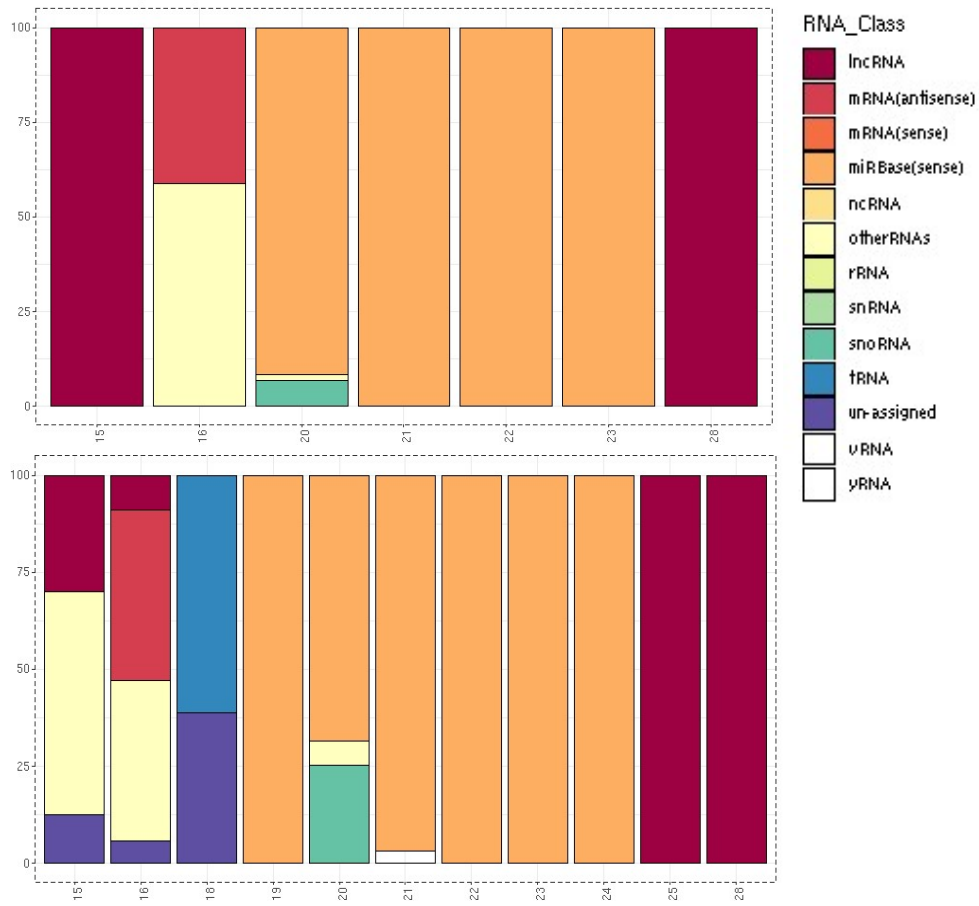


**Figure 4** - sRNABench annotation of small non-coding RNA in proliferating, tetraploid IMR-90 cells (n=2). Top and bottom diagram depicting each replicate. X-axis: read length [nt], y-axis: percentage of RNA classes per read length.

### 3.1.2 Differentially expressed miRNAs

To compare miRNA profiles of proliferating and senescent as well as diploid and tetraploid IMR-90 cells, differential expression analysis was performed utilizing sRNAde. Differentially overexpressed miRNAs with a p-value  $\leq 0.05$  were further functionally analyzed in the context of miRNA enrichment ontology using miEAA 2.1 (Aparicio-Puerta et al., 2023). In total, 100 differentially expressed miRNAs are found in the senescent IMR-90 small RNA sequencing data, with 49 being down- and 51 upregulated (Supplementary Table 5). Figure 5 depicts the top 30 differentially expressed miRNAs in senescent IMR-90 cells, with  $\log_2$  FC (fold changes) ranging from -3 (hsa-

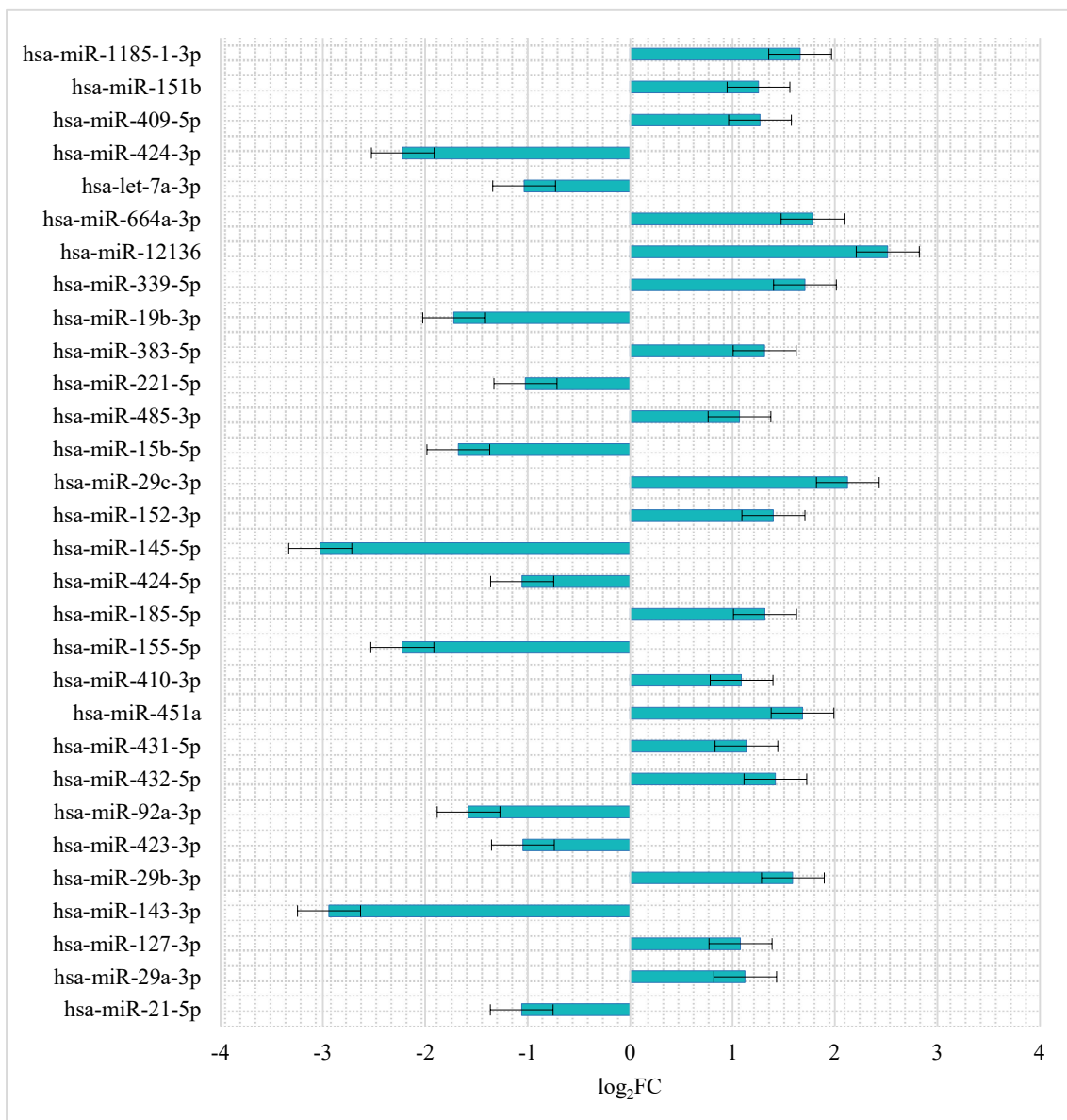


**Figure 5** - Top 30 differentially expressed miRNAs in senescent IMR-90 cells (n=2). X-axis:  $\log_2$  Fold Change as bars with standard error, Y-axis: annotation of human miRNAs.

miR-145-5p) to 2.5 (hsa-miR-12136). The 51 upregulated miRNAs in senescent IMR-90 cells were then checked for possible functional connections to diseases by utilizing miEAA (Figure 6). The observed senescence-associated upregulation of miRNAs is, inter alia, linked to Alzheimer disease, Huntington disease, various types of cancer e.g., lung cancer and lung disease.

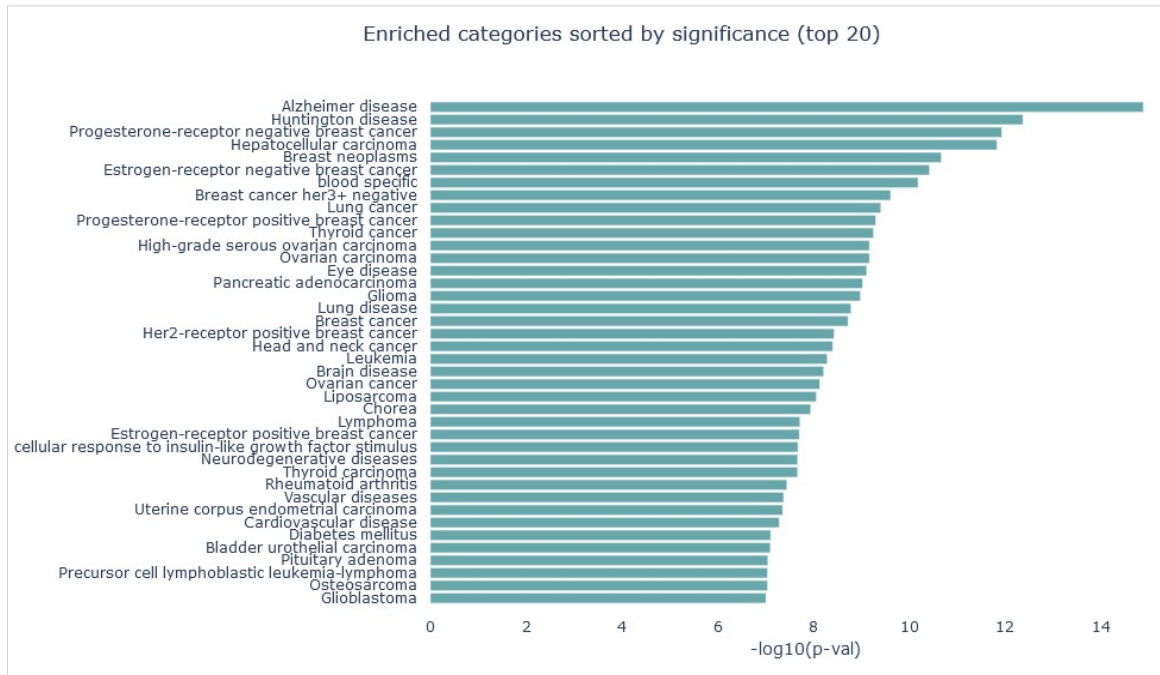


**Figure 6** - Barchart of top 20 enriched categories (diseases) sorted by significance of upregulated miRNAs in senescent IMR-90 cells (n=2), created with miEAA. X-axis:  $-\log_{10}(p\text{-value})$ , Y-axis: diseases associated with the upregulation of assorted miRNAs.

The tetraploid samples which served as a cancer precursor model were additionally analyzed for differentially expressed miRNAs to elucidate differences and similarities in contrast to the senescent samples. In total, the tetraploid samples (n=2) contain 36 differentially expressed miRNAs, of which 14 are under- and 22 are overexpressed, respectively (Figure 7). The  $\log_2FC$  range from -7 (has-miR-1915-5p) to 7.8 (hsa-miR-5193). Comparing the over- and underexpressed miRNAs ( $p\text{-value} \leq 0.05$ ) in the tetraploid and senescent small RNA sequencing data, only 7 in total are shared (Figure 8). Hsa-miR-145-5p, hsa-miR-3138, hsa-miR-138-5p and hsa-miR-15b-3p are downregulated in both tetraploid and senescent IMR-90 cells, while hsa-miR-668-3p, hsa-miR-127-3p and hsa-miR-4423-5p are upregulated.

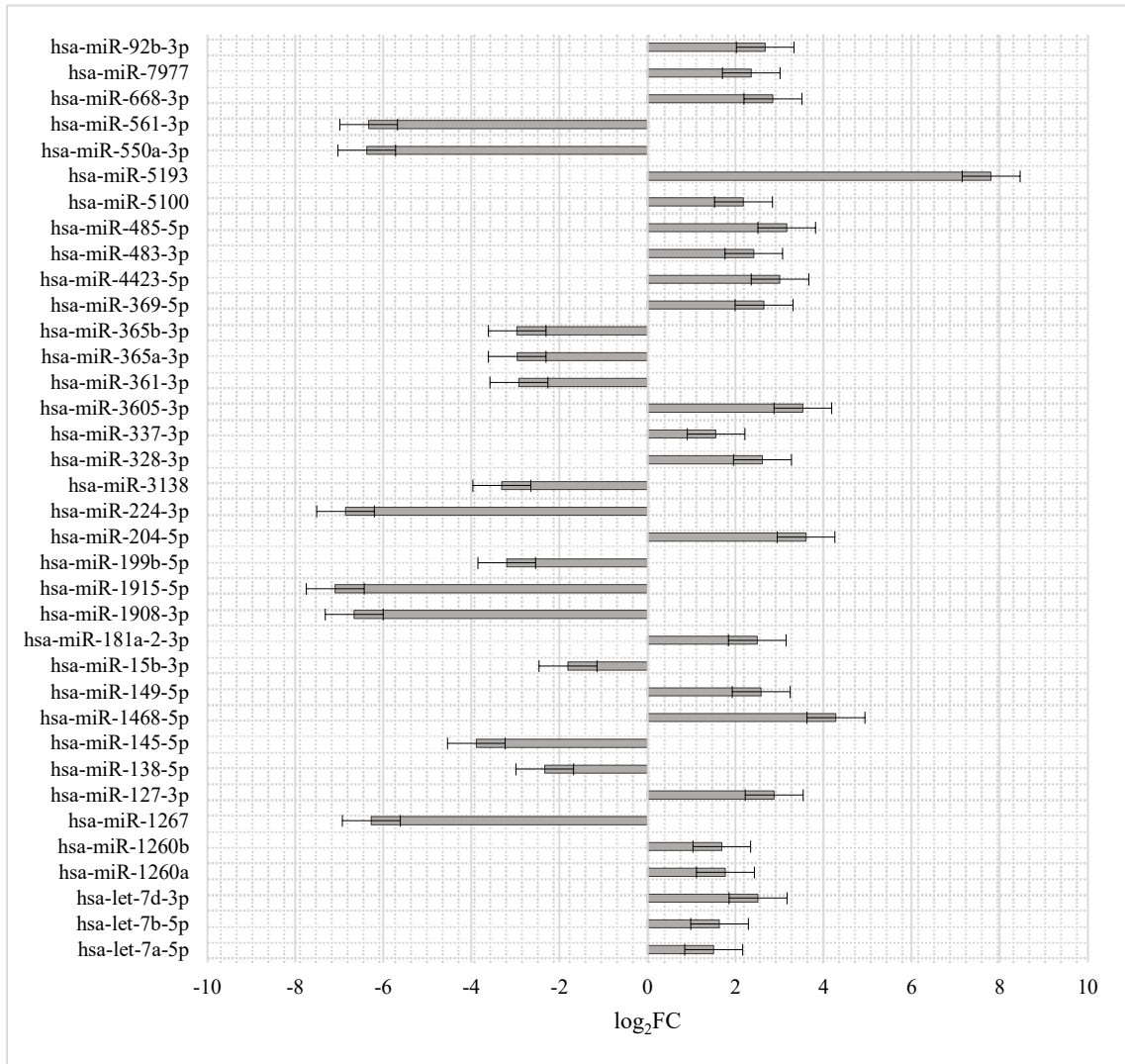


**Figure 7** - Differentially expressed miRNAs in tetraploid IMR-90 cells (n=2). X-axis: log<sub>2</sub> Fold Change as bars with standard error; Y-axis: annotation of human miRNAs.

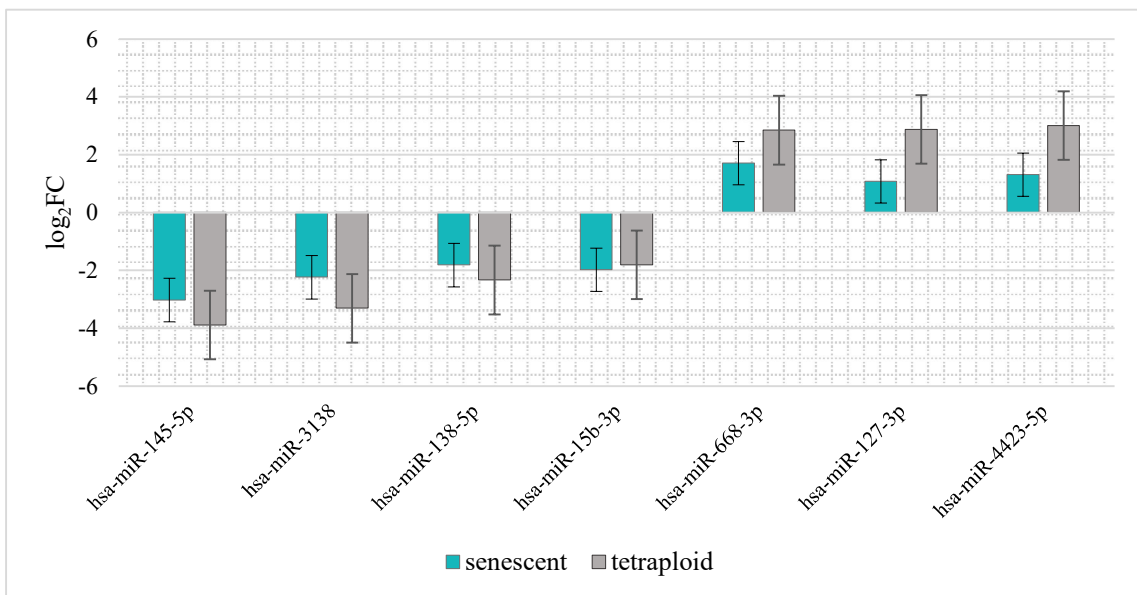


**Figure 8** - Shared differentially expressed miRNAs in tetraploid and senescent IMR-90 cells (n=2). Y-axis: log<sub>2</sub> Fold Change as bars with standard error; X-axis: annotation of human miRNAs.

The 22 differentially overexpressed miRNAs in tetraploid IMR-90 cells in comparison to proliferating cells were subsequently checked for functional properties linked to diseases using miEAA (Figure 9). Several diseases are associated with the upregulated miRNAs such as Alzheimer's, multiple sclerosis, cardiovascular disease, and malignant cancers such as colon adenocarcinoma, prostate cancers, glioblastoma and thyroid cancer.

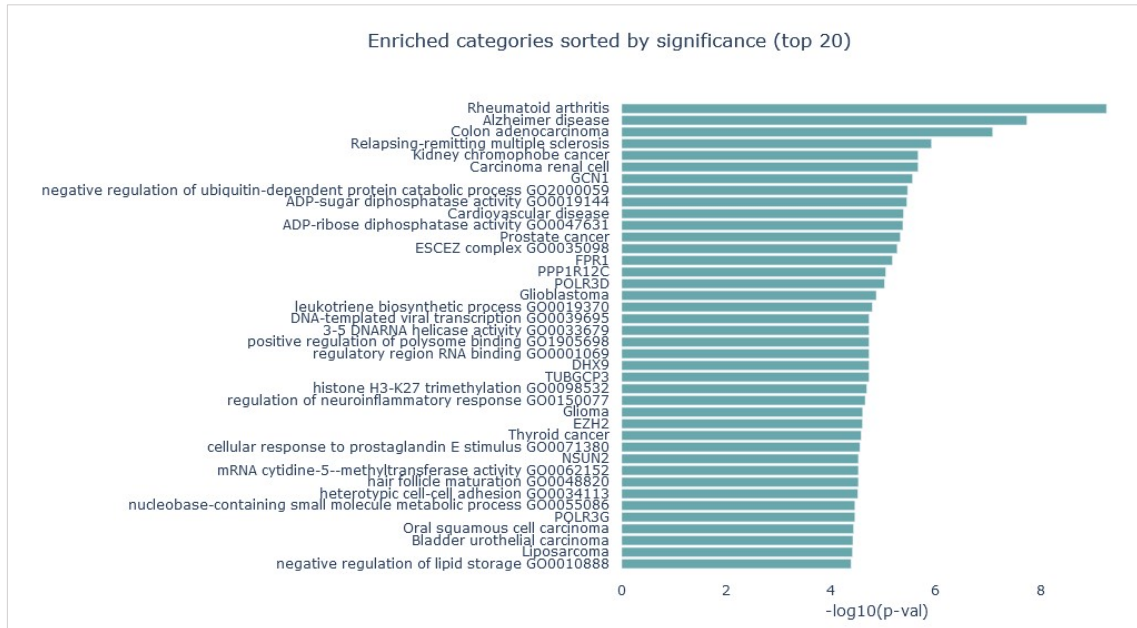


**Figure 9** - Barchart of top 20 enriched categories (diseases) sorted by significance of upregulated miRNAs in tetraploid IMR-90 cells (n=2), created with miEAA. X-axis:  $-\log_{10}(p\text{-value})$ , Y-axis: diseases associated with the upregulation of assorted miRNAs.

### 3.1.3 Senescence-associated miRNA in common marmosets

In order to obtain more insight on conservation of miRNA profiles and thus their possible functional relevance in the context of primate cellular senescence, small RNA sequencing data from proliferating and senescent common marmoset lung fibroblasts was additionally analyzed (adult, ♂; n=1). In total, 22,144,299 clean reads were generated for the proliferating fibroblasts (*Cja\_Prolif*) and 20,261,744 for the senescent fibroblasts (*Cja\_Sen*; Supplementary Table 1). Common marmosets share a common ancestor with humans about 35 mya and represent a fundamental model in age-related diseases, as their short lifespan (avg. 5-7 years) and close phylogenetic relation to humans allow to draw conclusions on possibly conserved physiological processes. Cellular senescence was assessed by applying the senescence-associated  $\beta$ -galactosidase assay to proliferating and senescent lung fibroblasts (Supplementary Figure 3). Clean data provided by BGI was annotated using Unitas and RNA class abundancies were compared between proliferating

and senescent common marmoset small RNA sequencing data. The top 20 most abundant miRNA (Figure 10) show up- and downregulation patterns, ranging from -2.5 fold change (miR-21-5p) to 1.18 fold change (miR-127-3p).

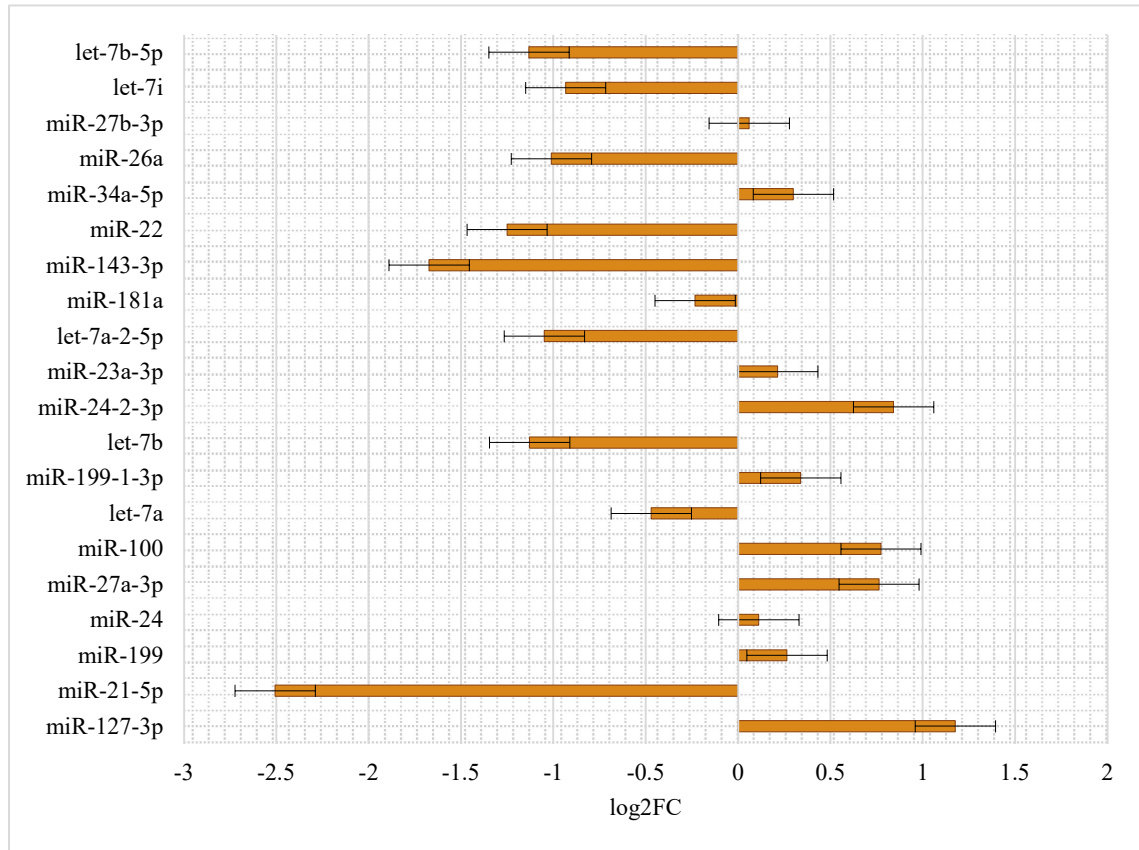


**Figure 10** - Top 20 up- and downregulated miRNAs in senescent common marmoset lung fibroblasts (adult, male, n=1). X-axis: annotation of miRNAs; Y-axis:  $\log_2FC$  as bars with standard error.

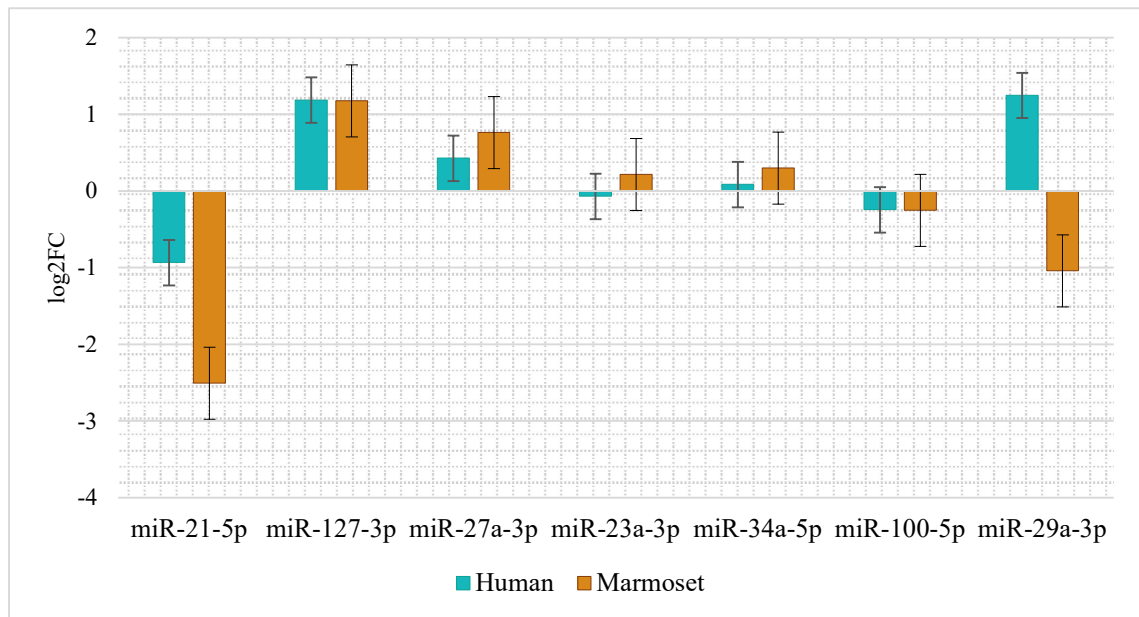


**Figure 11** - comparison of senescence-associated miRNAs in common marmoset (orange) and human IMR-90 lung fibroblast (turquoise) small RNA sequencing data. X-axis: annotation of miRNAs; Y-axis:  $\log_2FC$  as bars with standard error.



In an interspecies comparison, several senescence-associated miRNAs identified in senescent IMR-90 cells show similar enrichment and depletion patterns upon comparing proliferating with senescent cells in common marmoset lung fibroblasts. Especially miR-21-5p is significantly downregulated in the senescent marmoset sample ( $-2.5 \log_2\text{FC}$ , Figure 11), while miR-127-3p is upregulated. Interestingly, in contrast to the upregulation of miR-29a-3p in human lung fibroblasts ( $1.25 \log_2\text{FC}$ ), the homologue of the common marmoset is downregulated ( $-1 \log_2\text{FC}$ ).

### 3.1.4 Senescence-associated miRNA inhibition

To further investigate the impact of senescence-associated miRNA in the context of cellular integrity and cell cycle hallmarks, hsa-miR-29a-3p which is upregulated in senescent cells was chosen for miRNA inhibition. Inhibition was performed on proliferating IMR-90 cells for 48 hours, RNA was isolated and cDNA synthesis and RT-qPCR performed immediately post inhibition and in addition one week later to assess the efficiency of the transfection on miRNA expression level, target gene expression and expression of several senescence-associated mRNAs (*SIRT1*, *MMP3*, *IL6*, *IFNA1*, *LMNB1*; Supplementary Table 8-10).

With this approach, hsa-miR-29a-3p was successfully inhibited in proliferating IMR-90 cells whereas transfection in senescent IMR-90 cells did not yield conclusive results. The following experiments are thus mainly focused on proliferating IMR-90 cells. After 48 hours of RNAiMAX transfection, the miR-29a-3p expression is downregulated in proliferating IMR-90 cells by a factor of  $-4.5$ . After 7 days, the replated transfected cells almost entirely restored the initial miR-29a-3p expression (Figure 12A). One of miR-29a-3p target genes, *COL1A1*, is accordingly upregulated after 48 hours transfection with the miRNA inhibitor ( $0.69 \log_2\text{FC}$ ; Figure 12B). After 7 days, with restored miR-29a-3p expression, *COL1A1* expression is downregulated by  $-1.26 \text{FC}$  in the transfected samples respectively. With the established miR-29a-3p inhibition, non-treated proliferating and transfected cells at 7 days post inhibition were X-Gal treated to assess the activity of senescence-associated  $\beta$ -Galactosidase (Figure 13B & C). The proliferating, non-treated cells are  $\beta$ -Galactosidase negative (Figure 13B), while the transfected IMR-90 cells, 7 days post inhibition, express a distinctive activity of  $\beta$ -Galactosidase (blue staining), as well as an enlarged cell morphology. The investigation of senescence-associated mRNA expression utilizing RT-qPCR of proliferating, senescent and miR-29a-3p inhibited IMR-

90 cells primarily shows an enrichment (3.3 log<sub>2</sub>FC) of *SIRT1* expression in the freshly transfected samples (0 days post inhibition; Figure 13A), with a slight decrease to 2.4 log<sub>2</sub>FC after 7 days post inhibition. The senescent, non-treated control has a decreased *SIRT1* expression (-1.14 log<sub>2</sub>FC) in comparison to the proliferating, non-treated control. Further, *LMNB1* expression is increased by 0.9 log<sub>2</sub>FC in transfected samples 0 days post inhibition and reduced to a remaining overexpression of 0.4 log<sub>2</sub>FC after a week. The *LMNB1* expression of the senescent control is highly downregulated by -4.6 log<sub>2</sub>FC.

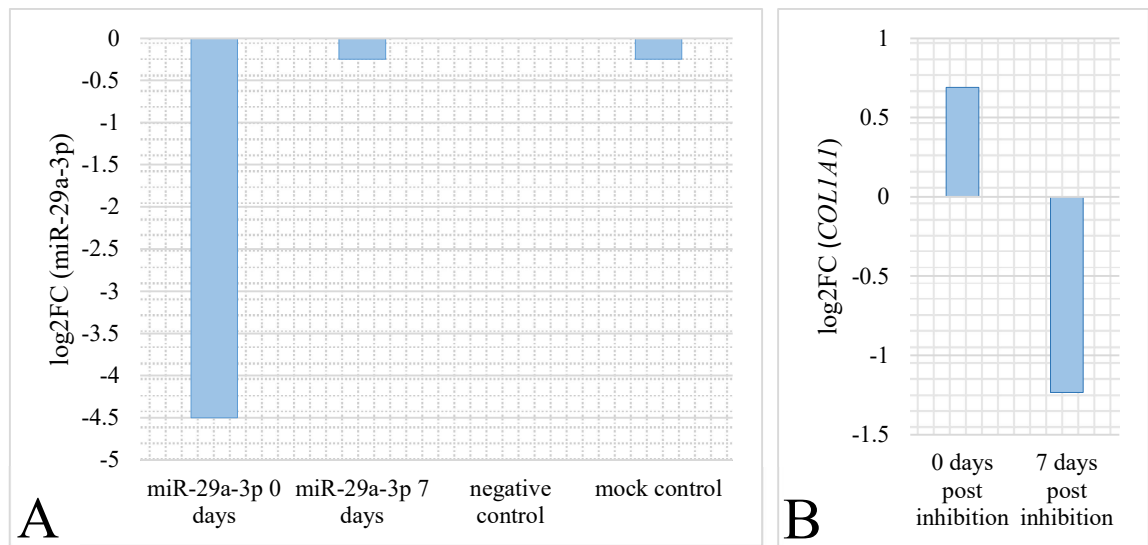


**Figure 12** – expression of *hsa-miR-29a-3p* (A) and its' target gene *COL1A1* (B) in transfected IMR-90 cells immediately after and 7 days post inhibition. X-axis: samples; Y-axis: log<sub>2</sub>FC expression, normalized via proliferating, non-treated samples.

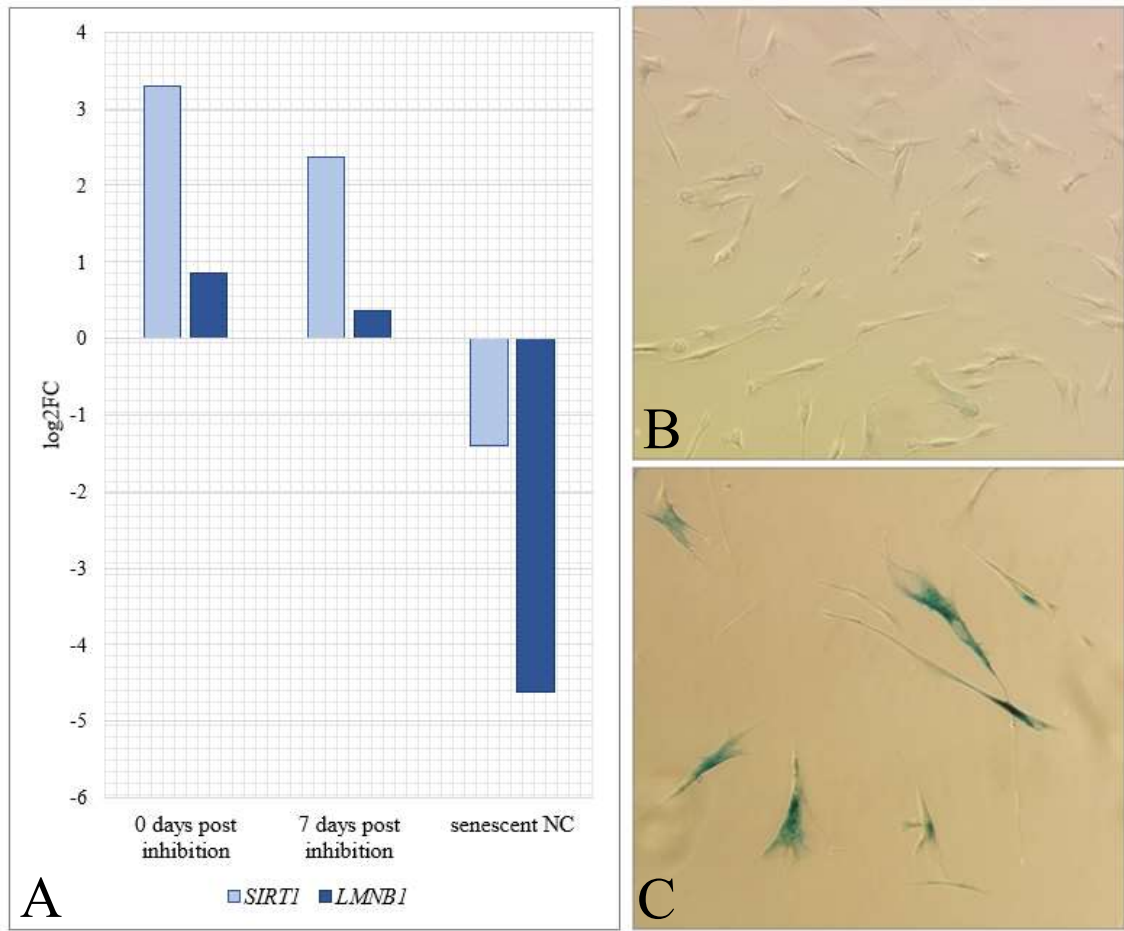


**Figure 13** – (A) mRNA expression of *SIRT1* and *LMNB1* in transfected, proliferating IMR-90 cells immediately after and 7 days post inhibition, such as senescent non-treated IMR-90 cells; X-axis: samples, Y-axis log<sub>2</sub>FC; (B) lightmicroscopic image (100x) of proliferating X-Gal treated IMR-90 cells. (C) lightmicroscopic image (100x) of miR-29a-3p inhibited, X-Gal treated IMR-90 cells 7 days post inhibition.

### 3.1.5 Transcriptomics in senescent and tetraploid IMR-90 cells

Gene expression changes are an inherent component of cellular processes in senescence and early tumorigenesis and help to identify patterns and heterogeneities of both occurrences in many mammalian organisms. To complement the small RNA sequencing analysis which implements a size fractionation of the RNA pool, enriching fragments below 50 nt, transcriptome sequencing was performed. This analysis included mapping of the generated RNA-seq data of proliferating, tetraploid and senescent IMR-90 cells to the human genome (hg38) by applying the standard bowtie2 routine. To pinpoint global differences between the gene expression patterns in senescent and tetraploid transcriptome data, transcript expression was quantified into read count files using Salmon, followed by transformation of transcript-level abundancies to gene-level

estimates utilizing tximport and finally performing differential expression analysis using DESeq2. Overall, 1576 genes were significantly ( $p\text{-value} \leq 0.05$ ) differentially expressed in senescent IMR-90 cells ( $n=2$ ), with 808 genes being downregulated and 768 upregulated (Figure 14A). In the tetraploid transcriptome data ( $n=2$ ), 1763 genes were differentially expressed, with 443 being downregulated and 1320 upregulated (Figure 14B). The top 20 differentially expressed genes for both sample data sets are highlighted in the respective volcano plots (Figure 14). Significantly downregulated genes in senescent IMR-90 transcriptome data include *TNFAIP2*, *MFAP2*, *SRGN*, *ZACN*, *GSTM5*, *NNAT*, *RPL36A*, *AC087632.1* – and *SCOC-AS1*, *ZNF385D*, *CYP1B1*, *GLIDR*, *RAB39B* for the tetraploid data. The upregulated genes of the top 20 markups contain *CTBP1-AS*, *AC126335.2*, *CHL1*, *WSCD1*, *PTPN11*, *FRMD3*, *AC138035.1*, *PKDIP5*, *STARD4-AS1*, *SLC27A6*, *WNT16* and *GOLGA8M* for the senescent data. As for the tetraploid data, more differentially expressed genes hold upregulation features, which is also reflected in the top 20 genes, including *SLC26A1*, *ACKR3*, *PTPN11*, *HLA-L*, *ACER2*, *CBR3-AS1*, *CD160*, *REST*, *ATP7A*, *STAT5B*, *RANBP2*, *GDNF-AS1*, *TRHDE-AS1* and *UHRF1*. To further identify senescence-associated motifs in the transcriptomic data and elucidate similarities and dissimilarities within the cancer precursor model, a gene set (SenMayo) established by Saul et al. (2022) was checked for significantly up- or downregulated genes (Supplementary Table 6 & 7). A total of 88 senescence-associated genes were investigated that showed enrichment in two cohorts of the study. In summary, the senescent data set included 7 significantly differentially expressed SenMayo genes, with four being downregulated (*PTGER2*, *HMBB1*, *CXCL12*, *CXCL1*) and three upregulated (*ANGPT1*, *ANGPTL4*, *FGF2*; Figure 15A). The tetraploid data contained 7 significantly differentially expressed SenMayo genes, with one showing downregulated (*PTGES*) and 6 upregulated (*NRG1*, *INHA*, *ANGPT1*, *SERPINE1*, *FGF2*, *EGFR*) properties, depicted in the respective volcano plot (Figure 15B).

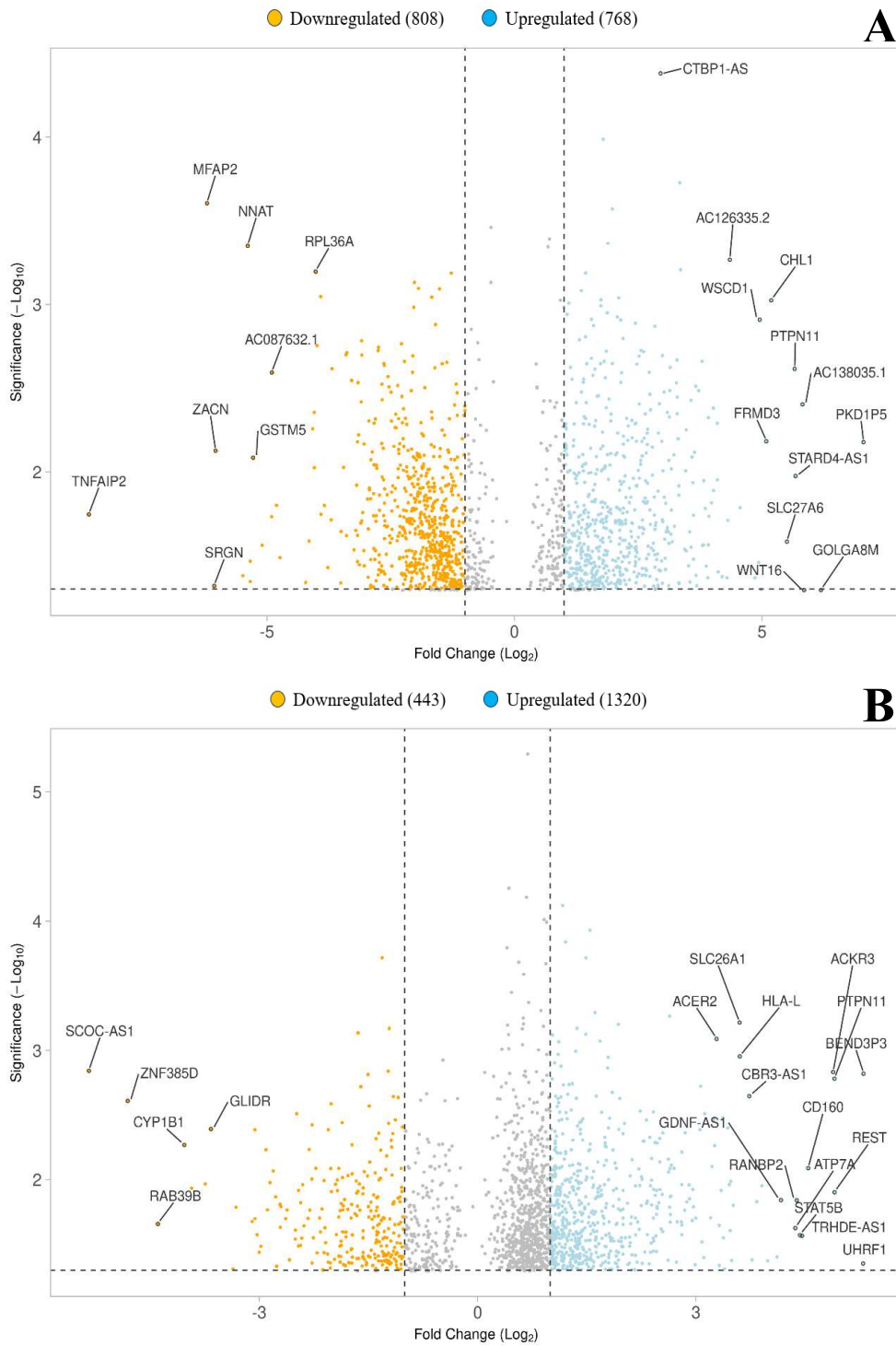


**Figure 14** – Volcano plots of differentially expressed genes in senescent (**A**) and tetraploid (**B**) IMR-90 transcriptomic sequencing data. Top 20 differentially expressed genes marked as hits. Orange: downregulated genes  $\geq -1 \log_2FC$ ; Blue: upregulated genes  $\geq 1 \log_2FC$ ; Grey: genes not meeting criteria ( $\log_2FC < 1$ ); created with VolcaNoseR.

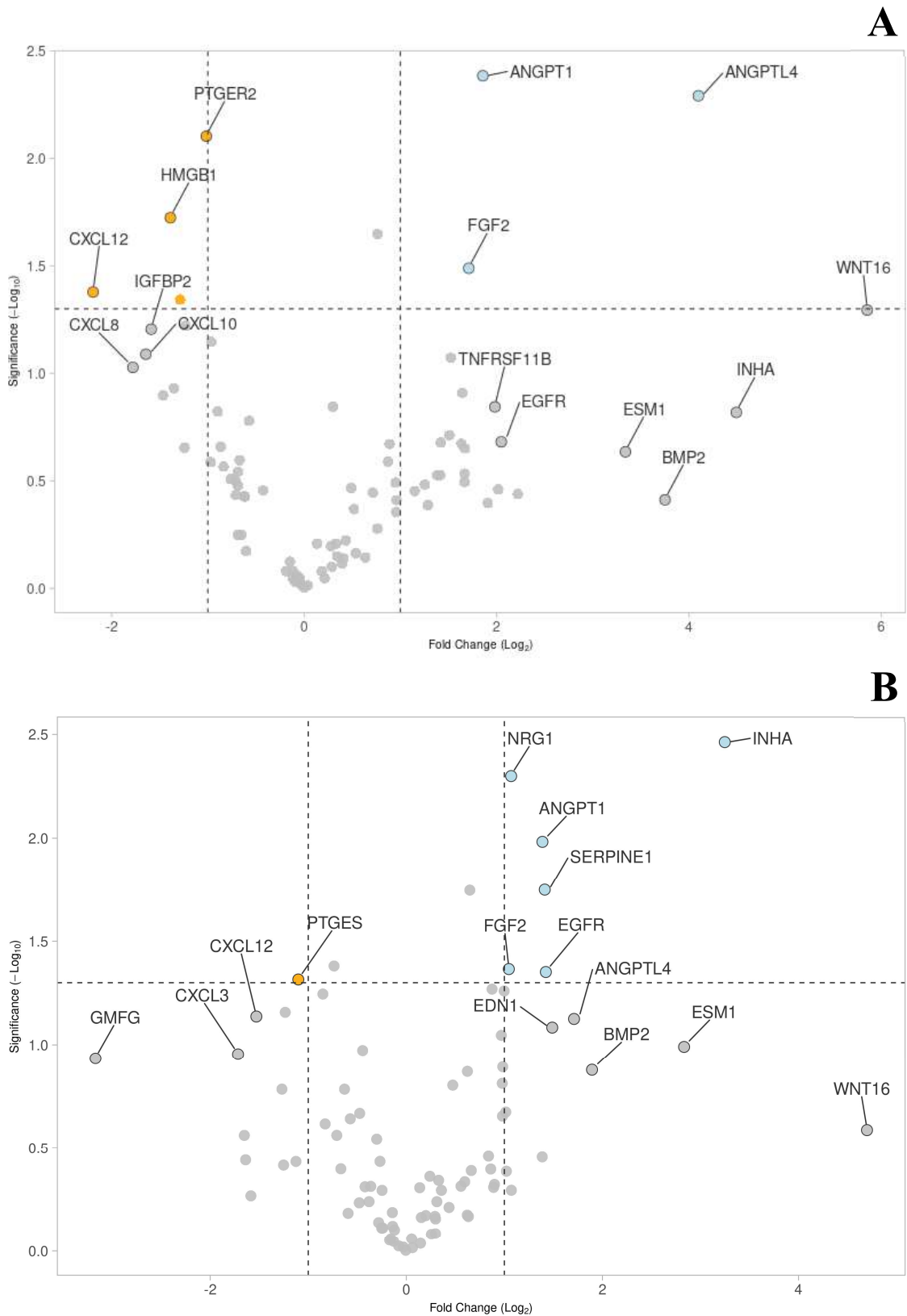


**Figure 15** - Volcano plots of differentially expressed senescence-associated genes (SenMayo set; Saul et al. 2022) in senescent (A) and tetraploid (B) IMR-90 transcriptomic sequencing data. Significant differentially expressed genes marked. Blue: downregulated genes; Orange: upregulated genes; Grey: genes not meeting criteria ( $p \geq 0.05$ ); created with VolcanoR.

## 3.2 Discussion

### 3.2.1 Small RNA sequencing in senescent and tetraploid lung fibroblasts

Several studies have been previously conducted on non-coding RNA to analyze the phenomenon of cellular senescence – with an emphasis on long non-coding RNAs that exceed 200 nt in length and impact gene expression on transcriptional, post-transcriptional and post-translational levels (Yoon et al., 2013; Singh et al., 2013). Their role as important cell proliferation and aging modulators has been broadly investigated in the context of telomere stability (Samper et al., 2001), DNA methylation (Abdelmohsen et al., 2013; Yap et al., 2010) and inhibition of senescence (Tripathi et al., 2013; Kotake et al., 2011). In the field of small non-coding RNA, circRNAs have been subject of extensive research as so-called sponges for miRNAs, serving as “traps” to modulate their bioavailability and thus gene expression. Increased cellular senescence has been linked to circRNA networks such as circ-Foxo3 interacting with anti-senescent acting proteins and transcription factors in cardiac mammalian samples (Du et al., 2017) and circRNA-0077930 upregulating p16, p21 and KRAS in vascular smooth muscle cells (Wang et al., 2020). LncRNA and circRNA are proven to affect the modulation of senescence especially by interaction with miRNA. To further investigate up- and downregulations of miRNAs and other small RNA subclasses including YsRNA and tRFs within the context of cellular senescence and to pinpoint possible properties of tumorigenesis based on the cancer precursor model (tetraploid cells), small RNA sequencing and annotation were performed. The generated small RNA sequencing data (n=2) of diploid proliferating (control), tetraploid proliferating (cancer precursor model) and diploid senescent (cellular senescence model) IMR-90 cells allow a broad perspective on consistency and overall expression changes of small non-coding RNA profiles. Certain small RNA subclasses such as YRNA-derived small RNA fragments (YsRNA) and their source human YRNAs are proposed as biomarkers of tumorigenesis and cell proliferation (Hizir et al., 2017; Tolkach et al., 2017). In this study, they did not show consistent up- or downregulations in the tetraploid and senescent IMR-90 small RNA data, depicting a rather heterogenous output in the replicates (Supplementary Table 2-4, Figure 2-4). Additionally, tRNA derived fragments (tRFs) that are proven to regulate gene expression and suppress carcinogenic and cell proliferation-relevant transcripts of metastatic cells (Goodarzi et al., 2015), show highly heterogenic distribution patterns in the senescent and tetraploid

replicates (Supplementary Table 2-4, Figure 2-4). Thus, the opposing abundances of the two small RNA subclasses do not indicate them as suitable, stable biomarkers for cellular senescence on the level of small RNA transcripts in lung fibroblasts. However, as the most abundant small RNA subclass, miRNAs show a solid consistency in the generated small RNA sequencing data within the replicates (Supplementary Table 2-4, Figure 2-4). Therefore, changes in miRNA abundance patterns in senescent and tetraploid IMR-90 small RNA sequencing data were further analyzed to identify possible novel biomarker properties and check for consistency in comparison to other studies.

#### **3.2.2 miRNAs in the context of cellular senescence and early tumorigenesis**

To identify possible senescence and early tumorigenesis-associated patterns in the up- and downregulation of miRNAs in human lung fibroblasts, differential expression analysis was applied using sRNAde. The senescent small-RNA sequencing data (n=2) consists of 100 differentially expressed miRNAs, with 49 down- and 51 upregulated that show significantly altered expression patterns compared to the proliferating data (Supplementary Table 5). The role of miRNAs as essential modulators of aging hallmarks has been broadly confirmed. They not only regulate expression of cell cycle relevant genes directly – but also act as upstream inhibitors of such key components, making their role in the establishment and upkeep of senescence imperative (Munk et al., 2017). While most biomarkers for acute and chronic senescence are focused on gene expression, protein excretion and metabolic changes as discussed in chapter 1.3 and 1.4, senescence-associated miRNAs gain more and more attention as key players. Therefore, their implementation into the catalogue of solid senescence-biomarkers should remain obligatory. For example, as seen in the top 30 differentially expressed miRNAs in senescent IMR-90 cells (Figure 5), hsa-miR-21-5p is downregulated by  $-1 \log_2FC$  which corroborates the findings of Balint et al. (2021), who identified the accelerated expression of cellular senescence by inhibition of miR-21. The  $>2 \log_2FC$  upregulated hsa-miR-29c-3p is linked to the progression of the p21 and p16 pathway and thus, significantly influences the development of senescence as observed in mesenchymal stem cells by Shang et al. (2016). Hsa-miR-19b-3p is downregulated in the present data ( $-1.72 \log_2FC$ ), complementing several studies that identify the miRNA as an essential contributor to human aging and tumor suppression. Micro-array analysis performed by Hackl et al. (2010) revealed a significantly downregulated miRNA set (miR-17-92 cluster), including



miR-19b in several cultured cells, contributing to the overexpression of *CDKN1A* and thus, allowing the progression of cellular growth arrest. Additionally, miR-19b inhibits the tumor suppressor *TP53* when overexpressed, as well as targeting endogenous downstream transcripts such as *CDKN1A* and *BCL2LA* – both essential for senescence and apoptosis and therefore resulting in accelerated cell proliferation in human cancer cells, promoting metastasis (Fan et al., 2014). The transfection of hsa-miR-339-5p mimics in breast cancer cells provided further insight into the complex *TP53* pathway. The oncogene *MDM2* inhibits *TP53* expression and thus contributes to the upkeep of uncontrolled cell proliferation in several cancers. Jansson et al. (2015) identified the targeted repression of *MDM2* binding sites by miR-339-5p, enabling *TP53*-administered cell cycle responses to malignant cells by senescence induction. The sncRNA data of senescent IMR-90 cells supports the established connection to the induced proliferation arrest due to the herein observed upregulation of hsa-miR-339-5p (1.7 log<sub>2</sub>FC).

While many miRNAs investigated in the context of cellular senescence portray ideal candidates for biomarkers, their many targets and undiscovered modulating functions may hamper solid conclusions. For instance, hsa-miR-424-5p is -1.1 log<sub>2</sub>FC downregulated in the senescent data – which is observed in non-small cell lung cancer and thus associated with tumor progression. Re-expression of miR-424-5p led to proliferation arrest, resulting in the prevention of migration and invasion in non-small lung cancer cells (Zhang et al., 2017). Moreover, miR-424 is defined as a consistent biomarker for carcinoma in salivary samples (Scholtz et al., 2022). In addition, overexpression of hsa-miR-155-5p is connected to increased cellular senescence in young human mesenchymal stem cells and an inhibition assay even regenerated aged mesenchymal stem cells – decreasing the senescence phenotype (Hong et al., 2020). The senescent sncRNA data in my study depicts an ambiguous picture, with downregulation of hsa-miR-155-5p by -2.22 log<sub>2</sub>FC. Lastly, hsa-miR-143-3p is significantly downregulated in senescent IMR-90 cells (-2.94 log<sub>2</sub>FC). Research conducted by Osaki et al. (2011) revealed an observed downregulation of miR-143 in metastatic lung cells, implemented within a mouse model - and by overexpressing the miRNA via transfection the invasion rate was significantly reduced. Taken together, the described miRNAs in this paragraph show a correlation to cancer and metastasis – but are not causally linked to the induction or upkeep of cellular senescence. Rather the opposite is depicted. As the entrance into senescence may cause detrimental effects due to a multitude of metabolic

stressors, reactive oxygen species and DNA damage, the shared molecular expression patterns should not be unexpected as they are proven to display two sides of the same coin. It should be imperative to conduct more research on the shared patterns between the senescent and malignant cell structures. miRNA enrichment ontology revealed several diseases linked to the 51 upregulated miRNAs in senescent IMR-90 sncRNA data. Predominantly, Alzheimer disease and Huntington disease have been assigned as the top enriched categories – both highly associated with the decline of physiological functions due to organismal aging (Figure 6). Strikingly, the senescence-associated upregulated miRNAs show enriched patterns for several cancers, such as lung cancer and multiple organ carcinomas – thus highlighting the functional interplay of senescence and tumorigenesis.

The tetraploid IMR-90 sncRNA data – acting as the early tumorigenesis model - contains 36 differentially expressed miRNAs (Figure 7). Interestingly, only 7 of them depict similar up- or downregulations compared to the senescent data, including miR-145-5p with a  $-3 \log_2FC$  decrease in the senescent IMR-90 cells and a  $-3.9 \log_2FC$  decrease in the tetraploid data (Figure 8). Overall, miR-145-5p shows high downregulation patterns in several cancers, including ovarian (Pan et al., 2022), prostate (Sun et al., 2021) and colorectal cancer (Chen et al., 2020). While the tetraploid sncRNA data reflects these findings, miR-145-5p expression is displaying an ambiguous outcome for the senescent data, thus further research is warranted to embed this miRNA into the process of cellular senescence. A significant upregulation shared in the tetraploid and senescent data is observed for hsa-miR-127-3p. With an upregulation of  $1.1 \log_2FC$  in the senescent and  $2.87 \log_2FC$  in the tetraploid data – miR-127-3p is known to repress cell proliferation and drive senescence by targeting *BCL6* in lung fibroblasts (Chen et al., 2013). As a vital part in tumor suppressor pathways, the upregulation of miR-127 has been causally observed in cell-cycle arrested carcinoma cells (Shin et al., 2013). With the consistency in the senescent data of IMR-90 cells, miR-127-3p proves to be a solid biomarker for the naturally occurring cell proliferation arrest in healthy fibroblasts - accompanying the already established catalog. Simultaneously, directly overexpressing miR-127-3p through miRNA mimic transfections has proven to trigger tumor-suppressor pathways in several cancer cells by inducing cell cycle arrest (Bi et al., 2016; Du et al., 2020), strengthening the correlation between the upregulation of miR-127 and induced cellular senescence. The tetraploid sncRNA data depict an upregulation of the respective miRNA as well. A

decrease in expression levels may be expected in the tetraploid samples to accurately reflect tumorigenesis patterns. However, the correlation between induced tetraploidy and stress responses in cells means that the activation of tumor suppressor pathways by miRNA regulators is highly probable. Nonetheless, as the tetraploid model only offers limited insight into the mechanisms of cancer and usually depicts early onset changes towards tumorigenesis, deviating expression profiles can be expected. It should be noted that the relationship between cause and effect in tetraploid cells regarding tumorigenesis is not yet fully understood. Therefore, miRNA up- and downregulations are not reliable standalone biomarkers for tumorigenesis in tetraploid cell lines and should only be considered in the context of cancer-related pathway expression patterns. This is also reflected in the ambiguous patterns of the let-7 miRNA group in the tetraploid sncRNA data. hsa-let-7d-3p (2.5 log<sub>2</sub>FC), hsa-let-7b-5p (1.6 log<sub>2</sub>FC) and hsa-let-7a-5p (1.5 log<sub>2</sub>FC) are significantly upregulated. Interestingly, numerous studies performed on let-7 in cancer have reported elevated expression levels – such as ovarian cancer (Tang et al., 2013), leukemia (Careccia et al., 2009) and esophageal cancer (Ma et al., 2017). However, the prevailing observation in cancer research is a substantial decrease of let-7 levels in most tumor tissues including melanoma (Schultz et al., 2008), prostate (Kang et al., 2017), liver (Shi et al., 2017), lung (Zhao et al., 2014) and gastric cancer (Tang et al., 2016). When examining the functional properties of significantly upregulated miRNAs in the context of diseases within the tetraploid data, it is noteworthy that the main enriched categories are connected to inflammatory-related diseases such as rheumatoid arthritis, Alzheimer's disease and multiple sclerosis - as well as several malignant cancers including colon, renal, and prostate carcinomas (Figure 9). While the miRNA ontology data must be viewed with caution due to the small number of upregulated miRNAs in the tetraploid data (23 in total, Figure 7) and thus only provides limited evidence, the established research on miRNA and their impact on cell cycle intervention pathways emphasizes the connection between senescence and tetraploidy – which I cautiously interpret as early onset tumorigenesis in this thesis. The shared increase of miRNAs relevant to both cancer progression and inflammation creates an auspicious opportunity to explore the interaction of cell proliferation arrest and – on the other side of the same coin - excessive cell proliferation, and aberrant replication.

### 3.2.3 miRNA in the context of primate cellular senescence

As crucial regulators across species, miRNAs are highly conserved. While numerous studies predominantly focus on the functional aspects, it is apparent that the wider view regarding the use of small non-coding RNA as phylogenetic markers is also pertinent. To further describe cellular senescence in primates, I incorporated lung fibroblasts from an adult common marmoset into the analysis of small non-coding RNAs, with a specific emphasis on miRNAs - the subclass with the most consistent read-out in the replicates of IMR-90 cells. Common marmosets share a common ancestor with humans, dating back to about 35 million years ago. They are a valuable model for studying age-related diseases due to their short lifespan (averaging 5-7 years) and close phylogenetic relation with humans. This allows for drawing conclusions on conceivably conserved physiological processes. I successfully implemented the senescence-associated  $\beta$ -galactosidase assay for the common marmoset lung fibroblasts and was able to obtain sncRNA data for both proliferating and senescent cells (n=1; Supplementary Figure 3). The acquired sequencing data was annotated using Umitas and miRNA expression patterns were analyzed (Figure 10). When comparing the miRNA expression levels of senescent IMR-90 sncRNA data and annotated miRNA levels in senescent common marmoset lung fibroblasts, numerous overlaps can be identified (Figure 11). Particularly, the expression of miR-21-5p - which is stated to be downregulated in the context of cellular senescence, as mentioned above - shows a sharp decrease in the sncRNA data of senescent common marmoset lung fibroblasts ( $-2.5 \log_2FC$ , Figure 10). Interestingly, the let-7 miRNA class is downregulated in the marmoset sncRNA data, as observed in the senescent IMR-90 data (Figure 10). This conforms with the inconsistency which is also highlighted for the upregulated tetraploid let-7 data, as let-7 is identified as a tumor suppressor and is thus frequently upregulated in the senescence of cells (Lee & Dutta, 2007; Wang et al., 2022). However, as both cell lines originate from lung fibroblasts, further research is required to investigate whether there are organ-specific changes that could be causally linked to the observed downregulation. miR-127-3p expression is upregulated in both senescent cell models and the tetraploid sncRNA data – which is in accordance with the abovementioned studies that connect the miRNA pathways interactions with cell proliferation arrest and senescence maintenance. However, a difference in miR-29a-3p expression is apparent between human and marmoset lung fibroblasts. The analysis demonstrates significant upregulation of miR-29a-3p in the human sncRNA data (Figure 5) in contrast to the

detected depletion in the senescent marmoset data as compared to the proliferative state of both (Figure 11). Whether a direct association between miR-29a-3p and the initiation, maintenance and upkeep of cellular senescence can be established in human lung fibroblasts remains to be explored. Research conducted on human miR-29a-3p has focused on neurodegenerative diseases such as Parkinson's and has observed significant downregulation in affected neuronal tissue (Chi et al., 2018).

#### **3.2.4 miR-29a-3p as a biomarker for cellular senescence**

Most studies investigating elevated expression of miR-29a-3p in the context of cell proliferation and senescence utilize aged mice as model organisms. Lyu and colleagues (2018) found a causal link between miR-29 and the promotion of murine senescence through the reduction of H4K20me3. This epigenetic alteration occurred when the TGF- $\beta$  pathway was activated. In a comparative study of young and old mice across multiple organs, miR-29a demonstrated protective properties by reducing cell proliferation in aging tissues that are susceptible to fibrosis – particularly in cardiac tissue (Rusu-Nastase et al., 2021). As numerous target genes of miR-29a transcribe collagen genes, this miRNA has demonstrated its potential as a viable biomarker for healthy aging in tissues across the whole organism. In the context of diseases affecting the lung, miR-29a-3p downregulation was observed in patients diagnosed with acute respiratory distress syndrome (ARDS) and in mice displaying acute lung injury (ALI). However, the respective experiments involving miR-29a-3p mimics and inhibitors were solely carried out on murine lung samples. Cui et al. (2022) demonstrated the anti-inflammatory properties of miR-29a-3p via overexpression through injection in mice with acute lung injury. Altogether, miR-29a-3p has promising characteristics for further analyses in the context of cellular senescence in the human lung fibroblasts model. To evaluate the impact of hsa-miR-29a-3p on cellular integrity and cell cycle processes, the senescence-associated upregulated miRNA was selected for inhibition in proliferating IMR-90 cells. Transfecting miRNA inhibitors via lipofection in senescent cells proved challenging due to the low cell count and apoptotic response to the reagents. Further experimentation is required to examine the consequences of miR-29a-3p downregulation in IMR-90 cells undergoing senescence. The inhibition of hsa-miR-29a-3p in proliferating cells was successful. Expression of miR-29a-3p, the control miRNA let-7a and genes of interest were assessed utilizing RT-qPCR.

The expression of miR-29a-3p is downregulated ( $-4.5 \log_2FC$ ) in comparison to the non-treated control (Figure 12A). However, the treated cells show a near-complete restoration of their initial miR-29a-3p expression after one week, indicating the cells' rapid capacity to retain the conserved miRNA. The miRNA's target gene *COL1A1* exhibits an upregulation in the treated cells and a subsequent downregulation after seven days, mirroring the process of miRNA restoration (Figure 12B). Although the inhibition is rapidly compensated, certain alterations in biomarkers relevant to the cell cycle and senescence are evident. The downregulation of the genes *SIRT1* and *LMNB1* is broadly recognized as a solid biomarker for cellular senescence. The nuclear lamina of cells undergoes continuous changes during mitosis, exhibiting a highly dynamic structure. The instability of *LMNB1* mRNA that codes for one of the structural proteins, Lamin B1, is significantly linked with cellular senescence (Freund et al., 2012). The reduction of *SIRT1* mRNA within senescent cells is hypothesized to be a programmed event to communicate with the immune system, limiting tumor development. *SIRT1* downregulates the expression of various SASP components, including IL-6. The establishment of the SASP plays a crucial role in the immunosurveillance of possibly malignant cells, as documented by Xu and colleagues (2020). The decrease of both biomarkers is reflected in the results of the RT-qPCR for the non-treated senescent IMR-90 samples (Figure 13A). Interestingly, the transfected IMR-90 cells display a strong increase in *SIRT1* mRNA and a slight increase in *LMNB1* mRNA immediately after the miR-29a-3p inhibition experiments (48 hours after induction). After 7 days, the transfected cells exhibit a decrease in the abundance of mRNA for *SIRT1* and *LMNB1*, resulting in an expression that closely mimics the non-treated, proliferating control in culture. While the consistent downregulated expression of *SIRT1* in senescent cells is evident, its epigenetic regulatory patterns in the context of tumorigenesis and cancer display contradictions, as reviewed by Alves-Fernandes & Jasiulionis (2019). Irregular patterns of *LMNB1* expression, specifically overexpression, play a role in the development of tumors. Yang et al. (2022) researched the potential therapeutic target of *LMNB1* in cancer treatment. They found that a higher detection of *LMNB1* transcript correlates with a negative prognosis for effective treatment. Knockdown experiments were conducted, as described by Li et al. (2022), which confirmed that *LMNB1* mRNA inhibition led to the progression of cellular senescence in adenocarcinoma. This finding may enhance the possibility of developing effective therapeutic options for malignant cancers. As previously noted, the depletion of

*LMNB1* in fibroblasts undergoing senescence is a natural occurrence. Depletion and severe mutation of *LMNA* also occurs in patients with Hutchinson-Gilford progeria, a disease strongly linked with early onset of aging phenotypes (Taimen et al., 2009). Interestingly, Dreesen et al. (2013) conducted a study to determine if changes in *LMNB1* expression were related to senescence as a cause or a consequence. Their research revealed that increasing the expression through experimentation impedes proliferation and leads to senescence in the treated dermal fibroblasts. Consistent with these findings, the anti-miR-29a-3p treated, proliferating IMR-90 cells which show an upregulation of *LMNB1* (Figure 13A) have slower population doubling in cell culture and are phenotypically enlarged and flattened. 7 days post inhibition, the transfected cells that underwent phenotypical changes were subjected to the X-gal assay for evaluating senescence initiation. As shown in Figure 13C, the assay results are positive. It is unclear whether the observed senescence-related morphology and metabolic change can be attributed directly to the miR-29a-3p inhibition or is instead an indirect result of the cell regulatory processes that compensate for the downregulation of the miRNA. The same applies to the observed increase in expression of *LMNB1*. *SIRT1* was identified as a target of hsa-miR-29a-3p through TargetScan (Human Release 7.1; Agarwal et al., 2015), alongside a total of 3538 potential transcripts. However, *LMNB1* is not annotated as a potential target. Further research is needed to clarify the correlation between the decrease in miR-29a-3p expression in proliferating IMR-90 cells, the increase in *LMNB1* expression, and the development of senescence-related morphology accompanied by an elevated level of  $\beta$ -galactosidase. Since miR-29a-3p is upregulated in senescent IMR-90 cells as opposed to the proliferating state, it stands to reason that downregulating miR-29a-3p may contribute to the promotion of longevity. Nonetheless, the downregulation of proliferating cells led to the accumulation of potential stress reactions and the emergence of senescence- and early tumorigenesis-associated patterns, as revealed by the limited number of observed biomarkers. While further research and a wider array of biomarkers must be employed, in addition to a comparative analysis of miR-29a-3p inhibition in senescent cells - utilizing an adjusted inhibition protocol that stabilizes the viability of senescent cells when treated with the reagents – first indications point towards the potential of antagonistic pleiotropy for miRNAs – especially miR-29a-3p in this study. With numerous targets, miR-29a-3p plays a crucial role in proliferating IMR-90 cells.

Inhibiting this microRNA to counteract the subsequent buildup in aging cells, however, has proven to have unfavorable consequences.

### **3.2.5 Implications of transcriptomics in senescent and tetraploid cells**

Gene expression changes are associated with cellular processes during senescence and early tumorigenesis, aiding in the recognition of patterns and heterogeneities in numerous mammalian species. Supplementary to the small RNA sequencing analysis, which fractionates the RNA pool to enrich fragments below 50 nt, transcriptome sequencing was executed. This analysis involved mapping the RNA-seq data generated from proliferating, tetraploid, and senescent IMR-90 cells to the human genome (hg38) using the standard bowtie2 method. To identify overall distinctions in gene expression patterns between senescent and tetraploid transcriptome data, transcript expression was measured and recorded in read count files with Salmon. Following this, transcript-level abundances were converted to gene-level estimates using tximport, and ultimately, differential expression analysis was conducted with DESeq2. In comparison, up- and downregulations are evenly distributed throughout the senescent data (Figure 14A). However, according to the obtained tetraploid transcriptome, 75 % of genes show significant upregulation in the differentially expressed transcripts (see Figure 14B). Saul and colleagues (2022) discovered a novel set of genes, known as SenMayo, that effectively detects senescence in various aging tissues. Common senescence markers possess limits in their detectability, given their tissue-specificity and low transcriptome-wide expression levels and thus significance. The SenMayo set excludes these markers, but determining senescence necessitates their inclusion prior to further analyses. Examples of such markers include p21/p16 expression, X-Gal assay, and SASP detection. To identify senescence-associated patterns in the transcriptomic data and elucidate similarities and differences within the cancer precursor model, I analyzed SenMayo genes for significant up- or downregulations (Figure 15). In total, the senescent transcriptome data reveals the upregulation of 51 genes from the SenMayo set, which consists of 88 genes (Supplementary Table 6). Of the 51 upregulated genes, 21 demonstrate a fold change of greater than 1, while only four genes display significant differential expression ( $p$ -value  $< 0.05$ ). Compared to the senescent data, 48 of the SenMayo genes associated with senescence are upregulated in the tetraploid transcriptome data (Supplementary Table 7). Among the overexpressed genes, a total of 16 show a  $\log_2FC$  greater than 1, and



6 are significantly differentially expressed (p-value < 0.05). The usefulness of the SenMayo gene set as a reliable biomarker for senescent IMR-90 cells is uncertain, as only 24 % of the genes showed at least twofold enrichment. However, it should be noted that the expression of senescence-associated markers depends on the length of time a cell spends in the growth arrested state. Thus, cells and tissues in the early stages of senescence may not exhibit expression changes as severe as those in late senescence. The IMR-90 cells used in this study were harvested within a week of entering proliferation arrest, determined by a plateau of PDL increase and subsequent  $\beta$ -galactosidase detection. The process of adapting the cellular structure to late senescence requires changing expression patterns compared to early stages, to regulate the dynamics of the new pathway while preserving cell viability (Alessio et al., 2021). Senescence-associated gene expression changes and their relation to pathways implicated in early tumorigenesis and induced tetraploidy are partially reflected in the SenMayo expressions. However, only 18 % of genes were enriched two-fold or more. Thus, additional research in transcriptomics is necessary to clarify the connection between transcript enrichment and depletion during early tumorigenesis and senescence. This should also incorporate a comparison of single cell transcriptomics.

#### **3.2.6 Conclusions of small RNA and transcriptomic analysis in the context of cellular senescence**

The sncRNA and transcriptomic analyses presented in this thesis offer insights that could enhance future investigations into cellular senescence and its link to early tumorigenesis. MiRNA provide stable biomarkers for aging in cellular senescent IMR-90 cells. Several miRNAs have been found to be up- or downregulated, reflecting previous research. However, the various targets and unknown modulating functions of these miRNAs may hinder sound conclusions, as their diverse expression patterns sometimes yield deviating outcomes compared to the described observations in numerous studies as seen in my analysis. Overall, senescent and tetraploid IMR-90 cells show shared, increased miRNA expression patterns relevant to cancer progression and inflammation as depicted in miRNA ontology analysis, offering a promising occasion to further examine the interplay between cell proliferation arrest and, conversely, excessive cell proliferation and aberrant replication. Most studies on miR-29a-3p in the context of senescence are primarily focused on murine systems. Several target genes of miR-29a encode collagen proteins,

which demonstrates the potential of this miRNA as a viable biomarker for healthy aging in tissues throughout the organism. With the obtained information from previous studies, miR-29a-3p shows promising characteristics for further examination as a solid senescence marker in human fibroblasts and should thus be used more intensively in human research. Given that miR-29a-3p is upregulated in senescent IMR-90 cells rather than the proliferating state, reducing miR-29a-3p levels could potentially enhance longevity. Nonetheless, the miR-29a-3p inhibition in proliferating cells resulted in the potential accumulation of stress reactions and the emergence of patterns associated with senescence and early tumorigenesis, as indicated by the limited number of observed biomarkers. Inhibiting this microRNA to prevent the accumulation of aging cells has produced unfavorable results, suggesting a link to the antagonistic pleiotropy model. For further investigation of other non-coding RNAs like lncRNA, it should be noted that the used NGS methodology – small non-coding RNA and transcriptomic NGS - is insufficient to offer a complete representation of lncRNAs in the results. Nonetheless, lincipedia's gtf-files make annotation tools accessible for conducting comparative quantitative analyses in terms of differential expression. Fully developed identification and categorization of lncRNAs based on biological mechanism and function is yet to be achieved. Only a limited number of long non-coding RNAs have been functionally annotated, especially in cancer research. The varying reliability of these annotations poses a challenge to conducting a study with sufficient statistical power, as cautioned by Klapproth et al. (2021). However, there is confidence that the understanding of lncRNA profiles and their contribution to the processes of senescence and aging will improve soon. It should be noted that the duration of cell growth arrest has a potential effect on senescence-related marker expression during subsequent investigations of senescent IMR-90 cells, as evidenced by my thesis's transcriptomic data. As a result, changes in expression detectable in cells and tissues in the early stages of senescence may not be as evident as those seen in later stages. The IMR-90 cells used in this study were acquired roughly within a week after reaching the proliferation arrest stage, as evidenced by a plateau in PDL increase and subsequent detection of  $\beta$ -galactosidase. Altering the cellular structure for late senescence entails adjusting expression patterns that differ from those observed in early stages. Including various time frames of senescence ought to be essential for future studies of senescence biomarkers in small non-coding and transcriptomic profiles in human model systems.

## **4 Generation of somatic de novo structural variation as a hallmark of cellular senescence in human lung fibroblasts**

*This chapter has been submitted to Frontiers in Cell and Developmental Biology, Epigenomics, and Epigenetics and is currently undergoing peer review. It has been included in this dissertation as the first draft. Any citations used within the chapter have been incorporated into the references section of this thesis, and the formatting of the presented figures and tables has been adjusted to be included as a sub-chapter.*

**Valentina Woronzow<sup>1\*</sup>, Jonas Möhner<sup>1</sup>, Daniel Remane<sup>1,2</sup>, Hans Zischler<sup>1\*</sup>**

<sup>1</sup>Division of Anthropology, Institute of Organismic and Molecular Evolution, Faculty of Biology, Johannes Gutenberg University Mainz, Mainz, Germany

<sup>2</sup>HOX Life Science GmbH, Frankfurt, Hessen, Germany

**\* Correspondence:**

Hans Zischler, Valentina Woronzow

zischler@uni-mainz.de, vaworonz@uni-mainz.de

**Keywords: cellular senescence, SVA, retrotransposition, somatic mosaicism, RDA, numts, mtDNA (Min.5-Max. 8)**

### **4.1 Abstract**

Cellular senescence is characterized by replication arrest in response to stress stimuli. Senescent cells accumulate in aging tissues and can trigger organ-specific and possibly systemic dysfunction. Although senescent cell populations are heterogeneous, a key feature is that they exhibit epigenetic changes. Epigenetic changes such as loss of repressive constitutive heterochromatin could lead to subsequent LINE-1 derepression, a phenomenon often described in the context of senescence or somatic evolution. LINE-1 elements encode the retroposition machinery and reverse transcription generates cDNA from autonomous and nonautonomous TEs that can potentially reintegrate into genomes and cause structural variants. Another feature of cellular senescence is mitochondrial dysfunction caused by mitochondrial damage. In combination with impaired mitophagy, which is characteristic of senescent cells, this could lead to cytosolic mtDNA accumulation and, as a genomic consequence, integrations of mtDNA into nuclear DNA

(nDNA), resulting in mitochondrial pseudogenes called *numts*. Thus, both phenomena could cause structural variants in aging genomes that go beyond epigenetic changes. We therefore compared proliferating and senescent IMR-90 cells in terms of somatic *de novo numts* and integrations of a non-autonomous composite retrotransposons - the so-called SVA elements - that hijack the retropositional machinery of LINE-1. We applied a subtractive and kinetic enrichment technique using proliferating cell DNA as a driver and senescent genomes as a tester for the detection of nuclear flanks of *de novo* SVA integrations. Coupled with deep sequencing we thus obtained a genomic readout for SVA retrotransposition occurring during cellular senescence in the IMR-90 model. A total of 1695 *de novo* integrations were detected in senescent IMR-90 cells, of which 333 were unique. Furthermore, by comparing the genomes of proliferative and senescent IMR-90 cells by deep sequencing or after enrichment of nuclear DNA using AluScan technology, we identified a total of 81 *de novo numts* with perfect identity to both mtDNA and nuclear hg38 flanks. In summary, we present evidence for age-dependent structural genomic changes by paralogization that go beyond epigenetic modifications. We hypothesize, that the structural variants we observe potentially impact processes associated with replicative aging of IMR-90 cells.

## 4.2 Introduction

Cellular senescence has received increasing attention as a fundamental factor in chronic disease and functional decline in older age. Senescent cells enter a permanent growth arrest after surpassing a limited number of cell divisions while remaining metabolically active (Hayflick & Moorhead, 1961). They are characterized by a whole range of different features, including disturbances in mitochondrial dynamics - changes in mitochondrial morphology due to fission and fusion processes, and both epigenetic and genetic alterations, e.g. phenomena linked to telomere attrition. While some characteristics are considered beneficial – such as remodeling features and tumor suppression – senescent cells accumulate in aging tissue and take part in inflammation responses and tumorigenesis, actively losing their regenerative capacities (Li et al., 2020; Farfariello et al., 2022). Epigenetic changes such as the loss of repressive constitutive heterochromatin and subsequent LINE-1 derepression (Simon et al. 2019), as well as faulty mitochondrial quality control mechanisms have the potential to give rise to somatic structural genomic variants in senescent cells. The former phenomenon triggering mobilization and possibly

insertional mutagenesis of both autonomous LINEs and non-autonomous SINEs. In addition, escape of mtDNA from mitochondria is usually associated with mitochondrial damage and mitophagy, which is impaired in senescent cells *in vitro* and *in vivo* (Dalle Pezze et al., 2014; García-Prat et al., 2016), possibly leading to cytosolic mtDNA accumulation and as a genomic consequence to integrations of mtDNA into nuclear DNA (nDNA), resulting in mitochondrial pseudogenes called *numts*. Thus, both sorts of DNA mobilization connect to age-associated hallmarks as summarized by López-Otín et al. (2023) and potentially cause structural variants. The upregulation of TE-expression – mainly autonomous LINE-1 – in senescent cells has been described (De Cecco et al. 2019) and repeatedly confirmed. Moreover, several reporter-based approaches to detect somatic integrations of non-autonomous retrotransposons (e.g., SVA, Hancks et al. 2011), together with qPCR approaches to distinguish copy number variations in young and aged cells of Alu-SINEs suggest that somatic TE integrations tissue-specifically increase as cells age (Morgan et al., 2017). A genome-wide qualitative and quantitative analysis of the genomic consequences of TE-derepression and mobilization, i.e., the landscape of somatic *de novo* integrations during senescence of a cellular model system to study *in vitro* cell aging such as human IMR-90 cells (Sherwood et al., 1988) is still pending. We therefore compared proliferating and senescent IMR-90 cells, the latter phenotypically defined by the senescence associated secretory phenotype (SASP), with respect to somatic *de novo numts* and integrations of a non-autonomous retrotransposon – the so called SVA-elements - that hijack the retropositional machinery of LINE-1. The SINE-VNTR-Alu retroposons are the "youngest" class of hominoid-specific TEs, preferentially found in gene- and GC-rich regions and possibly co-regulating nearby genes. Since they exhibit high mobility in the human germline, we investigated whether this is also reflected in somatic cells and during the processes of senescence due to replicative exhaustion. Due to the rarity of these *de novo* structural variations caused by retropositions, we used a representational difference analysis approach (RDA, Lisitsyn et al., 1993). This subtractive and kinetic enrichment technique, that is able to detect small differences between complex genomes, was coupled with deep sequencing. More precisely, we PCR-amplify the upstream flank of the 5' SVA region using SVA outward primers in combination with flank-adaptors and thus generate a representation of SVA flanks in proliferating and senescent IMR-90 cells. The sample of proliferating cells was used in a 100-fold excess as driver, denatured and hybridized to the tester senescent DNA that was

linked to an RDA-adaptor and subsequently used as PCR template. The resulting products were deep sequenced and bioinformatically checked with a customized pipeline, as outlined in our previous work (Möhner et al. 2023). Our ultimate goal was to get both qualitative - such as target site characteristics - and semi-quantitative information on the senescence associated SVA retropositions, the latter mainly because these integrations are regarded as rare genomic changes (Rokas & Holland 2000) without exhibiting reversals and parallelisms in different cell lineages. To further extend our investigation of mobile DNA such as SVAs, we implemented a comparative method to detect possible interorganelar transfer of DNA between mitochondria – characterized by senescence-related mitochondrial dysfunction associated with impaired mitophagy (Korolchuk et al., 2017) – and the nucleus. Total DNA of proliferating and senescent IMR-90 cells were whole genome sequenced and in addition, we followed a strategy of specifically enriching nuclear sequences applying an AluScan PCR with primers anchored in Alu-SINEs as described by Mei et al. (2011). The resulting Inter-Alu representations of both proliferating and senescent nuclear genomes were then NGS-sequenced. Results of both experimental approaches were bioinformatically scanned for sequences that perfectly matched both mtDNA - with the fast evolving D-loop sequences specifically acquired from our IMR-90 sequencing data - and flanking nuclear DNA in a continuous 150 bp read of the WGS and the AluScan NGS data. The obtained sequences, containing both mtDNA and nDNA, were then filtered to exclude hg38- annotated *numts* (UCSC) and checked for possible target site patterns and functional properties.

## 4.3 Material and Methods

### 4.3.1 Sample preparation: cell culture and SA- $\beta$ -Gal activity

Human fetal lung fibroblasts (IMR-90) were cultivated in Dulbecco's modified Eagle's medium (DMEM, Gibco™ Thermo Fisher Scientific, 11965092), supplemented with 10 % fetal bovine serum (FBS, Gibco™ Thermo Fisher Scientific, A5256701). Proliferating IMR-90 cells were used as controls and cultured until replicative exhaustion is reached to obtain senescent IMR-90 cells. Cell growth was assessed by calculating population doubling level of each cell passage. Senescence-associated  $\beta$ -galactosidase activity was estimated using an adapted staining protocol. Proliferating and senescent

#### 4 Generation of somatic de novo structural variation as a hallmark of cellular senescence in human lung fibroblasts

cells were harvested using 1X PBS washing solution and 0,05 % trypsin-EDTA (Gibco™ Thermo Fisher Scientific, 25300104).

##### 4.3.2 DNA isolation

Cells were harvested ( $5 \times 10^6$  per sample), resuspended in 1X PBS and treated with RNase A (20 mg/mL) for 20 minutes at 37 °C. Enzyme inactivation was performed with Proteinase K (40 mg/mL). DNA isolation steps were completed according to the QIAamp® DNA Mini Kit (Qiagen, 51304).

##### 4.3.3 RNA isolation

Harvested cells ( $1-5 \times 10^6$  per sample) were resuspended in ZymoResearch® RNA Lysis Buffer and treated according to manufacturer's protocol (Quick-RNA Miniprep Kit, ZymoResearch®, R1055). By adding 2:1 EtOH (>99 %) to the lysate sample at the column binding step, smaller RNA fragments were enriched.

##### 4.3.4 RNA-Sequencing

2 µg total RNA of proliferating and senescent IMR-90 cells were 150 paired-end mRNA sequenced, resulting in raw data as FASTQ files provided by Novogene Co., Ltd. using the Illumina NovaSeq 6000 platform.

##### 4.3.5 Differential Expression Analysis

The provided transcriptomic data of proliferating and senescent IMR-90 cells was further analysed by quantifying transcript expression into read count files using Salmon (Patro et al., 2017), transforming the generated transcript-level abundancies to gene-level estimates utilizing tximport (Soneson et al., 2015) and finally performing differential expression analysis using DESeq2 (Love et al., 2014). Fold changes and p-values were checked for genes of interest, including mitochondrial clearance, integrity and mitophagy genes and genes in close relation to open chromatin and cell proliferation.

##### 4.3.6 Local BLAST+ of transcriptomic data

FASTQ files of proliferating and senescent IMR-90 cell transcriptomes were mapped to the human genome (hg38) using Bowtie2 (Langmead & Salzberg, 2012). SAM files

generated in this way were transformed to sorted BAM files and finally to FASTA files containing only mapped reads using samtools (Danecek et al., 2021). Next, we ran local BLAST analyses of the transcriptome data with SVA query sequences to evaluate retrotransposon RNA abundance. To this end, we obtained SVA subfamily consensus sequences (SVA\_A to SVA\_F) from the DFAM database (<https://dfam.org>, Storer et al., 2021). The SVA subfamily sequences were aligned and checked for subfamily-specific informative regions. To minimize redundant hits due to the composite and tandem repetitive character of the SVA sequence, a 200 nt-query from the 5' region of the SVAs was chosen as query sequence. Blastn-settings included `-perc_identity 100` to retrieve exclusively 100 % identical hits. Hits were corrected for the overall alignment rate in the respective datasets as determined by Bowtie2.

#### **4.3.7 Representational difference analysis (RDA) of SVAs**

Representational difference analysis including laboratory steps such as PCR, hybridization and RDA amplifications and bioinformatical steps were performed as previously described (Möhner et al., 2023). 100 ng DNA obtained from proliferating (used as driver) and senescent (used as tester) IMR-90 cells were applied, respectively. 150 paired-end NGS data (FASTQ files) of the final PCR products including possible *de novo* insertions of SVAs in senescent IMR-90 cells (n=3) were generated on the Illumina NovaSeq 6000 platform by Novogene Co., Ltd.

#### **4.3.8 Genomic target sites and Gene Ontology analysis of SVA integrations**

Genomic target site coordinates of *de novo* SVA insertions were extracted as BED files applying a customized bioinformatical pipeline as previously described (Möhner et al., 2023). We used the HOMER software to detect specific target site features (AnnotatePeaks.pl) and gene ontology analysis was performed by extracting gene IDs from annotated peak files and scanning them for biological processes using EnrichR (Chen et al., 2013; Kuleshov et al., 2016, Xie et al., 2021), comparing identified functions ( $p \leq 0.05$ ).

#### **4.3.9 Human Whole Genome Sequencing (hWGS)**

1.5 µg total DNA was isolated from proliferating and senescent IMR-90 cells as previously described (2.2) and library preparation and sequencing was performed with a



3X coverage by Novogene Co., Ltd. on the Illumina NovaSeq 6000 platform and PE150 strategy obtaining raw reads as FASTQ files.

#### 4.3.10 AluScan-PCR and Next Generation Sequencing

To reduce the background of multicopy mtDNA, we additionally applied an “Alu-anchored scan” or “AluScan” to enrich for nuclear DNA sequences between Alu-sequences. This PCR method was described by Mei et al. (2011) and uses primers that bind to specific Alu-elements, the most abundant, Short Interspersed Nuclear Elements (SINEs) in the human nuclear genome exceeding a million of copies. We used the AluY278T18-, AluY66H21- and R12A267-primers according to the protocol outlined in Mei et al. (2011) and performed a PCR starting from 100 ng input DNA of both proliferating and senescent cells with 35 cycles using the Qiagen PCR Taq Core Kit (201223, Qiagen). The resulting heterogeneous PCR products were then purified using the QIAquick PCR Purification Kit (28104, Qiagen) and deep sequenced (150 PE) by Novogene Co., Ltd on the Illumina NovaSeq 6000 resulting in FASTQ files that were subsequently bioinformatically processed as outlined below.

#### 4.3.11 Bioinformatical scanning of *de novo numts*

To investigate possible *de novo* insertions of mtDNA into the nuclear DNA, a customized BASH script was established to detect *numt*-flanking regions in senescent and proliferating IMR-90 cells. For all extracted FASTA files from the hWGS and AluScan-Seq data a BLAT search with the complete IMR-90 mtDNA and the fast-evolving D-Loop, which was assembled from our WGS data, was performed (Kent, 2002). By utilizing the UCSC-PslScore script, output files with 100 % identical mtDNA hits of all data sets were filtered with respect to the alignment coverage. Each alignment exceeding 130 nt in length was discarded to finally get informative genomic flanking sites of a minimum size of 20 nt. Mitochondrial alignment fractions were then subtracted from the whole sequence reads and the remaining sequence read of  $\geq 20$  nt in length was mapped to the human genome hg38 using BLAT to search for possible integration sites. By using the UCSC-cDNAMFilter we then extracted alignments with a minimum query length of 95 %, uniquely mapped reads, gapless alignments and further deleted any hits that contained remaining mitochondrial segments in the flanking sequences. The BED files of proliferating IMR-90 data sets generated in this way – containing filtered genomic

positions of possible *de novo numt* target sites – are then subtracted from the senescent IMR-90 data sets utilizing BEDtools intersect (Quinlan et al., 2010). By that, we managed to obtain target sites specific to senescent IMR-90 cells. Those BED files were then further processed by subtracting known genomic coordinates of *numts* (hg19 liftover to hg38) and further checking every read associated with a possible *de novo numt* by performing a NCBI BLAST search throughout all known genomic databases for taxid 9606 (human), thus excluding already annotated *numts*.

#### **4.3.12 Genomic target sites and Gene Ontology analysis of *de novo numts***

We further analysed *de novo numts* of senescent IMR-90 cells by checking which mitochondrial genes were recruited for the integration and further, which genomic target sites were affected by the integration process. We first applied a BLAST alignment for all mapped mtDNA segments in our final *de novo numts* FASTA files and annotated their mitogenomic features. For the flanking regions – excluding mtDNA related fractions – we utilized HOMER to annotate the coordinates of the integrations on hg38 (AnnotatePeak.pl). Annotated gene names from the HOMER output were then extracted and checked for Gene Ontology of biological processes using EnrichR.

## 4.4 Results

### 4.4.1 RNA abundance of SVAs and genes critically influencing chromatin remodeling in proliferative and senescent IMR-90 cells

To obtain RNA sequencing data for both proliferative and senescent IMR-90 cells, a 150PE strategy was applied. First, we determined the overall alignment rate of our transcriptome data using Bowtie2. Second, we examined the expression of SVA and thus the availability of SVA messages for the onset of SVA mobilization in IMR-90 cells. To this end, we investigated the expression of SVA\_A - SVA\_F in our transcriptome data from proliferating and senescent IMR-90 cells using the consensus sequences of the SVA subfamilies as queries. More precisely, the 5' sequences of the six SVA subtypes A-F were truncated to a length of 200 nt, and we used NCBI BLAST+ (blastn) to align them to the hg38-mapped IMR-90 transcriptome. While the first 200 nt of SVA\_A was almost absent in our data (senescent: 0.16 RPM; proliferating: 0.013 RPM), we detected an overall increase in SVA expression with log<sub>2</sub> fold changes ranging from 1.08 in SVA\_B to 1.63 in SVA\_D for the senescent datasets (Figure I). Interestingly, the most normalized read counts were found for SVA\_C (4.3 RPM with an FC of 1.26), SVA\_E (3.3 RPM with an FC of 1.2), and SVA\_D (8 RPM with an FC: 1.63). Beside the mobilization of TEs, a successful reintegration is controlled and regulated by a variety of different factors, among them the methylation of CpGs. Both the dynamics of chromatin and changes of transcriptional networks are central with respect to aging associated changes (De Cecco et al. 2013). To get an idea of the age-associated dynamics related to chromatin remodeling, we examined the presumably epigenetically controlled transcript abundance of genes involved in chromatin remodeling and cell proliferation in the transcriptome data of proliferative and senescent IMR-90. By performing differential expression analysis, we observed a decrease in *DNMT1* transcripts in the senescent IMR-90 data (FC: -1.16), followed by *CDCA7* (FC: -2.75), *LMNB1* (FC: -3), and *HMGB2* (FC: -2.15), indicating marked age-associated dynamics of chromatin remodeling (Figure II). We hypothesize that downregulation of key components that trigger chromatin remodeling dynamics associated with replicative exhaustion of IMR-90 cells increases chromatin accessibility. The differential and age-dependent expression of the abovementioned genes provides a

#### 4 Generation of somatic de novo structural variation as a hallmark of cellular senescence in human lung fibroblasts

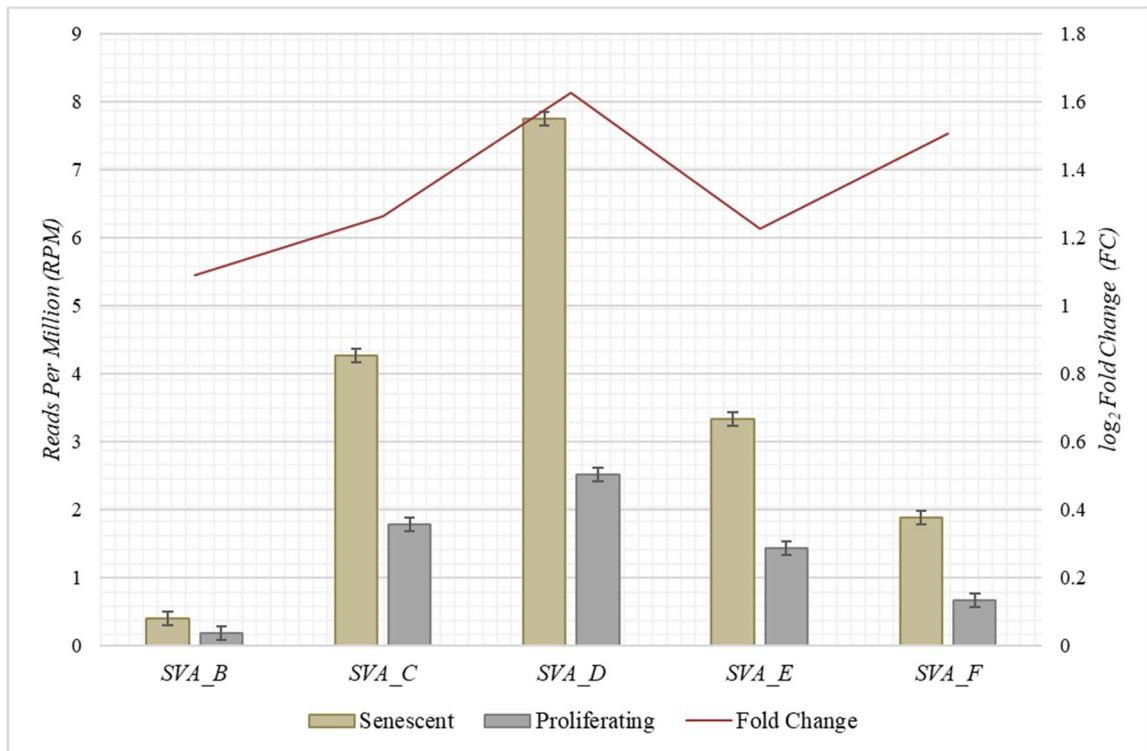


**Figure I** - RNA abundance of SVA\_B – SVA\_F in senescent and proliferating IMR-90 cells, determined by NCBI BLAST+ (blastn) alignment of 5' SVA sequences (200 nt) to Bowtie2 mapped transcriptomic data. Normalized aligned reads ( $n = 2$ ) depicted as Reads Per Million (RPM; left y-axis) with standard error shown as bars and  $\log_2$  Fold Change (FC; right y-axis).

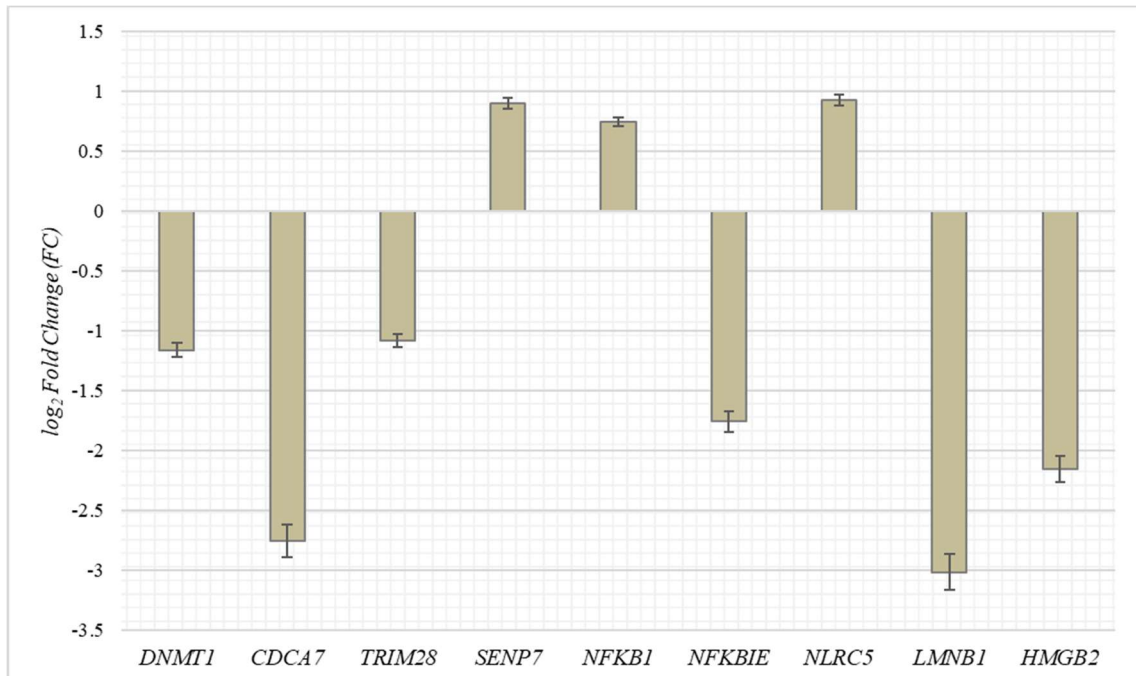


**Figure II** - Expression of genes associated with cell proliferation and chromatin remodeling (GO) in senescent IMR-90 cells ( $n = 2$ ).  $\log_2$  Fold Changes (y-axis) depicted for nine GOI with standard error displayed as bars (x-axis).

functional basis for the systematic effect of poisoning reintegration targets for SVAs after hijacking the LINE-1 machinery.

#### 4.4.2 Active *de novo* SVA retrotransposition in cellular senescent IMR-90 cells

Somatic *de novo* integrations of non-autonomous SVAs in senescent IMR-90 cells were investigated using the RDA enrichment technique (Lisitsyn et al., 1993), with tailored modifications and additional deep sequencing techniques (Möhner et al., 2023). Three batches of replicative senescent IMR-90 cells (Sen\_1-3) were treated accordingly as tester samples to identify novel integrations occurring during the process of senescence. Proliferating IMR-90 cell DNA served as driver samples that represent 5'-flanks of both evolutionary fixated SVA integrations and polymorphic ones. Only the tester samples are covalently ligated to specific RDA primers, which ensured an exponential enrichment of SVA flanks that are absent in the driver sample. The resulting PCR-enriched and deep sequenced SVA flanks were analysed using a customized bioinformatical pipeline. To scan for novel integration properties, previously annotated SVAs (hg38) were filtered out from the data sets and the remaining flanking sequences were mapped to the human genome (hg38) using BLAT v.36 (Kent, 2002), to determine specific coordinates for novel SVA insertion events and their genomic target sites. Overall, we detected a total of 1223 SVA insertions in the first sample (Sen\_1), of which 159 hg38 flanking coordinates were unique. The second sample (Sen\_2) contained 44 total and 30 unique SVA flanks and 428 total and 144 unique were discovered in the third sample (Sen\_3), respectively. We then checked for shared positions of *de novo* integrations and found five SVA target site coordinates which showed an overlap between all three samples (Figure IIIA & IIIB). Global chromosomal distribution was analysed using the positional BED files containing all SVA flanks in the three data sets. Total read counts of *de novo* SVA flanks were logarithmically corrected and possible differences and similarities have been featured between the three samples. As for Sen\_1, most flanking regions were detected on chromosome 8 (271 flanks), followed by chromosome X (235 flanks) and chromosome 21 (135 flanks). Sen\_3 shares the most *de novo* integration flank-counts with Sen\_1 on chromosome 8, with a total abundance of 210 flanking sequences. In addition, for the third sample, 33 flanks are found on chromosome 2 and 31 flanks on chromosome 11. Sen\_1 and Sen\_3 exhibit multiple target site locations scattered across the entire genome, resulting in a highly diverse landscape of SVA integrations (Figure IIIC). These findings suggest ample evidence for active SVA retrotransposition in the context of cellular senescence and highlight that the herein presented senescence-associated abundance of chromosomal targets deviates from known SVA integration patterns. Overall genomic

4 Generation of somatic de novo structural variation as a hallmark of cellular senescence in human lung fibroblasts

SVA density in humans is more prominent on chromosomes 1, 17, 19 and 22 (Wang et al., 2005), whereas our results on somatic and age-associated SVA retropositions suggest integration preferences on chromosomes 2, 8, 12, 21 and X in senescent IMR-90 cells.

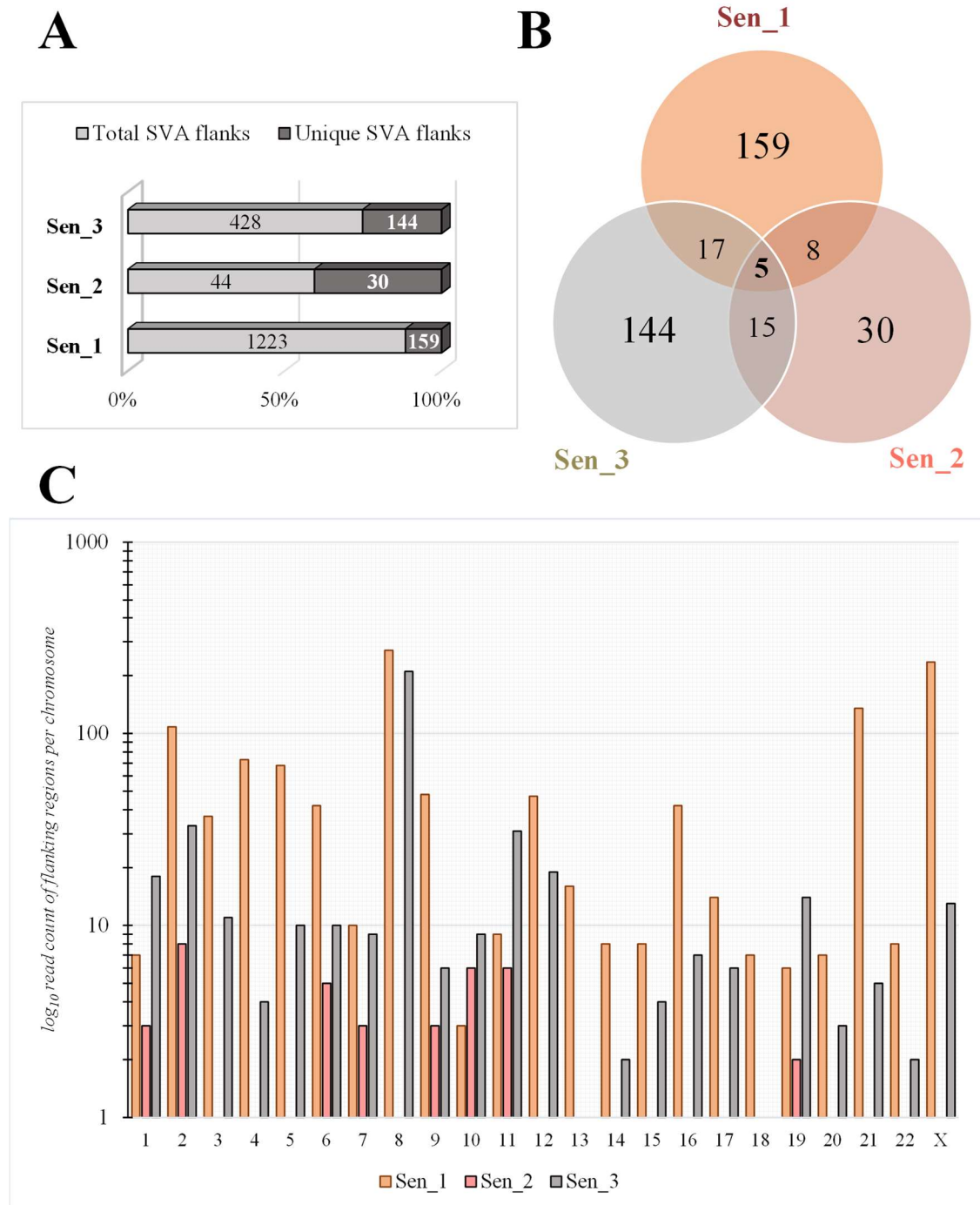


**Figure III** - Quantity and chromosomal distribution of somatic de novo integrations of non-autonomous SVAs in senescent IMR-90 cells ( $n = 3$ ). **(A)** Total and unique SVA integration flanks in the three samples (Sen\_1 – Sen\_3) displayed in % and shown as bars. **(B)** Venn diagram of the unique, shared SVA integrations between all three RDA samples (Sen\_1 – Sen\_3). **(C)** Distribution of chromosomal SVA flanking regions (Sen\_1 – Sen\_3) displayed as  $\log_{10}$  of total read counts ( $y$ -axis) per chromosome ( $x$ -axis).

#### 4.4.3 Genomic target sites of *de novo* SVA integrations

Following the chromosomal distribution analysis, target site coordinates of the three samples were annotated using HOMER software, thereby elucidating preferred locations with respect to genomic features and preferred locations of senescence-associated integrations. Interestingly, retrotransposons such as LINES, SINEs and LTRs appear to be favored targets for *de novo* SVA insertions in all three senescent data sets. Sen\_1 exhibits most annotated integration targets in LTRs (32.7 %, Figure 4), followed by LINE-1 with 30.2 % and SINEs in form of Alu elements (14.5 %). With 53.3 %, Sen\_2 displays most integration targets in LTR regions, followed by Alu SINEs (26.7 %) and promoter regions (6.7 %). The third replicate reveals most target sites in Alu-SINEs (43.8 %), LINE-1 (17.4 %) and LTRs (17.4 %). In summary, *de novo* SVA insertions in senescent IMR-90 cells take place in regions already affected by previous retrotranspositions, next to a less pronounced fraction located in intronic (2.5 % [Sen\_1], 3.3 % [Sen\_2], 4.9 % [Sen\_3]) and intergenic (6.9 % [Sen\_1] and 5.6 % [Sen\_3]) regions (Figure IV).

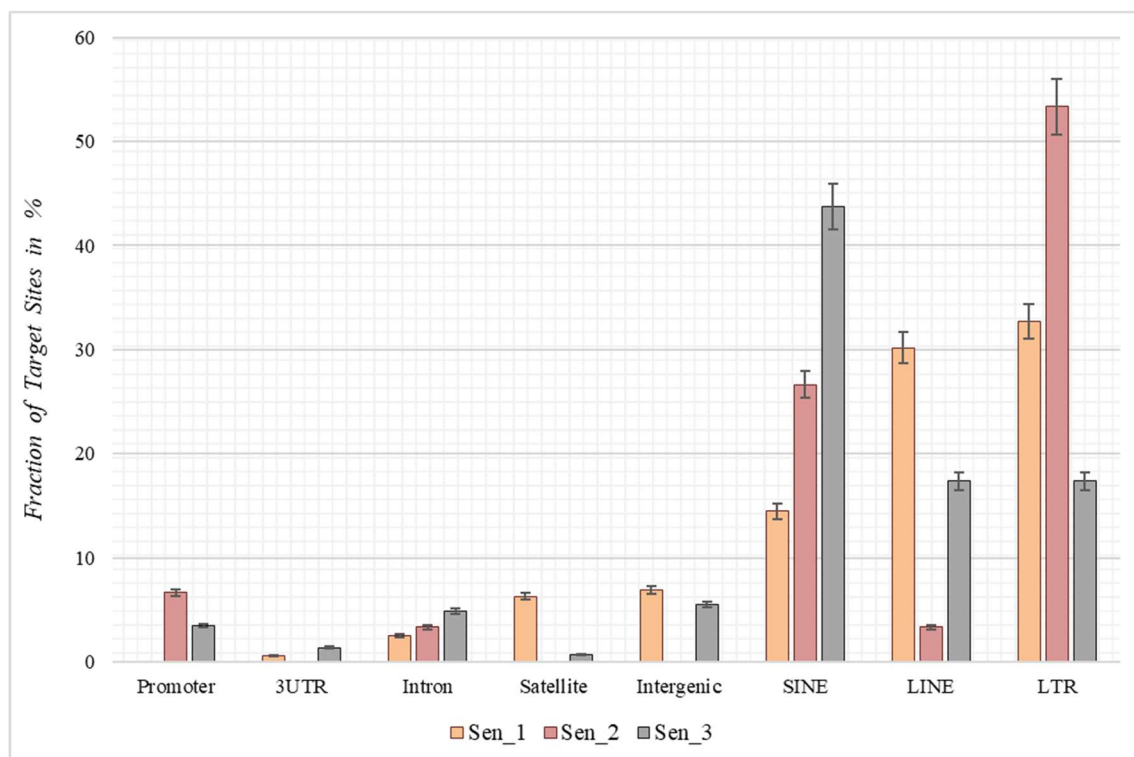


**Figure IV** - Annotation of genomic features of *de novo* SVA integrations in senescent IMR-90 cells (Sen\_1 – Sen\_3; n = 3). Annotated features (HOMER, x-axis) for each sample displayed as % fraction (y-axis) of all target sites. Features on x-axis are (from left to right): Promoter-TSS from -1 kb to +100 bp (Promoter), 3'-untranslated region (3UTR), intronic region (Intron), satellite region (Satellite), intergenic region (Intergenic), SINE transposons (SINE), LINE transposons (LINE) and long terminal repeats (LTR).

#### 4.4.4 SVA integrations localize in close proximity to genes associated with mitosis and cell proliferation

To further investigate functional patterns of senescence associated SVA retrotransposition, HOMER annotated target sites in intronic, 5'- and 3'-UTR, exonic and promoter regions were analysed for Gene Ontologies of biological processes using EnrichR, while intergenic regions were excluded in the process. The estimated gene ontologies ( $p \leq 0.05$ ) of biological processes for the three data sets revealed a connection between preferred target locations of senescence-associated SVAs and processes linked to mitosis (Table I), i.e. genes associated with regulation of spindle organization (GO:0090224), nuclear migration (GO:0007097), establishment of spindle orientation (GO:0051294), establishment of mitotic spindle localization (GO:0040001) and orientation (GO:0000132). Additionally, genes participating in the regulation of hippo signaling (GO:0035330), a pathway linked to cell differentiation and modulation of cell proliferation in growing tissues (Meng et al., 2016) are in close proximity to some SVA retrotransposition coordinates that may be affected by senescence associated reintegration processes.

#### 4.4.5 Cytosolic mtDNA accumulation in cellular senescent IMR-90 cells

Due to the importance of senescence-related mitochondrial dysfunction associated with impaired mitophagy and mitochondrial clearance processes, we asked whether an interorganellar transfer of mobile DNA – more precisely the paralogization of mtDNA to *numts* – is characteristic for cellular senescent IMR-90 cells. Total DNA of proliferating and senescent cells were whole genome sequenced and bioinformatically processed (n=2). Prior to detecting a possible interorganellar transfer of DNA between mitochondria and the nucleus, we checked for mtDNA quantity and overall distribution in our WGS data. Whole mitochondrial DNA (D38112) was thus split into 1000 nt subsequences and the fast-evolving D-Loop sequence was assembled from our WGS data. These sequences were used as queries in a local NCBI BLAST+ (*blastn*, 100 % *perc\_identity*) to analyse proliferating and senescent WGS databases. Overall, the mtDNA read counts (reads per million, RPM) show a substantial increase ranging from 1.3 to 1.46 FC (fold change) in the senescent samples throughout all 1000 nt mtDNA subranges (Figure V). Lowest relative read counts were observed for the mitochondrial genome position 8001-9000 nt (senescent: 277 RPM; proliferating: 103 RPM), where the transcript for ATPase subunit



#### 4 Generation of somatic de novo structural variation as a hallmark of cellular senescence in human lung fibroblasts

6 (7941-8621 nt) and cytochrome c oxidase subunit 3 are located (8621-9404 nt). We detected the highest read counts for the query positions 6000-7001 nt (senescent: 596 RPM; proliferating: 222 RPM) including the sequences for cytochrome c oxidase subunit 1 (5327-6868 nt), tRNA-Ser (6868-6939 nt) and tRNA-Asp (6941-4008 nt).

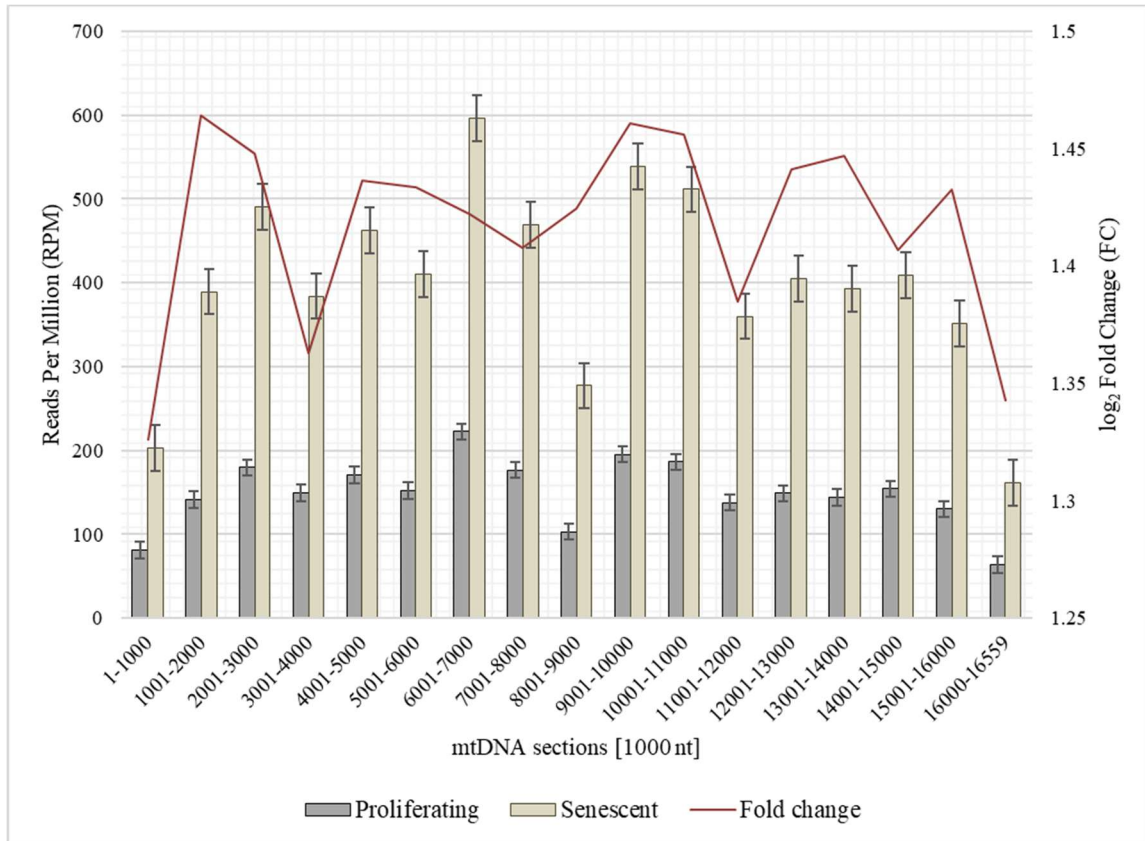


**Figure V** - Abundance of mtDNA copies in proliferating and senescent IMR-90 cells. mtDNA sequence (D38112 with the IMR-90 cell-specific D-Loop) is sectioned in 1000 nt fractions from 1 – 16559 bp (x-axis), aligned read counts (RPM, left y-axis) are displayed as bars with standard error for proliferating and senescent data, fold change (FC) is depicted as a secondary graph overlay (y-axis).

#### 4.4.6 Cellular senescence drives *de novo* nuclear integration events of mtDNA

To define *de novo* transferred mtDNA in the nucleus of senescent IMR-90 we applied a customized bioinformatical pipeline, defining full length-reads with both 100 % identity to IMR-90-mtDNA and hg38 genomic DNA. To extract genomic coordinates of *de novo numts* target sites we analysed two standard WGS datasets for each the proliferating and senescent IMR-90 cells. In addition, we enriched the nuclear genome information against a background of the multycopy-mtDNA by amplifying the regions between Alu-SINES, the most abundant SINE with respect to copy number in the human genome. To this end, the AluScan method (Mei et al. 2011) was applied as suggested by the authors and the amplicates were deep sequenced. All NGS results were scanned for mtDNA insertions

by reads partially consisting of perfect identical mtDNA and nuclear flank sequence. By eliminating known hg38-annotated *numts* and intersecting the numt coordinates of the senescent sample with genomic numt coordinates of the proliferating sample, we excluded germline-specific *numts* within IMR-90 cells and obtained unique target sites that can be further investigated in the context of cellular senescence. In total, we managed to identify 79 *de novo numts* in senescent IMR-90 of which 13 were found in the first WGS data set, 55 in the second WGS data set and 11 in the AluScan Seq data (Figure VIA).

#### 4.4.7 mtDNA mobility and *numts*

We identified 79 *de novo numts* with perfect identity to mtDNA and nuclear hg38 flanks in senescent IMR-90 cells and thus wanted to further evaluate the abundance and distribution of specific mtDNA regions, i. e. a potential preferential mobility of certain mtDNA regions. Therefore, mtDNA-like sequence fractions of our data were annotated by alignment to the mitochondrial genome (D38112) complemented by the IMR-90 specific D-Loop sequence. 6 % of these mtDNA-like sequence fractions within our *de novo numts* represent paralogs of the D-Loop (Figure VIB). Most abundant mtDNA fragments of *de novo numts* belong to *MT-ND5* with 10 %, followed by *MT-CYB* (9 %) and equally *MT-RNR2*, *MT-ND1*, *MT-ND2*, *MT-CO1*. *MT-CO2* (8 %). Further, *MT-RNR2*, *MT-ND1* and *MT-ND2* share the same feature count in our senescent data (7.6 %).

**A**

<i>Numts</i>	hWGS1	hWGS2	Aluscan-Seq
<b>Total identified <i>numts</i></b>	70	102	33
<b><i>Bedtools</i> subtract proliferating <i>numts</i></b>	33	94	12
<b><i>Bedtools</i> subtract hg38 annotated <i>numts</i></b>	13	55	11

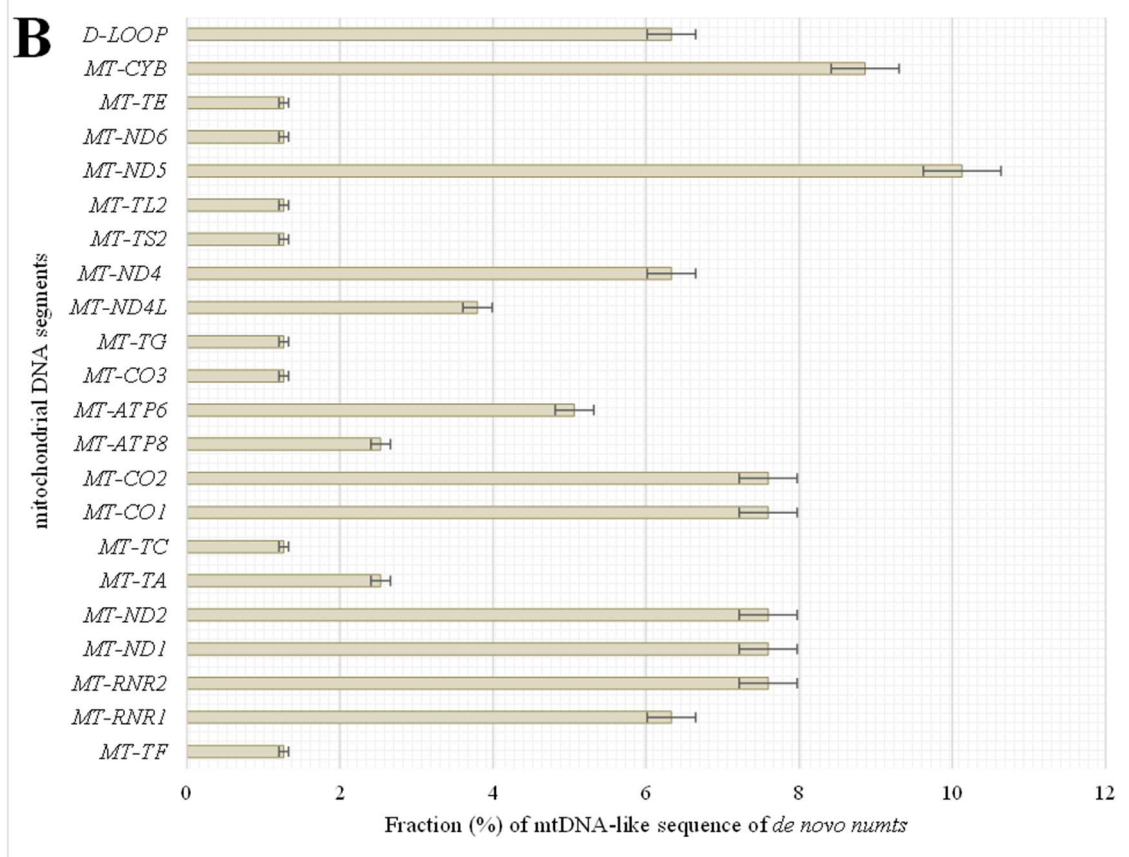


**Figure VI** - Quantity of identified *numts* and distribution of their mtDNA like segments in senescent IMR-90 cells. **(A)** Table of all *numts* (total read counts) identified in the three data sets: hWGS1, hWGS2 and Aluscan-Seq. **(B)** Abundance and distribution of mtDNA-like segments of all *de novo numts* (= 79) as % with standard error (*y*-axis), displayed as bars.

#### 4.4.8 Mitochondrial quality control and somatic interorganellar transfer

To get further insight in the integrity and quality control of mitochondria during the senescence process and the possible association with an increased mobility during senescence, we investigated genes and their abundance in proliferating and senescent IMR-90 cells associated with mitochondrial integration, clearance and mitophagy. Specific genes, that might be associated with mtDNA accumulation and depletion in the

#### 4 Generation of somatic de novo structural variation as a hallmark of cellular senescence in human lung fibroblasts

context of cellular senescence, were chosen (Szkarczyk et al., 2014; Srinivasainagendra et al., 2017; Livingston et al., 2019). Differential expression analysis of the transcriptomic data of proliferating and senescent IMR-90 cells (n=2) was performed and fold changes checked for the GOI. In total, 27 genes associated with mitochondrial pathways were checked for differences in expression. Interestingly, while mRNA could be observed for all genes in the proliferating and senescent data sets, we did not detect any significant expression differences except for three genes (Figure VII). As for the mitochondrial integrity genes, *MSRB2* expression is decreased in senescent cells (FC: -1;  $p \leq 0.05$ ) whereas *MFN2* expression is highly increased (FC: 2.2;  $p \leq 0.05$ ). Additionally, one gene of the mitochondrial clearance family is enriched in senescent cells: *BCL2L13* (FC: 1.4;  $p \leq 0.05$ ). Beside the above-mentioned accumulation of mtDNA during senescence, we thus observed changes in the expression for several genes actively involved in mitochondrial homeostasis in senescent IMR-90 cells.

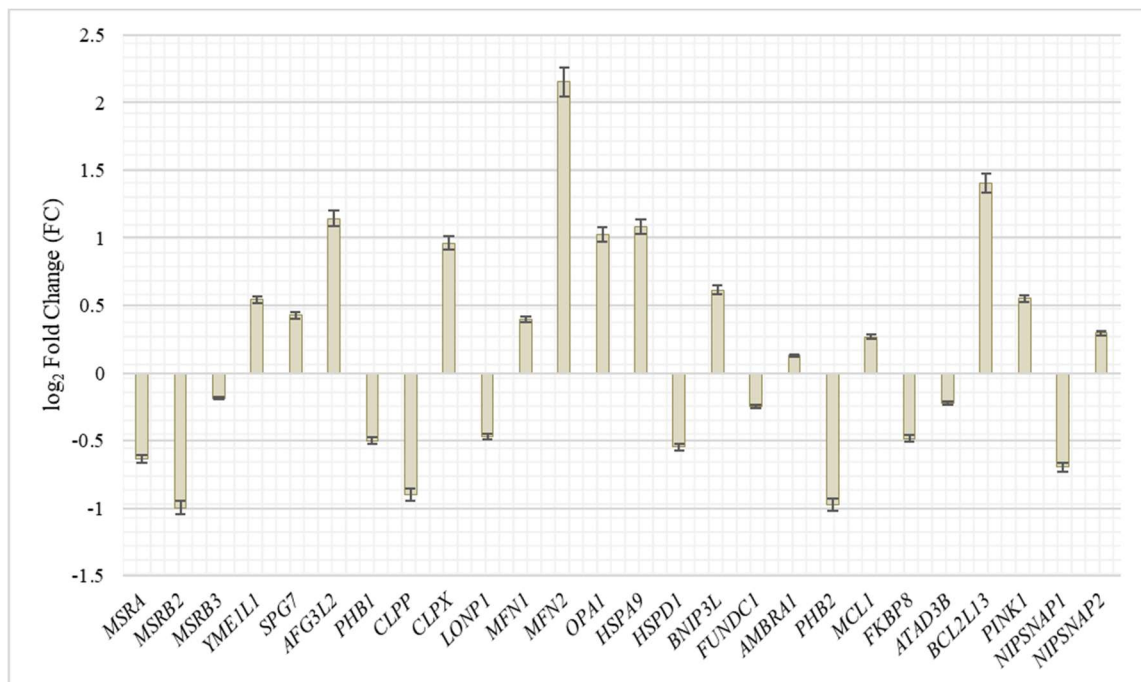


**Figure VII** - Expression of genes associated with mitochondrial integrity, clearance and mitophagy in senescent IMR-90 cells (n = 2). Log<sub>2</sub> Fold Changes (y-axis) depicted for 26 GOI with standard error displayed as bars (x-axis).

#### 4.4.9 Target sites of *de novo numts* in senescent IMR-90 cells and Gene Ontology

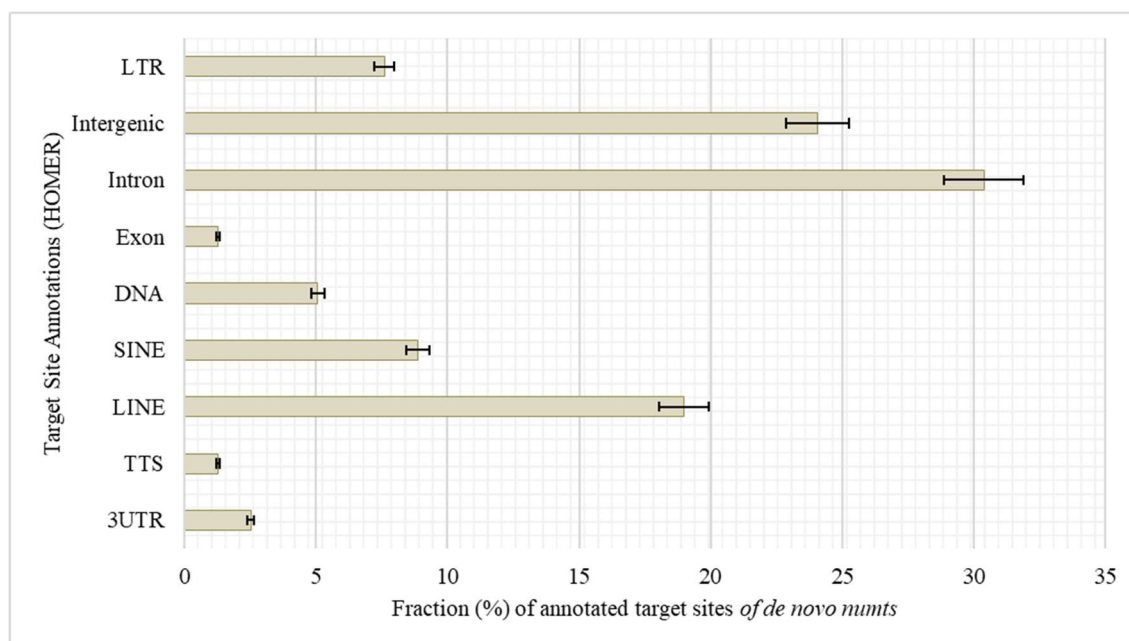


**Figure VIII** - Annotation of genomic features of *de novo numts* in senescent IMR-90 cells. Annotated features with respect to the sum of all HOMER-annotated features (y-axis) for each sample displayed as % fraction (x-axis) of all target sites. Features on y-axis are (from top to bottom): long terminal repeats (LTR), intergenic region (Intergenic), intronic region (Intron), exonic region (Exon), DNA, satellite region (Satellite), SINE transposons (SINE), LINE transposons (LINE), transcription termination site from -100 bp to +1 kbp (TTS) and 3'-untranslated region (3UTR).

Looking into possible target sites of senescence-associated *de novo numts*, we utilized HOMER AnnotatePeaks.pl to obtain peak annotations of the genomic coordinates. Most target sites can be found in introns (30 %), followed by intergenic regions (24 %), LINEs (19 %) and SINEs (9 %, Figure VIII). To check for specific biological processes being affected by *numt* integration, gene names extracted from the HOMER output (43 genes in total) – thus excluding intergenic regions – were analysed using EnrichR. Looking specifically into processes characterized by significant p-values, we observed multiple target sites in close connection to biological processes such as intercellular communication and cellular integrity upkeep with the positive regulation of gap junction assembly (GO:1903598), regulation of actin filament-based process (GO:0032970), regulation of actin cytoskeleton organization (GO:0032956) and - in addition - a direct link to the mitochondrial metabolism through the affected malate metabolic process (GO:0006108) and the calcium ion import (GO:0070509, Table II). Remarkably, genes associated with regulation of heterochromatin formation (GO:0031445) were affected as well.

## 4.5 Discussion

Consistent with the data obtained for human LF1 diploid fibroblast cells (De Cecco et al., 2019), we observe a transcriptional upregulation of SVA elements in IMR-90 cells as well. First, our RNAseq-data comparing proliferative and senescent IMR-90 mirror the observed increase in SVA message. To differentially screen for RNA of the different SVA families we searched the RNA-databases correcting for the overall alignment rate and querying with the informative 5' portion of SVA, thus avoiding misalignments due to the internally repetitive structure of SVAs. Though the SVA elements in general were transcriptionally upregulated we observed that this upregulation preferably affects SVA\_D most strongly. Previous research elucidated that SVA\_B and SVA\_D are the most abundant within the human genome, a dependency of copy number and level of transcription is only mirrored for SVA\_D-transcripts in our data (Wang et al., 2005). The human-specific SVA\_E and SVA\_F are expressed to a comparatively lower extent, however fold changes as obtained comparing proliferative and senescent cells suggest an accumulation of the both in a senescence-associated manner.

Whether the abundance of the 5' SVA as described herein also reflects the diversity in the transcriptional units of SVAs mainly due to differing 5' TSS is not clear, since the preferred mode of SVA transcription is varying in different cell types (Hancks & Kazazian 2010). A decrease in the methyltransferase *DNMT1* transcription (-1.16 FC) that occurs in the process of senescence as described by (Young & Smith, 2001) could be observed in our data in addition, pinpointing towards DNA methylation being effective to control SVA transcription. A possible pre-transcriptional control mechanism of SVA transcription might be CpG methylation, which could be however both systemic and specific at the same time and possibly dependent on the age of the TEs (Ewing et al., 2020). The nanopore sequencing approach by Ewing et al. (2020) has recently uncovered the complex nature of SVA methylation possibly influencing the spatial-temporal expression patterns of SVA and probably getting even more complex when considering age-associated changes. Therefore, we regard our obtained expression data as a rough proxy of potentially mobilizable SVA retroposons that increase in abundance with age. Our IMR-90 data thus recapitulate the observation of age-related reactivated TEs which is observed across species (Bravo et al., 2020, Giordani et al., 2021). In addition, we examined genes that play important roles in cell proliferation and global chromatin

changes such as *LMNB1* – which is part of the nuclear lamina – and observed an overall decrease in transcript abundance in our senescent transcriptomic IMR-90 data (-3 FC). Downregulation of *LMNB1* is defined as a key trigger of chromatin remodeling as outlined by Shah et al (2013). *HMGB2* encodes a chromatin-associated protein of the high mobility group family, and its' expression is altered during replicative exhaustion as described by Aird and coworkers (2016). We observed a decrease for *HMGB2* (-2.15 FC) in the senescent IMR-90 transcriptome which is consistent with the observation of Aird et al. (2016). Finally, we detected a depletion of *CDCA7* (-2.75 FC) in the senescent transcriptomic data, which is closely linked to *DNMT1* expression and an overall hypomethylation at centromeric repeats as reviewed by Vukic & Daxinger (2019). Thus, our transcriptomic data of replicative exhausted IMR-90 cells provide evidence for a dynamic remodeling of chromatin and thus a changed accessibility of reintegration target sites. In line with this, De Cecco et al. (2013) hypothesized that the chromatin of repetitive elements becomes relatively more open during replicative exhaustion. We therefore asked whether this not only mobilizes non-autonomous SVA elements allowing a hijacking of the L1 machinery but also triggers *de novo* reintegration with respect to their genomic targets. To obtain maximum sensitivity in tracing *de novo* SVA integrations we applied an RDA based enrichment technique, in that we represented the 5'flanks of SVAs. The RDA is based on a hybridization of PCR fragments from two genomes under scrutiny - proliferative vs. senescent - in that driver 5' SVA flanks from proliferating cells are given in excess and hybridized to senescent tester representations of 5' SVA flanks, that were ligated to RDA-primers. Ideally, only fragments that originated in the senescent genomes could then be amplified exponentially thus finding the SVA-related differences between the genomes. The results from deep sequencing were scanned for fixated and germline transmitted SVA elements, thus hg38-annotated SVAs were excluded. Moreover, and since we perform intraindividual tester-driver comparisons, we also experimentally represent the fraction of presence/absence-polymorphic SVA-elements in both driver and tester increasing the specificity for *de novo* SVA integrations. In the three replicate experimental settings we could detect 1223, 44, and 428 SVA *de novo* integrations from that 159, 30 and 144 were unique, respectively. The differing read counts and degree of mosaicism represent the individual unique events of SVA *de novo* integrations taking place at different PDL stages and on different lineages during somatic evolution towards senescence as each DNA sample input for the three batches was isolated from IMR-90

cells which underwent replicative exhaustion independently. SVA integrations represent rare genomic changes which has been observed in previous research (Raiz et al., 2012) and is further documented by the observation that of all detected *de novo* SVA insertions only five target site coordinates shared an overlap in our data. In conclusion and in an extension to the experiments with induceable and marked SVA retropositions (Hancks et al. 2011) we provide ample evidence for a marked genomic impact of mobile SVAs during cellular senescence. We present data as obtained by a highly sensitive and specific method to trace *de novo* formed SVA integration sites which showed that active *de novo* SVA mobilization, hijacking of the retrotranspositional machinery and reintegration is ongoing and frequently taking place in senescent IMR-90 cells. To come back to the status of open chromatin pertaining to the repetitive elements in senescent genomes, we next checked the localization of the *de novo* SVA integrations. To this end, BED-files with *de novo* integration coordinates were first annotated to hg38 revealing that LINEs, SINEs and LTRs are the preferred targets of *de novo* integration mirroring the open chromatin status. In an extension to these global patterns of *de novo* SVA integrations, we checked if SVA integrations localize in close proximity to genes. We thus assembled a list of *de novo* integrations for the HOMER functionally annotated intronic or 5' and 3' regulatory regions with the respective genes. We applied EnrichR to get information about the GO-annotation of these genes, from that the most significant fell into processes linked to mitosis, spindle organization, nuclear migration and hippo signalling. In a broad sense we found that *de novo* integrations preferably reintegrate in close proximity to genes involved in pathways linked to cell proliferation and proliferation modulation. We hypothesize that the relevant genes of these processes are characterized by an open chromatin status in senescent cells thus providing easily attainable target structures for the reintegration of SVA cDNA. This observation clearly indicates that in addition to a systemic effect of *de novo* SVA integrations, e.g. by promoting genome instability as described for "jumping" Alu SINEs (Lai et al., 2019), gene-specific and SVA-mediated effects are also possible, ranging from changes in gene regulation to insertional mutagenesis, and may be associated with changes in transcriptional networks and functional decline.

It is generally accepted that cytoplasmic DNA is an efficient damage-associated molecular pattern (DAMP) that triggers the innate immune system responses associated with aging. Beside reverse transcribed autonomous and non-autonomous TEs, another



source of cytoplasmic DNA arises upon release of mtDNA from the mitochondrial compartment. This release, among other things, serves as a rate-determining step for numtogenesis, as summarized by Singh et al. (2017). The mtDNA copy number, together with impaired mitophagy characteristic of old cells, contributes to the cytoplasmic mtDNA quantity possibly initiating the interorganellar transfer into the nucleus. Concordantly, studies in rats have shown that the amount of mtDNA in the nucleus increases with the age of individuals in liver and brain (Caro et al. 2010). Therefore, we first checked in our hWGS data whether we can observe an increase in mtDNA copy number associated with IMR-90 senescence. To this end, we queried the WGS data of proliferating and senescent IMR-90 cells ( $n = 2$ ) with mtDNA sequences partitioned into 1000-nt fragments and with the rapidly evolving D-loop sequences assembled from our IMR-90 WGS data. By comparing proliferative and senescent cells, we obtained evidence for an increase in mtDNA copy number in senescent cells. A decrease in mtDNA copy number, or mtDNA depletion, is seen in many cancers (Abd Radzak et al., 2022). Vice versa, it has been speculated that the accumulation of mtDNA in senescent cells may be a key factor in suppressing tumorigenesis or inflammatory responses (Miwa et al., 2022). This positive effect could be counteracted by increased leakage of mitochondrial genetic material first into the cytoplasm and being eventually transferred into the nucleus. Several scenarios favoring interorganellar transfer have been proposed, including scenarios leading to mitochondrial membrane disruption, such as excessive production of reactive oxygen species, release of cytochrome c, and mitophagy, the latter being impaired in senescent cells. As reviewed by Kumar and Reichert (2021), dysfunctional mitochondria are subjected to different quality control mechanisms, with different pathways operating at different extents of mitochondrial damage. Complete mitochondria are removed by mitophagy in response to severe mitochondrial damage or failure of other quality control mechanisms. Removal of mitochondria is known to negatively affect the development of many features associated with senescence, including SASP, while maintaining cell cycle arrest (Hubackova et al., 2019).

To determine whether critical components belonging to the functional units of mitochondrial clearance, mitophagy, and mitochondrial integrity have different age-associated expression profiles, we performed RNAseq of proliferative and senescent IMR-90 cells. Of the 26 genes analyzed for this purpose, three genes show significant changes in their expression, with *MSRB2* downregulated in our senescent data and *MFN2*

and *BCL2L13* upregulated. We speculate that these changes in expression of genes actively involved in mitochondrial homeostasis in senescent IMR-90 cells reflect impaired mitochondrial quality control, most likely leading to cytoplasmic mtDNA accumulation in cellular senescent IMR-90 cells. According to Barja (2017), mitochondrial ROS production breaks mtDNA into mtDNA fragments that are subsequently transferred to the nucleus. It is widely believed that this extrachromosomal DNA is often used as a filler or glue in NHEJ repair of DSB. Consistent with this, Hazkani-Covo and Covo (2008), comparing pedigree-specific *numts* in humans and chimpanzees with the rhesus outgroup, uncovered sequence patterns before and after numtogenesis characterized by microhomologies and nucleotide additions reminiscent of NHEJ. Obviously, this filler strategy appears to be evolutionarily conserved. We therefore wondered whether cellular senescence drives *de novo* nuclear integration events of mtDNA in IMR-90 cells and pursued two experimental strategies, first by bioinformatic screening of WGS data and second after enrichment of nuclear DNA by an AluScan-PCR approach. Regarding the first approach, a recently published analysis on human brain and circulating immune cells together with an analysis of human fibroblasts revealed a gradual accumulation of *numts* with age (Zhou et al.2023), using WGS data and applying bioinformatic screens for mtDNA paralogs physically linked to GRCh37 chromosomal flanks. In our datasets obtained for the two experimental approaches comparing proliferative and senescent IMR-90, we managed to identify 79 *de novo numts* of which 13 were found in the first WGS data set, 55 in the second WGS data set and 11 in the AluScan Seq data. We interpret the lower number of detectable *de novo numts* in the AluScan dataset as a result of a non-optimal representation of the Alu-intervening segments and the fact that *numts* integrate in remnants of transposable elements such as e.g. SINEs at a frequency of 9 % (see below). The latter cannot be represented by our strategy applying Alu-outward primers. In general, we corroborate data as obtained for brain regions, PBMC and fibroblasts from humans as well as data on yeast aging which is apparently influenced by the migration of mtDNA into the nucleus, too (Cheng & Ivessa, 2010). Thus, numtogenesis increases with age over a broad evolutionary divergence and is recapitulated in the IMR-90 system. To examine if there are mtDNA regions with a higher mobility rate in the process of numtogenesis, we checked which mitogenomic segments were part of our *de novo numts* sequences in our BLAT output data. Our results on mtDNA mobility and *numts* uncovered, that *de novo* integrated

#### 4 Generation of somatic *de novo* structural variation as a hallmark of cellular senescence in human lung fibroblasts

mtDNA paralogs consisted of segments/genes decoding MT-ND5 (10 %), followed by MT-CYB (9 %) and MT-RNR2, MT-ND1, MT-ND2, MT-CO1. MT-CO2 (8 %). Furthermore, MT-RNR2, MT-ND1 and MT-ND2 share the same feature count in our senescent data (7.6 %) and with a lower fraction of 6 %, *de novo numts* apparently originate from the IMR-90 specific D-Loop. Overall, we cannot recognize a significantly preferred mobility with respect to different mtDNA regions. To elucidate a possible gene-specific impact caused by insertional mutagenesis, somatic target sites of *de novo numts* in senescent IMR-90 cells were first annotated for hg38 features applying HOMER software. We observed most target sites of senescence-associated *de novo numts* in introns (30 %), followed by intergenic regions (24 %), LINEs (19 %) and SINEs (9 %, Figure VIII). For the latter we speculate that the above-mentioned open chromatin status pertaining to TEs in senescent cells renders these sequences more amenable to integrations. At last we scrutinized, if mitochondrial dysfunction is merely an epiphenomenon of senescence, or to what extent dysfunctional mitochondria, caused by insertional mutagenesis into specific genes, can possibly trigger the senescent phenotype. Several human diseases, including Pallister–Hall syndrome and mucopolipidosis, can be initiated by mtDNA insertion mutagenesis of nuclear DNA (reviewed in Srinivasainagendra et al. 2017) and we therefore checked the Gene Ontology assignment of *de novo numts* by using EnrichR (biological processes) after applying a HOMER routine to our dataset and obtaining the associated gene names. Interestingly we found several GO annotations possibly affecting mitochondrial homeostasis and mitochondrial metabolism such as Malate Metabolic Process (GO:0006108) and – as observed for the *de novo* SVA integrations – Regulation of Heterochromatin Formation (GO:0031445).

Overall, we obtained evidence for mobile elements that actively cause age-dependent structural genomic changes that go beyond epigenetic modifications. Similar to the consequences of telomere attrition, the chance to cause larger scale rearrangements due to unequal recombination mechanisms caused by TEs is likely to be increased by TE-*de novo* integrations. Moreover, the structural variants thus generated could lead to insertional mutagenesis of relevant genes or changes in their regulation, potentially impacting processes associated with replicative aging of IMR-90 cells. Finally, our results demonstrate that non-autonomous SVA elements efficiently exploit the L1-machinery in trans in an age-dependent manner, leading to cytoplasmic cDNA derived from both SVAs, and probably other non-autonomous TEs - as well as from LINE1. De Cecco et al

(2013) stated that L1 cDNA is an important inducer of IFN-I in senescent cells, and it is reasonable to assume that this promotes an age-associated sterile inflammation, dubbed inflammaging. The same holds for cytoplasmic DNA from other sources such as mtDNA triggering IFN-1 responses which can be differentiated in both intracellular and extracellular effective pathways (West et al, 2015). Efficient counterstrategies to reduce the generation and the genomic effects of mobile cDNA and the associated innate immune response are likely candidates to therapeutically influence healthspan.

#### **4.6 Author Contributions**

Conceptualization: VW and HZ; Methodology: VW, HZ and JM; Bioinformatic analysis: VW, JM and DR; Data interpretation: VW and HZ; Figures, Tables, Graphics: VW; Manuscript writing: VW and HZ; All authors listed have made a substantial, direct, and intellectual contribution to the work, reviewed and edited the manuscript and approved the final version.

#### **4.7 Conflict of Interest**

*The authors declare that the research was conducted in the absence of any commercial or financial relationships that could be construed as a potential conflict of interest.*

#### **4.8 Funding**

This work was financially supported by the Johannes Gutenberg-University of Mainz (Inneruniversitäre Forschungsförderung Stufe I "Differentielle SVA-Retroposonmuster als Indikatoren somatischer Genommosaike des Menschen " to HZ).

#### **4.9 Acknowledgments**

This publication is based on data collected as part of VW's dissertation project at the Department of Biology, Johannes Gutenberg University, Mainz, Germany. We thank members of the Centre for Healthy Ageing (CHA) Mainz for discussions, especially the Hajieva and Moosmann Groups (UMC and CHA) for kindly providing and introducing the IMR-90 cellular system to us. We further want to gratefully acknowledge the expert technical assistance of M.Weisser. Additionally, we want to thank S. Klag for carrying out the pilot mtDNA copy number experiments.

## 4.10 Tables

**Table 1** - EnrichR, biological processes) of de novo SVA retrotranspositions in cellular senescent IMR-90 cells (n = 3); Top 30 GOs with  $p \leq 0.05$ .

Term (Enrichr GO; biological processes)	p-value	q-value
Cardiac Muscle Cell-Cardiac Muscle Cell Adhesion (GO:0086042)	0.00296305	0.66259636
Positive Regulation Of Glucose Import (GO:0046326)	0.00532376	0.66259636
Regulation Of Cardiac Muscle Cell Action Potential (GO:0098901)	0.00734697	0.66259636
snRNA Transcription By RNA Polymerase II (GO:0042795)	0.00855826	0.66259636
Positive Regulation Of Glucose Transmembrane Transport (GO:0010828)	0.00976783	0.66259636
Brain Morphogenesis (GO:0048854)	0.01036166	0.66259636
Cell-Cell Adhesion Via Plasma-Membrane Adhesion Molecules (GO:0098742)	0.01226151	0.66259636
Adult Locomotory Behavior (GO:0008344)	0.01231711	0.66259636
Defense Response To Tumor Cell (GO:0002357)	0.01231711	0.66259636
snRNA Transcription (GO:0009301)	0.01231711	0.66259636
Neuromuscular Process Controlling Balance (GO:0050885)	0.01441991	0.66259636
Regulation Of Oxidoreductase Activity (GO:0051341)	0.01441991	0.66259636
Regulation Of Glucose Import (GO:0046324)	0.01472339	0.66259636
Cell-Cell Junction Organization (GO:0045216)	0.0164963	0.66259636
Protein Trimerization (GO:0070206)	0.01666547	0.66259636
Protein Homotrimerization (GO:0070207)	0.01666547	0.66259636
Regulation Of Monoatomic Ion Transmembrane Transporter Activity (GO:0032412)	0.01731924	0.66259636
Retrograde Axonal Transport (GO:0008090)	0.01904927	0.66259636
Regulation Of Wnt Signaling Pathway (GO:0030111)	0.02050741	0.66259636
Nuclear Migration (GO:0007097)	0.02156693	0.66259636
Regulation Of NMDA Receptor Activity (GO:2000310)	0.02156693	0.66259636
Regulation Of Neurotransmitter Receptor Activity (GO:0099601)	0.0222359	0.66259636
Regulation Of Axonogenesis (GO:0050770)	0.0222359	0.66259636
Positive Regulation Of Neurogenesis (GO:0050769)	0.02279263	0.66259636
Transepithelial Transport (GO:0070633)	0.02421413	0.66259636
Positive Regulation Of NLRP3 Inflammasome Complex Assembly (GO:1900227)	0.02698667	0.66259636
Cellular Response To Radiation (GO:0071478)	0.03147657	0.66259636
Hydrogen Peroxide Catabolic Process (GO:0042744)	0.03289138	0.66259636
Heterophilic Cell-Cell Adhesion Via Plasma Membrane Cell Adhesion Molecules (GO:0007157)	0.0331838	0.66259636
G Protein-Coupled Receptor Signaling Pathway, Coupled To Cyclic Nucleotide Second Messenger (GO:0007187)	0.03493835	0.66259636
Cellular Response To Ionizing Radiation (GO:0071479)	0.03858846	0.66259636
Vesicle Transport Along Microtubule (GO:0047496)	0.03924923	0.66259636
Negative Regulation Of Cell Junction Assembly (GO:1901889)	0.0460298	0.66259636
Positive Regulation Of Cellular Metabolic Process (GO:0031325)	0.04644502	0.66259636
Negative Regulation Of Cellular Biosynthetic Process (GO:0031327)	0.04774848	0.66259636
Signal Transduction In Response To DNA Damage (GO:0042770)	0.0485232	0.66259636
Negative Regulation Of Lipid Biosynthetic Process (GO:0051055)	0.04956946	0.66259636
Regulation Of Hippo Signaling (GO:0035330)	0.04956946	0.66259636
Regulation Of Synapse Organization (GO:0050807)	0.04956946	0.66259636

#### 4 Generation of somatic de novo structural variation as a hallmark of cellular senescence in human lung fibroblasts

**Table II** - Gene Ontology (EnrichR, biological processes) of de novo numts in cellular senescent IMR-90 cells; Top 10 GOs with  $p \leq 0.05$ .

<b>Term (Enrichr GO; biological processes)</b>	<b>p-value</b>	<b>q-value</b>
Regulation Of Actin Filament-Based Process (GO:0032970)	0.008644	0.189158
Positive Regulation Of Gap Junction Assembly (GO:1903598)	0.009961	0.189158
Positive Regulation Of Catabolic Process (GO:0009896)	0.010904	0.189158
Malate Metabolic Process (GO:0006108)	0.013918	0.189158
Regulation Of Heterochromatin Formation (GO:0031445)	0.013918	0.189158
Negative Regulation Of T Cell Apoptotic Process (GO:0070233)	0.013918	0.189158
Regulation Of Actin Cytoskeleton Organization (GO:0032956)	0.014276	0.189158
Regulation Of Gap Junction Assembly (GO:1903596)	0.015891	0.189158
UDP-N-acetylglucosamine Biosynthetic Process (GO:0006048)	0.015891	0.189158
Neuronal Ion Channel Clustering (GO:0045161)	0.015891	0.189158

## 5 Conclusion of the present thesis

With the present work, I aim to elucidate genetic and epigenetic phenomena implicated in cellular senescence and early tumorigenesis. The first part of this thesis addresses epigenetic modifications utilizing sncRNA and transcriptomic profiles in senescent and tetraploid IMR-90 cells. miRNAs are evaluated as reliable aging biomarkers due to their conserved nature, high abundance in mammalian genomes and stable expression profiles. My analysis revealed several highly upregulated miRNA expression patterns that are shared between senescent and tetraploid IMR-90 cells and are closely associated with cancer progression and inflammation. This provides an opportunity for further examination of the relationship between senescence-associated patterns and excessive cell proliferation, abnormal replication, and stress-induced growth arrest. It should be noted that the diverse expression patterns observed for some miRNAs in the senescent and early tumorigenesis model suggest that many unknown modulating functions – possibly linked to the high number of targets – are yet to be uncovered. The significant upregulation of miR-29a-3p in IMR-90 cells undergoing senescence indicates its potential as a biomarker for aging in my study. One could argue that downregulating miR-29a-3p may in turn have beneficial effects on cell proliferation. However, the inhibition leads to stress accumulation and the emergence of senescence-associated features in the treated, proliferating IMR-90 cells. This suggests an antagonistic pleiotropy of the respective miRNA. Further investigation is needed to clarify the correlation between miR-29a-3p and cellular senescence, while examining its effect on cell proliferation and healthy aging. Additional markers for aging should be included in studies and experiments conducted in proliferating and senescent cells. Furthermore, it is crucial to verify the consistency of these findings in other organs and primate cell cultures, as well as malignant tissues.

The second part of this thesis, which has been submitted as a first draft manuscript to *Frontiers in Cell and Developmental Biology, Epigenomics, and Epigenetics* and is currently undergoing peer review, explores structural variations in aging genomes that extend beyond epigenetic alterations in the model of senescent IMR-90 cells. SVA elements are hominoid-specific transposable elements. They utilize the retrotranspositional machinery of LINE-1 making them vulnerable to remobilization and integration in the aging genome. Furthermore, cellular senescence is characterized by mitochondrial dysfunction, which leads to the accumulation of mtDNA in the cytosol.

This may result in possible integrations of mtDNA fragments in nuclear DNA as *numts*. Numerous integration sites were identified in senescent IMR-90 cells compared to their proliferating counterparts through comparative analyses of both SVA *de novo* insertions and *de novo numts*, suggesting that these structural variants could potentially impact processes associated with replicative aging.

The representational difference analysis of our first draft received feedback from reviewers, leading to the incorporation of suggested revisions in the updated version. As a result, I will address the comments in the conclusion of this thesis. Based on the experimental procedures, we do not expect to uncover a linear correlation between SVA transcript abundance and the emergence of structural variation due to reintegration. The elevated expression of possible SVA source RNAs is circumstantial evidence that could support the non-autonomous SVA retrotransposition observed in the data, as the expression of the LINE-1 machinery in senescent cells is generally accepted. The main objective of the study was to apply the concept of rare genomic events of SVA integrations, assessing the SVA-presence and -absence mosaicism in senescent cells as a clade marker retrotranspositional event without reversals or parallels. While a time course of retrotranspositional activity during the cell doubling towards senescence would be of interest, my work instead focuses on exploiting the clearly defined character polarity of SVA retropositions rather than yielding estimations of specific rates in the senescent IMR-90 cells. Regarding the sensitivity of the applied method, we utilize the fact that these retropositions are considered homoplasmy-free. For the detection of SVAs using PCR, we have implemented the primer system from the Me-Scan-SVA method developed by Ha et al (2016). This system has proven to be highly precise in detecting SVAs (over 90 %) and very sensitive when considering fixed SVA integrations (over 90 %) in the above-mentioned study. We agree with the reviewers that our data are insufficient for drawing definite conclusions regarding target site features and consequences of *de novo* retrotranspositions. Instead, we put more emphasis on the genomic variations we observe within the process of cells undergoing cellular senescence. On the other hand, and with the expression changes of several genes associated with chromatin remodeling observed, we assume an unspecific "multilocus" influence. Clearly, more investigation on DNA methylation and differential histone modifications should be performed in parallel by future studies. As the integrations we identified vary in frequency and represent rare genomic events, we agree with the reviewer's assertion that further investigation is



required to draw meaningful conclusions from the target enrichment analysis. However, we are confident that our approach gives solid information on structural variation caused by non-autonomous elements represented by the *de novo* SVA integrations and *de novo* numts.

## References

Abd Radzak, S. M., Mohd Khair, S. Z. N., Ahmad, F., Patar, A., Idris, Z., & Mohamed Yusoff, A. A. (2022). Insights regarding mitochondrial DNA copy number alterations in human cancer (Review). *International journal of molecular medicine*, *50*(2), 104. <https://doi.org/10.3892/ijmm.2022.5160>

Abdelmohsen, K., Panda, A., Kang, M. J., Xu, J., Selimyan, R., Yoon, J. H., Martindale, J. L., De, S., Wood, W. H., 3rd, Becker, K. G., & Gorospe, M. (2013). Senescence-associated lncRNAs: senescence-associated long noncoding RNAs. *Aging cell*, *12*(5), 890–900. <https://doi.org/10.1111/accel.12115>

Agarwal, V., Bell, G. W., Nam, J. W., & Bartel, D. P. (2015). Predicting effective microRNA target sites in mammalian mRNAs. *eLife*, *4*, e05005. <https://doi.org/10.7554/eLife.05005>

Aird, K. M., Iwasaki, O., Kossenkov, A. V., Tanizawa, H., Fatkhutdinov, N., Bitler, B. G., Le, L., Alicea, G., Yang, T. L., Johnson, F. B., Noma, K. I., & Zhang, R. (2016). HMGB2 orchestrates the chromatin landscape of senescence-associated secretory phenotype gene loci. *The Journal of cell biology*, *215*(3), 325–334. <https://doi.org/10.1083/jcb.201608026>

Alessio, N., Aprile, D., Cappabianca, S., Peluso, G., Di Bernardo, G., & Galderisi, U. (2021). Different Stages of Quiescence, Senescence, and Cell Stress Identified by Molecular Algorithm Based on the Expression of Ki67, RPS6, and Beta-Galactosidase Activity. *International journal of molecular sciences*, *22*(6), 3102. <https://doi.org/10.3390/ijms22063102>

Alves-Fernandes, D. K., & Jasiulionis, M. G. (2019). The Role of SIRT1 on DNA Damage Response and Epigenetic Alterations in Cancer. *International journal of molecular sciences*, *20*(13), 3153. <https://doi.org/10.3390/ijms20133153>

- Aparicio-Puerta, E., Hirsch, P., Schmartz, G. P., Kern, F., Fehlmann, T., & Keller, A. (2023). miEAA 2023: updates, new functional microRNA sets and improved enrichment visualizations. *Nucleic acids research*, 51(W1), W319–W325. <https://doi.org/10.1093/nar/gkad392>
- Aparicio-Puerta, E., Lebrón, R., Rueda, A., Gómez-Martín, C., Giannoukakos, S., Jaspez, D., Medina, J. M., Zubkovic, A., Jurak, I., Fromm, B., Marchal, J. A., Oliver, J., & Hackenberg, M. (2019). sRNAbench and sRNAtoolbox 2019: intuitive fast small RNA profiling and differential expression. *Nucleic acids research*, 47(W1), W530–W535. <https://doi.org/10.1093/nar/gkz415>
- Argüelles, S., Guerrero-Castilla, A., Cano, M., Muñoz, M. F., & Ayala, A. (2019). Advantages and disadvantages of apoptosis in the aging process. *Annals of the New York Academy of Sciences*, 1443(1), 20–33. <https://doi.org/10.1111/nyas.14020>
- Baar, M. P., Brandt, R. M. C., Putavet, D. A., Klein, J. D. D., Derks, K. W. J., Bourgeois, B. R. M., Stryeck, S., Rijksen, Y., van Willigenburg, H., Feijtel, D. A., van der Pluijm, I., Essers, J., van Cappellen, W. A., van IJcken, W. F., Houtsmuller, A. B., Pothof, J., de Bruin, R. W. F., Madl, T., Hoeijmakers, J. H. J., Campisi, J., ... de Keizer, P. L. J. (2017). Targeted Apoptosis of Senescent Cells Restores Tissue Homeostasis in Response to Chemotoxicity and Aging. *Cell*, 169(1), 132–147.e16. <https://doi.org/10.1016/j.cell.2017.02.031>
- Baker, D. J., Perez-Terzic, C., Jin, F., Pitel, K. S., Niederländer, N. J., Jeganathan, K., Yamada, S., Reyes, S., Rowe, L., Hiddinga, H. J., Eberhardt, N. L., Terzic, A., & van Deursen, J. M. (2008). Opposing roles for p16Ink4a and p19Arf in senescence and ageing caused by BubR1 insufficiency. *Nature cell biology*, 10(7), 825–836. <https://doi.org/10.1038/ncb1744>
- Balint, V., Ninkovic, D. S., Anastasov, N., Lazic, S., Kovacevic-Grujicic, N., Stevanovic, M., & Lazic, A. (2021). Inhibition of miR-21 Promotes Cellular Senescence in NT2-Derived Astrocytes. *Biochemistry. Biokhimiia*, 86(11), 1434–1445. <https://doi.org/10.1134/S0006297921110079>

- Barja, G. (2017). The Cell Aging Regulation System (CARS). *Reactive Oxygen Species*, 3(9), 148–183. Retrieved from <https://www.rosj.org/index.php/ros/article/view/82>
- Basisty, N., Kale, A., Jeon, O. H., Kuehnemann, C., Payne, T., Rao, C., Holtz, A., Shah, S., Sharma, V., Ferrucci, L., Campisi, J., & Schilling, B. (2020). A proteomic atlas of senescence-associated secretomes for aging biomarker development. *PLoS biology*, 18(1), e3000599. <https://doi.org/10.1371/journal.pbio.3000599>
- Berman, J. R., & Kenyon, C. (2006). Germ-cell loss extends *C. elegans* life span through regulation of DAF-16 by *kri-1* and lipophilic-hormone signaling. *Cell*, 124(5), 1055–1068. <https://doi.org/10.1016/j.cell.2006.01.039>
- Bi, L., Yang, Q., Yuan, J., Miao, Q., Duan, L., Li, F., & Wang, S. (2016). MicroRNA-127-3p acts as a tumor suppressor in epithelial ovarian cancer by regulating the BAG5 gene. *Oncology reports*, 36(5), 2563–2570. <https://doi.org/10.3892/or.2016.5055>
- Blasco M. A. (2005). Telomeres and human disease: ageing, cancer and beyond. *Nature reviews. Genetics*, 6(8), 611–622. <https://doi.org/10.1038/nrg1656>
- Bravo, J. I., Nozownik, S., Danthi, P. S., & Benayoun, B. A. (2020). Transposable elements, circular RNAs and mitochondrial transcription in age-related genomic regulation. *Development (Cambridge, England)*, 147(11), dev175786. <https://doi.org/10.1242/dev.175786>
- Careccia, S., Mainardi, S., Pelosi, A., Gurtner, A., Diverio, D., Riccioni, R., Testa, U., Pelosi, E., Piaggio, G., Sacchi, A., Lavorgna, S., Lo-Coco, F., Blandino, G., Levrero, M., & Rizzo, M. G. (2009). A restricted signature of miRNAs distinguishes APL blasts from normal promyelocytes. *Oncogene*, 28(45), 4034–4040. <https://doi.org/10.1038/onc.2009.255>
- Caro, P., Gómez, J., Arduini, A., González-Sánchez, M., González-García, M., Borrás, C., Viña, J., Puertas, M. J., Sastre, J., & Barja, G. (2010). Mitochondrial DNA sequences are present inside nuclear DNA in rat tissues and increase with age. *Mitochondrion*, 10(5), 479–486. <https://doi.org/10.1016/j.mito.2010.05.004>

- Chan, P. P., & Lowe, T. M. (2009). GtRNAdb: a database of transfer RNA genes detected in genomic sequence. *Nucleic acids research*, *37*(Database issue), D93–D97. <https://doi.org/10.1093/nar/gkn787>
- Chen, E. Y., Tan, C. M., Kou, Y., Duan, Q., Wang, Z., Meirelles, G. V., Clark, N. R., & Ma'ayan, A. (2013). Enrichr: interactive and collaborative HTML5 gene list enrichment analysis tool. *BMC bioinformatics*, *14*, 128. <https://doi.org/10.1186/1471-2105-14-128>
- Chen, J., Wang, M., Guo, M., Xie, Y., & Cong, Y. S. (2013). miR-127 regulates cell proliferation and senescence by targeting BCL6. *PloS one*, *8*(11), e80266. <https://doi.org/10.1371/journal.pone.0080266>
- Chen, Q., Zhou, L., Ye, X., Tao, M., & Wu, J. (2020). miR-145-5p suppresses proliferation, metastasis and EMT of colorectal cancer by targeting CDCA3. *Pathology, research and practice*, *216*(4), 152872. <https://doi.org/10.1016/j.prp.2020.152872>
- Cheng, X., & Ivessa, A. S. (2010). The migration of mitochondrial DNA fragments to the nucleus affects the chronological aging process of *Saccharomyces cerevisiae*. *Aging cell*, *9*(5), 919–923. <https://doi.org/10.1111/j.1474-9726.2010.00607.x>
- Chi, J., Xie, Q., Jia, J., Liu, X., Sun, J., Deng, Y., & Yi, L. (2018). Integrated Analysis and Identification of Novel Biomarkers in Parkinson's Disease. *Frontiers in aging neuroscience*, *10*, 178. <https://doi.org/10.3389/fnagi.2018.00178>
- Childs, B. G., Baker, D. J., Kirkland, J. L., Campisi, J., & van Deursen, J. M. (2014). Senescence and apoptosis: dueling or complementary cell fates?. *EMBO reports*, *15*(11), 1139–1153. <https://doi.org/10.15252/embr.201439245>
- Collado, M., Blasco, M. A., & Serrano, M. (2007). Cellular senescence in cancer and aging. *Cell*, *130*(2), 223–233. <https://doi.org/10.1016/j.cell.2007.07.003>
- Cui, Y., Wang, X., Lin, F., Li, W., Zhao, Y., Zhu, F., Yang, H., Rao, M., Li, Y., Liang, H., Dai, M., Liu, B., Chen, L., Han, D., Lu, R., Peng, W., Zhang, Y., Song, C., Luo, Y., & Pan, P. (2022). MiR-29a-3p Improves Acute Lung Injury by Reducing Alveolar Epithelial Cell PANoptosis. *Aging and disease*, *13*(3), 899–909. <https://doi.org/10.14336/AD.2021.1023>

- Dalle Pezze, P., Nelson, G., Otten, E. G., Korolchuk, V. I., Kirkwood, T. B., von Zglinicki, T., & Shanley, D. P. (2014). Dynamic modelling of pathways to cellular senescence reveals strategies for targeted interventions. *PloS computational biology*, *10*(8), e1003728. <https://doi.org/10.1371/journal.pcbi.1003728>
- Danecek, P., Bonfield, J. K., Liddle, J., Marshall, J., Ohan, V., Pollard, M. O., Whitwham, A., Keane, T., McCarthy, S. A., Davies, R. M., & Li, H. (2021). Twelve years of SAMtools and BCFtools. *GigaScience*, *10*(2), giab008. <https://doi.org/10.1093/gigascience/giab008>
- Davoli, T., & de Lange, T. (2011). The causes and consequences of polyploidy in normal development and cancer. *Annual review of cell and developmental biology*, *27*, 585–610. <https://doi.org/10.1146/annurev-cellbio-092910-154234>
- De Cecco, M., Criscione, S. W., Peckham, E. J., Hillenmeyer, S., Hamm, E. A., Manivannan, J., Peterson, A. L., Kreiling, J. A., Neretti, N., & Sedivy, J. M. (2013). Genomes of replicatively senescent cells undergo global epigenetic changes leading to gene silencing and activation of transposable elements. *Aging cell*, *12*(2), 247–256. <https://doi.org/10.1111/accel.12047>
- De Cecco, M., Ito, T., Petrashen, A. P., Elias, A. E., Skvir, N. J., Criscione, S. W., Caligiana, A., Broccoli, G., Adney, E. M., Boeke, J. D., Le, O., Beauséjour, C., Ambati, J., Ambati, K., Simon, M., Seluanov, A., Gorbunova, V., Slagboom, P. E., Helfand, S. L., Neretti, N., & ... Sedivy, J. M. (2019). L1 drives IFN in senescent cells and promotes age-associated inflammation. *Nature*, *566*(7742), 73–78. <https://doi.org/10.1038/s41586-018-0784-9>
- de Lange T. (2005). Shelterin: the protein complex that shapes and safeguards human telomeres. *Genes & development*, *19*(18), 2100–2110. <https://doi.org/10.1101/gad.1346005>
- Dimri, G. P., Lee, X., Basile, G., Acosta, M., Scott, G., Roskelley, C., Medrano, E. E., Linskens, M., Rubelj, I., & Pereira-Smith, O. (1995). A biomarker that identifies senescent human cells in culture and in aging skin in vivo. *Proceedings of the National*

---

*Academy of Sciences of the United States of America*, 92(20), 9363–9367.  
<https://doi.org/10.1073/pnas.92.20.9363>

Dreesen, O., Chojnowski, A., Ong, P. F., Zhao, T. Y., Common, J. E., Lunny, D., Lane, E. B., Lee, S. J., Vardy, L. A., Stewart, C. L., & Colman, A. (2013). Lamin B1 fluctuations have differential effects on cellular proliferation and senescence. *The Journal of cell biology*, 200(5), 605–617. <https://doi.org/10.1083/jcb.201206121>

Du, S. Y., Huang, X. X., Li, N. M., Lv, C. Y., Lv, C. H., Wei, M. L., Gao, Z., & Zhang, Y. P. (2020). MiR-127-3p inhibits proliferation of ovarian cancer in rats through down-regulating MAPK4. *European review for medical and pharmacological sciences*, 24(20), 10383–10390. [https://doi.org/10.26355/eurrev\\_202010\\_23388](https://doi.org/10.26355/eurrev_202010_23388)

Du, W. W., Yang, W., Chen, Y., Wu, Z. K., Foster, F. S., Yang, Z., Li, X., & Yang, B. B. (2017). Foxo3 circular RNA promotes cardiac senescence by modulating multiple factors associated with stress and senescence responses. *European heart journal*, 38(18), 1402–1412. <https://doi.org/10.1093/eurheartj/ehw001>

Ewing, A. D., Smits, N., Sanchez-Luque, F. J., Faivre, J., Brennan, P. M., Richardson, S. R., Cheetham, S. W., & Faulkner, G. J. (2020). Nanopore Sequencing Enables Comprehensive Transposable Element Epigenomic Profiling. *Molecular cell*, 80(5), 915–928.e5. <https://doi.org/10.1016/j.molcel.2020.10.024>

Faget, D. V., Ren, Q., & Stewart, S. A. (2019). Unmasking senescence: context-dependent effects of SASP in cancer. *Nature reviews. Cancer*, 19(8), 439–453. <https://doi.org/10.1038/s41568-019-0156-2>

Fan, Y., Yin, S., Hao, Y., Yang, J., Zhang, H., Sun, C., Ma, M., Chang, Q., & Xi, J. J. (2014). miR-19b promotes tumor growth and metastasis via targeting TP53. *RNA (New York, N.Y.)*, 20(6), 765–772. <https://doi.org/10.1261/rna.043026.113>

Farfariello, V., Gordienko, D. V., Mesilmany, L., Touil, Y., Germain, E., Fliniaux, I., Desruelles, E., Gkika, D., Roudbaraki, M., Shapovalov, G., Noyer, L., Lebas, M., Allart, L., Zienthal-Gelus, N., Iamshanova, O., Bonardi, F., Figeac, M., Laine, W., Kluza, J., Marchetti, P., Prevarskaya, N. (2022). TRPC3 shapes the ER-mitochondria Ca<sup>2+</sup> transfer

characterizing tumour-promoting senescence. *Nature communications*, 13(1), 956. <https://doi.org/10.1038/s41467-022-28597-x>

Feldser, D. M., & Greider, C. W. (2007). Short telomeres limit tumor progression in vivo by inducing senescence. *Cancer cell*, 11(5), 461–469. <https://doi.org/10.1016/j.ccr.2007.02.026>

Fergal J Martin, M Ridwan Amode, Alisha Aneja, Olanrewaju Austine-Orimoloye, Andrey G Azov, If Barnes, Arne Becker, Ruth Bennett, Andrew Berry, Jyothish Bhai, Simarpreet Kaur Bhurji, Alexandra Bignell, Sanjay Boddu, Paulo R Branco Lins, Lucy Brooks, Shashank Budhanuru Ramaraju, Mehrnaz Charkhchi, Alexander Cockburn, Luca Da Rin Fiorretto, Claire Davidson, Kamalkumar Dodiya, Sarah Donaldson, Bilal El Houdaigui, Tamara El Naboulsi, Reham Fatima, Carlos Garcia Giron, Thiago Genez, Gurpreet S Ghattaoraya, Jose Gonzalez Martinez, Cristi Guijarro, Matthew Hardy, Zoe Hollis, Thibaut Hourlier, Toby Hunt, Mike Kay, Vinay Kaykala, Tuan Le, Diana Lemos, Diego Marques-Coelho, José Carlos Marugán, Gabriela Alejandra Merino, Louise Paola Mirabueno, Aleena Mushtaq, Syed Nakib Hossain, Denye N Ogeh, Manoj Pandian Sakthivel, Anne Parker, Malcolm Perry, Ivana Piližota, Irina Prosovetskaia, José G Pérez-Silva, Ahamed Imran Abdul Salam, Nuno Saraiva-Agostinho, Helen Schuilenburg, Dan Sheppard, Swati Sinha, Botond Sipos, William Stark, Emily Steed, Ranjit Sukumaran, Dulika Sumathipala, Marie-Marthe Suner, Likhitha Surapaneni, Kyösti Sutinen, Michal Szpak, Francesca Floriana Tricomi, David Urbina-Gómez, Andres Veidenberg, Thomas A Walsh, Brandon Walts, Elizabeth Wass, Natalie Willhoft, Jamie Allen, Jorge Alvarez-Jarreta, Marc Chakiachvili, Bethany Flint, Stefano Giorgetti, Leanne Haggerty, Garth R Ilesley, Jane E Loveland, Benjamin Moore, Jonathan M Mudge, John Tate, David Thybert, Stephen J Trevanion, Andrea Winterbottom, Adam Frankish, Sarah E Hunt, Magali Ruffier, Fiona Cunningham, Sarah Dyer, Robert D Finn, Kevin L Howe, Peter W Harrison, Andrew D Yates & Paul Flicek (2023). Ensembl 2023, *Nucleic Acids Research*, Volume 51, Issue D1, Pages D933–D941, <https://doi.org/10.1093/nar/gkac958>

Franceschi, C., Capri, M., Monti, D., Giunta, S., Olivieri, F., Sevini, F., Panourgia, M. P., Invidia, L., Celani, L., Scurti, M., Cevenini, E., Castellani, G. C., & Salvioli, S. (2007). Inflammaging and anti-inflammaging: a systemic perspective on aging and longevity

- emerged from studies in humans. *Mechanisms of ageing and development*, 128(1), 92–105. <https://doi.org/10.1016/j.mad.2006.11.016>
- Freund, A., Laberge, R. M., Demaria, M., & Campisi, J. (2012). Lamin B1 loss is a senescence-associated biomarker. *Molecular biology of the cell*, 23(11), 2066–2075. <https://doi.org/10.1091/mbc.E11-10-0884>
- García-Prat, L., Martínez-Vicente, M., Perdiguero, E., Ortet, L., Rodríguez-Ubreva, J., Rebollo, E., Ruiz-Bonilla, V., Gutarra, S., Ballestar, E., Serrano, A. L., Sandri, M., & Muñoz-Cánoves, P. (2016). Autophagy maintains stemness by preventing senescence. *Nature*, 529(7584), 37–42. <https://doi.org/10.1038/nature16187>
- Gebert D, Hewel C, Rosenkranz D (2017). unitas: the universal tool for annotation of small RNAs. *BMC Genomics* 18(1):644.
- Ghafouri-Fard, S., Khoshbakht, T., Hussen, B. M., Baniahmad, A., Branicki, W., Taheri, M., & Eghbali, A. (2022). Emerging Role of Non-Coding RNAs in Senescence. *Frontiers in cell and developmental biology*, 10, 869011. <https://doi.org/10.3389/fcell.2022.869011>
- Giordani, G., Cavaliere, V., Gargiulo, G., Lattanzi, G., & Andrenacci, D. (2021). Retrotransposons Down- and Up-Regulation in Aging Somatic Tissues. *Cells*, 11(1), 79. <https://doi.org/10.3390/cells11010079>
- Goedhart, J., & Luijsterburg, M. S. (2020). VolcaNoseR is a web app for creating, exploring, labeling and sharing volcano plots. *Scientific reports*, 10(1), 20560. <https://doi.org/10.1038/s41598-020-76603-3>
- Goodarzi, H., Liu, X., Nguyen, H. C., Zhang, S., Fish, L., & Tavazoie, S. F. (2015). Endogenous tRNA-Derived Fragments Suppress Breast Cancer Progression via YBX1 Displacement. *Cell*, 161(4), 790–802. <https://doi.org/10.1016/j.cell.2015.02.053>
- Ha, H., Loh, J. W., & Xing, J. (2016). Identification of polymorphic SVA retrotransposons using a mobile element scanning method for SVA (ME-Scan-SVA). *Mobile DNA*, 7, 15. <https://doi.org/10.1186/s13100-016-0072-x>



- Hackl, M., Brunner, S., Fortschegger, K., Schreiner, C., Micutkova, L., Mück, C., Laschober, G. T., Lepperdinger, G., Sampson, N., Berger, P., Herndler-Brandstetter, D., Wieser, M., Kühnel, H., Strasser, A., Rinnerthaler, M., Breitenbach, M., Mildner, M., Eckhart, L., Tschachler, E., Trost, A., Bauer, J. W., Papak, C., Trajanoski, Z., Scheideler, M., Grillari-Voglauer, R., Grubeck-Loebenstein, B., Jansen-Dürr, P. & Grillari, J. (2010). miR-17, miR-19b, miR-20a, and miR-106a are down-regulated in human aging. *Aging cell*, 9(2), 291–296. <https://doi.org/10.1111/j.1474-9726.2010.00549.x>
- Han, S., & Brunet, A. (2012). Histone methylation makes its mark on longevity. *Trends in cell biology*, 22(1), 42–49. <https://doi.org/10.1016/j.tcb.2011.11.001>
- Hancks, D. C., & Kazazian, H. H., Jr (2010). SVA retrotransposons: Evolution and genetic instability. *Seminars in cancer biology*, 20(4), 234–245. <https://doi.org/10.1016/j.semcancer.2010.04.001>
- Hancks, D. C., Goodier, J. L., Mandal, P. K., Cheung, L. E., & Kazazian, H. H., Jr (2011). Retrotransposition of marked SVA elements by human L1s in cultured cells. *Human molecular genetics*, 20(17), 3386–3400. <https://doi.org/10.1093/hmg/ddr245>
- Hastie, N. D., & Allshire, R. C. (1989). Human telomeres: fusion and interstitial sites. *Trends in genetics : TIG*, 5(10), 326–331. [https://doi.org/10.1016/0168-9525\(89\)90137-6](https://doi.org/10.1016/0168-9525(89)90137-6)
- Hayflick, L., & Moorhead, P. S. (1961). The serial cultivation of human diploid cell strains. *Experimental cell research*, 25, 585–621. [https://doi.org/10.1016/0014-4827\(61\)90192-6](https://doi.org/10.1016/0014-4827(61)90192-6)
- Hazkani-Covo, E., & Covo, S. (2008). Numt-mediated double-strand break repair mitigates deletions during primate genome evolution. *PLoS genetics*, 4(10), e1000237. <https://doi.org/10.1371/journal.pgen.1000237>
- Heard, E., & Martienssen, R. A. (2014). Transgenerational epigenetic inheritance: myths and mechanisms. *Cell*, 157(1), 95–109. <https://doi.org/10.1016/j.cell.2014.02.045>
- Heinz, S., Benner, C., Spann, N., Bertolino, E., Lin, Y. C., Laslo, P., Cheng, J. X., Murre, C., Singh, H., & Glass, C. K. (2010). Simple combinations of lineage-determining

- transcription factors prime cis-regulatory elements required for macrophage and B cell identities. *Molecular cell*, 38(4), 576–589. <https://doi.org/10.1016/j.molcel.2010.05.004>
- Hizir, Z., Bottini, S., Grandjean, V., Trabucchi, M., & Repetto, E. (2017). RNY (YRNA)-derived small RNAs regulate cell death and inflammation in monocytes/macrophages. *Cell death & disease*, 8(1), e2530. <https://doi.org/10.1038/cddis.2016.429>
- Horvath S. (2013). DNA methylation age of human tissues and cell types. *Genome biology*, 14(10), R115. <https://doi.org/10.1186/gb-2013-14-10-r115>
- Hubackova, S., Davidova, E., Rohlenova, K., Stursa, J., Werner, L., Andera, L., Dong, L., Terp, M. G., Hodny, Z., Ditzel, H. J., Rohlena, J., & Neuzil, J. (2019). Selective elimination of senescent cells by mitochondrial targeting is regulated by ANT2. *Cell death and differentiation*, 26(2), 276–290. <https://doi.org/10.1038/s41418-018-0118-3>
- Jafri, A., Siddiqui, S., Rais, J., Ahmad, M. S., Kumar, S., Jafar, T., Afzal, M., & Arshad, M. (2019). Induction of apoptosis by piperine in human cervical adenocarcinoma via ROS mediated mitochondrial pathway and caspase-3 activation. *EXCLI journal*, 18, 154–164. <https://doi.org/10.17179/excli2018-1928>
- Jansson, M. D., Damas, N. D., Lees, M., Jacobsen, A., & Lund, A. H. (2015). miR-339-5p regulates the p53 tumor-suppressor pathway by targeting MDM2. *Oncogene*, 34(15), 1908–1918. <https://doi.org/10.1038/onc.2014.130>
- Kabacik, S., Lowe, D., Fransen, L., Leonard, M., Ang, S. L., Whiteman, C., Corsi, S., Cohen, H., Felton, S., Bali, R., Horvath, S., & Raj, K. (2022). The relationship between epigenetic age and the hallmarks of aging in human cells. *Nature aging*, 2(6), 484–493. <https://doi.org/10.1038/s43587-022-00220-0>
- Kang, M., Lee, K. H., Lee, H. S., Jeong, C. W., Ku, J. H., Kim, H. H., & Kwak, C. (2017). Concurrent treatment with simvastatin and NF- $\kappa$ B inhibitor in human castration-resistant prostate cancer cells exerts synergistic anti-cancer effects via control of the NF- $\kappa$ B/LIN28/let-7 miRNA signaling pathway. *PloS one*, 12(9), e0184644. <https://doi.org/10.1371/journal.pone.0184644>

- Kent W. J. (2002). BLAT--the BLAST-like alignment tool. *Genome research*, 12(4), 656–664. <https://doi.org/10.1101/gr.229202>
- Kirkwood, T.B. L., (1977). Evolution of ageing. *Nature*, 270: 301-304
- Klapproth, C., Sen, R., Stadler, P. F., Findeiß, S., & Fallmann, J. (2021). Common Features in lncRNA Annotation and Classification: A Survey. *Non-coding RNA*, 7(4), 77. <https://doi.org/10.3390/ncrna7040077>
- Korolchuk, V. I., Miwa, S., Carroll, B., & von Zglinicki, T. (2017). Mitochondria in Cell Senescence: Is Mitophagy the Weakest Link?. *EbioMedicine*, 21, 7–13. <https://doi.org/10.1016/j.ebiom.2017.03.020>
- Kotake, Y., Nakagawa, T., Kitagawa, K., Suzuki, S., Liu, N., Kitagawa, M., & Xiong, Y. (2011). Long non-coding RNA ANRIL is required for the PRC2 recruitment to and silencing of p15(INK4B) tumor suppressor gene. *Oncogene*, 30(16), 1956–1962. <https://doi.org/10.1038/onc.2010.568>
- Kozomara, A., & Griffiths-Jones, S. (2014). miRBase: annotating high confidence microRNAs using deep sequencing data. *Nucleic acids research*, 42(Database issue), D68–D73. <https://doi.org/10.1093/nar/gkt1181>
- Kujoth, G. C., Leeuwenburgh, C., & Prolla, T. A. (2006). Mitochondrial DNA mutations and apoptosis in mammalian aging. *Cancer research*, 66(15), 7386–7389. <https://doi.org/10.1158/0008-5472.CAN-05-4670>
- Kuleshov, M. V., Jones, M. R., Rouillard, A. D., Fernandez, N. F., Duan, Q., Wang, Z., Koplev, S., Jenkins, S. L., Jagodnik, K. M., Lachmann, A., McDermott, M. G., Monteiro, C. D., Gundersen, G. W., & Ma'ayan, A. (2016). Enrichr: a comprehensive gene set enrichment analysis web server 2016 update. *Nucleic acids research*, 44(W1), W90–W97. <https://doi.org/10.1093/nar/gkw377>
- Kumar, R., & Reichert, A. S. (2021). Autophagy promotes mitochondrial respiration by providing serine for one-carbon-metabolism. *Autophagy*, 17(12), 4480–4483. <https://doi.org/10.1080/15548627.2021.1909408>

- Lai, R. W., Lu, R., Danthi, P. S., Bravo, J. I., Goumba, A., Sampathkumar, N. K., & Benayoun, B. A. (2019). Multi-level remodeling of transcriptional landscapes in aging and longevity. *BMB reports*, *52*(1), 86–108. <https://doi.org/10.5483/BMBRep.2019.52.1.296>
- Langmead, B., & Salzberg, S. L. (2012). Fast gapped-read alignment with Bowtie 2. *Nature methods*, *9*(4), 357–359. <https://doi.org/10.1038/nmeth.1923>
- Lee, Y. S., & Dutta, A. (2007). The tumor suppressor microRNA let-7 represses the HMGA2 oncogene. *Genes & development*, *21*(9), 1025–1030. <https://doi.org/10.1101/gad.1540407>
- Li, F., Huangyang, P., Burrows, M., Guo, K., Riscal, R., Godfrey, J., Lee, K. E., Lin, N., Lee, P., Blair, I. A., Keith, B., Li, B., & Simon, M. C. (2020). FBP1 loss disrupts liver metabolism and promotes tumorigenesis through a hepatic stellate cell senescence secretome. *Nature cell biology*, *22*(6), 728–739. <https://doi.org/10.1038/s41556-020-0511-2>
- Li, J., Sun, Z., Cui, Y., Qin, L., Wu, F., Li, Y., Du, N., & Li, X. (2022). Knockdown of LMNB1 Inhibits the Proliferation of Lung Adenocarcinoma Cells by Inducing DNA Damage and Cell Senescence. *Frontiers in oncology*, *12*, 913740. <https://doi.org/10.3389/fonc.2022.913740>
- Lim, S., & Ganem, N. J. (2014). Tetraploidy and tumor development. *Oncotarget*, *5*(22), 10959–10960. <https://doi.org/10.18632/oncotarget.2790>
- Lisitsyn, N., Lisitsyn, N., & Wigler, M. (1993). Cloning the differences between two complex genomes. *Science (New York, N.Y.)*, *259*(5097), 946–951. <https://doi.org/10.1126/science.8438152>
- Liu, L., Wylie, R. C., Andrews, L. G., & Tollefsbol, T. O. (2003). Aging, cancer and nutrition: the DNA methylation connection. *Mechanisms of ageing and development*, *124*(10-12), 989–998. <https://doi.org/10.1016/j.mad.2003.08.001>
- Liu, N., Landreh, M., Cao, K., Abe, M., Hendriks, G. J., Kennerdell, J. R., Zhu, Y., Wang, L. S., & Bonini, N. M. (2012). The microRNA miR-34 modulates ageing and

neurodegeneration in *Drosophila*. *Nature*, 482(7386), 519–523.  
<https://doi.org/10.1038/nature10810>

Livingston, M. J., Wang, J., Zhou, J., Wu, G., Ganley, I. G., Hill, J. A., Yin, X. M., & Dong, Z. (2019). Clearance of damaged mitochondria via mitophagy is important to the protective effect of ischemic preconditioning in kidneys. *Autophagy*, 15(12), 2142–2162.  
<https://doi.org/10.1080/15548627.2019.1615822>

López-Otín, C., Blasco, M. A., Partridge, L., Serrano, M., & Kroemer, G. (2013). The hallmarks of aging. *Cell*, 153(6), 1194–1217. <https://doi.org/10.1016/j.cell.2013.05.039>

López-Otín, C., Blasco, M. A., Partridge, L., Serrano, M., & Kroemer, G. (2023). Hallmarks of aging: An expanding universe. *Cell*, 186(2), 243–278.  
<https://doi.org/10.1016/j.cell.2022.11.001>

Love MI, Huber W, Anders S (2014). “Moderated estimation of fold change and dispersion for RNA-seq data with DESeq2.” *Genome Biology*, 15, 550.  
[doi:10.1186/s13059-014-0550-8](https://doi.org/10.1186/s13059-014-0550-8)

Lyu, G., Guan, Y., Zhang, C., Zong, L., Sun, L., Huang, X., Huang, L., Zhang, L., Tian, X. L., Zhou, Z., & Tao, W. (2018). TGF- $\beta$  signaling alters H4K20me3 status via miR-29 and contributes to cellular senescence and cardiac aging. *Nature communications*, 9(1), 2560. <https://doi.org/10.1038/s41467-018-04994-z>

Ma, J., Zhan, Y., Xu, Z., Li, Y., Luo, A., Ding, F., Cao, X., Chen, H., & Liu, Z. (2017). ZEB1 induced miR-99b/let-7e/miR-125a cluster promotes invasion and metastasis in esophageal squamous cell carcinoma. *Cancer letters*, 398, 37–45.  
<https://doi.org/10.1016/j.canlet.2017.04.006>

Maegawa, S., Hinkal, G., Kim, H. S., Shen, L., Zhang, L., Zhang, J., Zhang, N., Liang, S., Donehower, L. A., & Issa, J. P. (2010). Widespread and tissue specific age-related DNA methylation changes in mice. *Genome research*, 20(3), 332–340.  
<https://doi.org/10.1101/gr.096826.109>

Mei, L., Ding, X., Tsang, S. Y., Pun, F. W., Ng, S. K., Yang, J., Zhao, C., Li, D., Wan, W., Yu, C. H., Tan, T. C., Poon, W. S., Leung, G. K., Ng, H. K., Zhang, L., & Xue, H.

- (2011). AluScan: a method for genome-wide scanning of sequence and structure variations in the human genome. *BMC genomics*, *12*, 564. <https://doi.org/10.1186/1471-2164-12-564>
- Meng, Z., Moroishi, T., & Guan, K. L. (2016). Mechanisms of Hippo pathway regulation. *Genes & development*, *30*(1), 1–17. <https://doi.org/10.1101/gad.274027.115>
- Mitelman F, Johansson B, Mertens F. (2010) Mitelman Database of Chromosome Aberrations and Gene Fusions in Cancer. <http://cgapnc.nih.gov/Chromosomes/Mitelman>.
- Miwa, S., Kashyap, S., Chini, E., & von Zglinicki, T. (2022). Mitochondrial dysfunction in cell senescence and aging. *The Journal of clinical investigation*, *132*(13), e158447. <https://doi.org/10.1172/JCI158447>
- Möhner, J., Scheuren, M., Woronzow, V., Schumann, S., & Zischler, H. (2023). RDA coupled with deep sequencing detects somatic SVA-retrotranspositions and mosaicism in the human brain. *Frontiers in cell and developmental biology*, *11*, 1201258. <https://doi.org/10.3389/fcell.2023.1201258>
- Morgan, R. G., Venturelli, M., Gross, C., Tarperi, C., Schena, F., Reggiani, C., Naro, F., Pedrinolla, A., Monaco, L., Richardson, R. S., & Donato, A. J. (2017). Age-Associated ALU Element Instability in White Blood Cells Is Linked to Lower Survival in Elderly Adults: A Preliminary Cohort Study. *PloS one*, *12*(1), e0169628. <https://doi.org/10.1371/journal.pone.0169628>
- Munk, R., Panda, A. C., Grammatikakis, I., Gorospe, M., & Abdelmohsen, K. (2017). Senescence-Associated MicroRNAs. *International review of cell and molecular biology*, *334*, 177–205. <https://doi.org/10.1016/bs.ircmb.2017.03.008>
- Pan, Y., Huang, Q., Peng, X., Yu, S., & Liu, N. (2022). Circ\_0015756 promotes ovarian cancer progression via the miR-145-5p/PSAT1 axis. *Reproductive biology*, *22*(4), 100702. <https://doi.org/10.1016/j.repbio.2022.100702>
- Patro, R., Duggal, G., Love, M. I., Irizarry, R. A., & Kingsford, C. (2017). Salmon provides fast and bias-aware quantification of transcript expression. *Nature Methods*.

- Pegoraro, G., & Misteli, T. (2009). The central role of chromatin maintenance in aging. *Aging, 1*(12), 1017–1022. <https://doi.org/10.18632/aging.100106>
- Peleg, S., Feller, C., Ladurner, A. G., & Imhof, A. (2016). The Metabolic Impact on Histone Acetylation and Transcription in Ageing. *Trends in biochemical sciences, 41*(8), 700–711. <https://doi.org/10.1016/j.tibs.2016.05.008>
- Quast, C., Pruesse, E., Yilmaz, P., Gerken, J., Schweer, T., Yarza, P., Peplies, J., & Glöckner, F. O. (2013). The SILVA ribosomal RNA gene database project: improved data processing and web-based tools. *Nucleic acids research, 41*(Database issue), D590–D596. <https://doi.org/10.1093/nar/gks1219>
- Quinlan, A. R., & Hall, I. M. (2010). BEDTools: a flexible suite of utilities for comparing genomic features. *Bioinformatics (Oxford, England), 26*(6), 841–842. <https://doi.org/10.1093/bioinformatics/btq033>
- Raiz, J., Damert, A., Chira, S., Held, U., Klawitter, S., Hamdorf, M., Löwer, J., Strätling, W. H., Löwer, R., & Schumann, G. G. (2012). The non-autonomous retrotransposon SVA is trans-mobilized by the human LINE-1 protein machinery. *Nucleic acids research, 40*(4), 1666–1683. <https://doi.org/10.1093/nar/gkr863>
- Rieder, C. L., & Palazzo, R. E. (1992). Colcemid and the mitotic cycle. *Journal of cell science, 102 (Pt 3)*, 387–392. <https://doi.org/10.1242/jcs.102.3.387>
- Rokas, A., & Holland, P. W. (2000). Rare genomic changes as a tool for phylogenetics. *Trends in ecology & evolution, 15*(11), 454–459. [https://doi.org/10.1016/s0169-5347\(00\)01967-4](https://doi.org/10.1016/s0169-5347(00)01967-4)
- Rosenkranz D. (2016). piRNA cluster database: a web resource for piRNA producing loci. *Nucleic acids research, 44*(D1), D223–D230. <https://doi.org/10.1093/nar/gkv1265>
- Rusu-Nastase, E. G., Lupan, A. M., Marinescu, C. I., Neculachi, C. A., Preda, M. B., & Burlacu, A. (2022). MiR-29a Increase in Aging May Function as a Compensatory Mechanism Against Cardiac Fibrosis Through SERPINH1 Downregulation. *Frontiers in cardiovascular medicine, 8*, 810241. <https://doi.org/10.3389/fcvm.2021.810241>

- Salminen, A., Ojala, J., & Kaarniranta, K. (2011). Apoptosis and aging: increased resistance to apoptosis enhances the aging process. *Cellular and molecular life sciences : CMLS*, *68*(6), 1021–1031. <https://doi.org/10.1007/s00018-010-0597-y>
- Samper, E., Flores, J. M., & Blasco, M. A. (2001). Restoration of telomerase activity rescues chromosomal instability and premature aging in *Terc*<sup>-/-</sup> mice with short telomeres. *EMBO reports*, *2*(9), 800–807. <https://doi.org/10.1093/embo-reports/kve174>
- Saul, D., Kosinsky, R. L., Atkinson, E. J., Doolittle, M. L., Zhang, X., LeBrasseur, N. K., Pignolo, R. J., Robbins, P. D., Niedernhofer, L. J., Ikeno, Y., Jurk, D., Passos, J. F., Hickson, L. J., Xue, A., Monroe, D. G., Tchkonina, T., Kirkland, J. L., Farr, J. N., & Khosla, S. (2022). A new gene set identifies senescent cells and predicts senescence-associated pathways across tissues. *Nature communications*, *13*(1), 4827. <https://doi.org/10.1038/s41467-022-32552-1>
- Scholtz, B., Horváth, J., Tar, I., Kiss, C., & Márton, I. J. (2022). Salivary miR-31-5p, miR-345-3p, and miR-424-3p Are Reliable Biomarkers in Patients with Oral Squamous Cell Carcinoma. *Pathogens (Basel, Switzerland)*, *11*(2), 229. <https://doi.org/10.3390/pathogens11020229>
- Schultz, J., Lorenz, P., Gross, G., Ibrahim, S., & Kunz, M. (2008). MicroRNA let-7b targets important cell cycle molecules in malignant melanoma cells and interferes with anchorage-independent growth. *Cell research*, *18*(5), 549–557. <https://doi.org/10.1038/cr.2008.45>
- Shaban, H. A., & Gasser, S. M. (2023). Dynamic 3D genome reorganization during senescence: defining cell states through chromatin. *Cell death and differentiation*, [10.1038/s41418-023-01197-y](https://doi.org/10.1038/s41418-023-01197-y). Advance online publication. <https://doi.org/10.1038/s41418-023-01197-y>
- Shah, P. P., Donahue, G., Otte, G. L., Capell, B. C., Nelson, D. M., Cao, K., Aggarwala, V., Cruickshanks, H. A., Rai, T. S., McBryan, T., Gregory, B. D., Adams, P. D., & Berger, S. L. (2013). Lamin B1 depletion in senescent cells triggers large-scale changes in gene expression and the chromatin landscape. *Genes & development*, *27*(16), 1787–1799. <https://doi.org/10.1101/gad.223834.113>



- Shang, J., Yao, Y., Fan, X., Shangguan, L., Li, J., Liu, H., & Zhou, Y. (2016). miR-29c-3p promotes senescence of human mesenchymal stem cells by targeting CNOT6 through p53-p21 and p16-pRB pathways. *Biochimica et biophysica acta*, 1863(4), 520–532. <https://doi.org/10.1016/j.bbamcr.2016.01.005>
- Sherwood, S. W., Rush, D., Ellsworth, J. L., & Schimke, R. T. (1988). Defining cellular senescence in IMR-90 cells: a flow cytometric analysis. *Proceedings of the National Academy of Sciences of the United States of America*, 85(23), 9086–9090. <https://doi.org/10.1073/pnas.85.23.9086>
- Shi, W., Zhang, Z., Yang, B., Guo, H., Jing, L., Liu, T., Luo, Y., Liu, H., Li, Y., & Gao, Y. (2017). Overexpression of microRNA let-7 correlates with disease progression and poor prognosis in hepatocellular carcinoma. *Medicine*, 96(32), e7764. <https://doi.org/10.1097/MD.00000000000007764>
- Shin, J. A., Li, C., Choi, E. S., Cho, S. D., & Cho, N. P. (2013). High expression of microRNA-127 is involved in cell cycle arrest in MC-3 mucoepidermoid carcinoma cells. *Molecular medicine reports*, 7(2), 708–712. <https://doi.org/10.3892/mmr.2012.1222>
- Simon, M., Van Meter, M., Ablueva, J., Ke, Z., Gonzalez, R. S., Taguchi, T., De Cecco, M., Leonova, K. I., Kogan, V., Helfand, S. L., Neretti, N., Roichman, A., Cohen, H. Y., Meer, M. V., Gladyshev, V. N., Antoch, M. P., Gudkov, A. V., Sedivy, J. M., Seluanov, A., & Gorbunova, V. (2019). LINE1 Derepression in Aged Wild-Type and SIRT6-Deficient Mice Drives Inflammation. *Cell metabolism*, 29(4), 871–885.e5. <https://doi.org/10.1016/j.cmet.2019.02.014>
- Singh, D. K., & Prasanth, K. V. (2013). Functional insights into the role of nuclear-retained long noncoding RNAs in gene expression control in mammalian cells. *Chromosome research : an international journal on the molecular, supramolecular and evolutionary aspects of chromosome biology*, 21(6-7), 695–711. <https://doi.org/10.1007/s10577-013-9391-7>
- Singh, K. K., Choudhury, A. R., & Tiwari, H. K. (2017). Numtogenesis as a mechanism for development of cancer. *Seminars in cancer biology*, 47, 101–109. <https://doi.org/10.1016/j.semcancer.2017.05.003>

- Soneson C, Love MI, Robinson MD (2015). “Differential analyses for RNA-seq: transcript-level estimates improve gene-level inferences.” *F1000Research*, 4. doi:10.12688/f1000research.7563.1
- Srinivas, U. S., Tan, B. W. Q., Vellayappan, B. A., & Jeyasekharan, A. D. (2019). ROS and the DNA damage response in cancer. *Redox biology*, 25, 101084. <https://doi.org/10.1016/j.redox.2018.101084>
- Srinivasainagendra, V., Sandel, M. W., Singh, B., Sundaresan, A., Mooga, V. P., Bajpai, P., Tiwari, H. K., & Singh, K. K. (2017). Migration of mitochondrial DNA in the nuclear genome of colorectal adenocarcinoma. *Genome medicine*, 9(1), 31. <https://doi.org/10.1186/s13073-017-0420-6>
- Stein, G. H., Drullinger, L. F., Soulard, A., & Dulić, V. (1999). Differential roles for cyclin-dependent kinase inhibitors p21 and p16 in the mechanisms of senescence and differentiation in human fibroblasts. *Molecular and cellular biology*, 19(3), 2109–2117. <https://doi.org/10.1128/MCB.19.3.2109>
- Storchova, Z., & Kuffer, C. (2008). The consequences of tetraploidy and aneuploidy. *Journal of cell science*, 121(Pt 23), 3859–3866. <https://doi.org/10.1242/jcs.039537>
- Storer, J., Hubley, R., Rosen, J., Wheeler, T. J., & Smit, A. F. (2021). The Dfam community resource of transposable element families, sequence models, and genome annotations. *Mobile DNA*, 12(1), 2. <https://doi.org/10.1186/s13100-020-00230-y>
- Sturmlechner, I., Durik, M., Sieben, C. J., Baker, D. J., & van Deursen, J. M. (2017). Cellular senescence in renal ageing and disease. *Nature reviews. Nephrology*, 13(2), 77–89. <https://doi.org/10.1038/nrneph.2016.183>
- Sun, J., Deng, L., & Gong, Y. (2021). MiR-145-5p Inhibits the Invasion of Prostate Cancer and Induces Apoptosis by Inhibiting WIP1. *Journal of oncology*, 2021, 4412705. <https://doi.org/10.1155/2021/4412705>
- Szklarczyk, R., Nootboom, M., & Osiewacz, H. D. (2014). Control of mitochondrial integrity in ageing and disease. *Philosophical transactions of the Royal Society of*

---

*London. Series B, Biological sciences*, 369(1646), 20130439.  
<https://doi.org/10.1098/rstb.2013.0439>

Taimen, P., Pflieger, K., Shimi, T., Möller, D., Ben-Harush, K., Erdos, M. R., Adam, S. A., Herrmann, H., Medalia, O., Collins, F. S., Goldman, A. E., & Goldman, R. D. (2009). A progeria mutation reveals functions for lamin A in nuclear assembly, architecture, and chromosome organization. *Proceedings of the National Academy of Sciences of the United States of America*, 106(49), 20788–20793.  
<https://doi.org/10.1073/pnas.0911895106>

Tanaka, K., Goto, H., Nishimura, Y., Kasahara, K., Mizoguchi, A., & Inagaki, M. (2018). Tetraploidy in cancer and its possible link to aging. *Cancer science*, 109(9), 2632–2640.  
<https://doi.org/10.1111/cas.13717>

Tang, R., Yang, C., Ma, X., Wang, Y., Luo, D., Huang, C., Xu, Z., Liu, P., & Yang, L. (2016). MiR-let-7a inhibits cell proliferation, migration, and invasion by down-regulating PKM2 in gastric cancer. *Oncotarget*, 7(5), 5972–5984.  
<https://doi.org/10.18632/oncotarget.6821>

Tang, Z., Ow, G. S., Thiery, J. P., Ivshina, A. V., & Kuznetsov, V. A. (2014). Meta-analysis of transcriptome reveals let-7b as an unfavorable prognostic biomarker and predicts molecular and clinical subclasses in high-grade serous ovarian carcinoma. *International journal of cancer*, 134(2), 306–318. <https://doi.org/10.1002/ijc.28371>

Tolkach, Y., Stahl, A. F., Niehoff, E. M., Zhao, C., Kristiansen, G., Müller, S. C., & Ellinger, J. (2017). YRNA expression predicts survival in bladder cancer patients. *BMC cancer*, 17(1), 749. <https://doi.org/10.1186/s12885-017-3746-y>

Tripathi, V., Shen, Z., Chakraborty, A., Giri, S., Freier, S. M., Wu, X., Zhang, Y., Gorospe, M., Prasanth, S. G., Lal, A., & Prasanth, K. V. (2013). Long noncoding RNA MALAT1 controls cell cycle progression by regulating the expression of oncogenic transcription factor B-MYB. *PLoS genetics*, 9(3), e1003368.  
<https://doi.org/10.1371/journal.pgen.1003368>

Victorelli, S., Salmonowicz, H., Chapman, J., Martini, H., Vizioli, M. G., Riley, J. S., Cloix, C., Hall-Younger, E., Machado Espindola-Netto, J., Jurk, D., Lagnado, A. B., Sales

- Gomez, L., Farr, J. N., Saul, D., Reed, R., Kelly, G., Eppard, M., Greaves, L. C., Dou, Z., Pirijs, N., Szczepanowska, K., Porritt, R. A., Huang, H., Huang, T. Y., Mann, D. A., Masuda, C. A., Khosla, S., Dai, H., Kaufmann, S. H., Zacharioudakis, E., Gavathiotis, E., LeBrasseur, N. K., Lei, X., Sainz, A. G., Korolchuk, V. I., Adams, P. D., Shadel, G. S., Tait, S. W. G. & Passos, J. F. (2023). Apoptotic stress causes mtDNA release during senescence and drives the SASP. *Nature*, 622(7983), 627–636. <https://doi.org/10.1038/s41586-023-06621-4>
- Vukic, M., & Daxinger, L. (2019). DNA methylation in disease: Immunodeficiency, Centromeric instability, Facial anomalies syndrome. *Essays in biochemistry*, 63(6), 773–783. <https://doi.org/10.1042/EBC20190035>
- Wang, C., Jurk, D., Maddick, M., Nelson, G., Martin-Ruiz, C., & von Zglinicki, T. (2009). DNA damage response and cellular senescence in tissues of aging mice. *Aging cell*, 8(3), 311–323. <https://doi.org/10.1111/j.1474-9726.2009.00481.x>
- Wang, H., Xing, J., Grover, D., Hedges, D. J., Han, K., Walker, J. A., & Batzer, M. A. (2005). SVA elements: a hominid-specific retroposon family. *Journal of molecular biology*, 354(4), 994–1007. <https://doi.org/10.1016/j.jmb.2005.09.085>
- Wang, S., Zhan, J., Lin, X., Wang, Y., Wang, Y., & Liu, Y. (2020). CircRNA-0077930 from hyperglycaemia-stimulated vascular endothelial cell exosomes regulates senescence in vascular smooth muscle cells. *Cell biochemistry and function*, 38(8), 1056–1068. <https://doi.org/10.1002/cbf.3543>
- Wang, Y., Zhao, J., Chen, S., Li, D., Yang, J., Zhao, X., Qin, M., Guo, M., Chen, C., He, Z., Zhou, Y., & Xu, L. (2022). Let-7 as a Promising Target in Aging and Aging-Related Diseases: A Promise or a Pledge. *Biomolecules*, 12(8), 1070. <https://doi.org/10.3390/biom12081070>
- West, A. P., Khoury-Hanold, W., Staron, M., Tal, M. C., Pineda, C. M., Lang, S. M., Bestwick, M., Duguay, B. A., Raimundo, N., MacDuff, D. A., Kaech, S. M., Smiley, J. R., Means, R. E., Iwasaki, A., & Shadel, G. S. (2015). Mitochondrial DNA stress primes the antiviral innate immune response. *Nature*, 520(7548), 553–557. <https://doi.org/10.1038/nature14156>

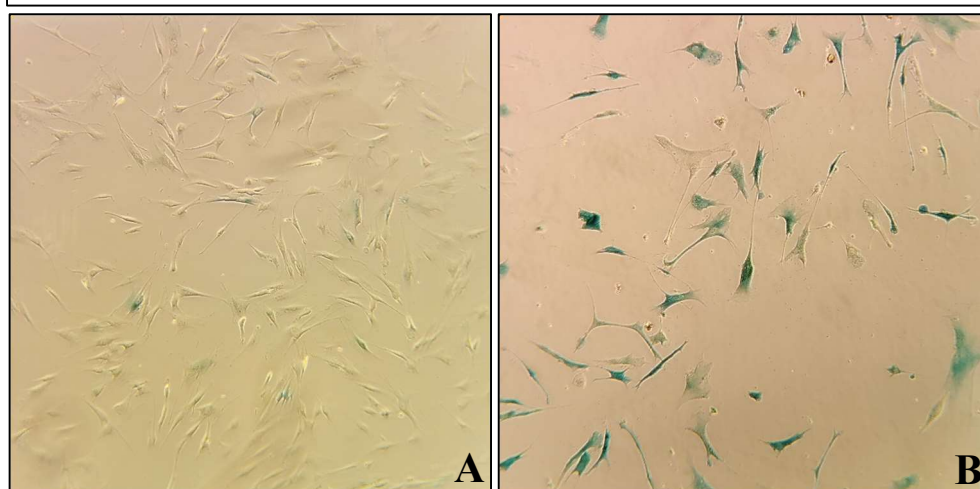
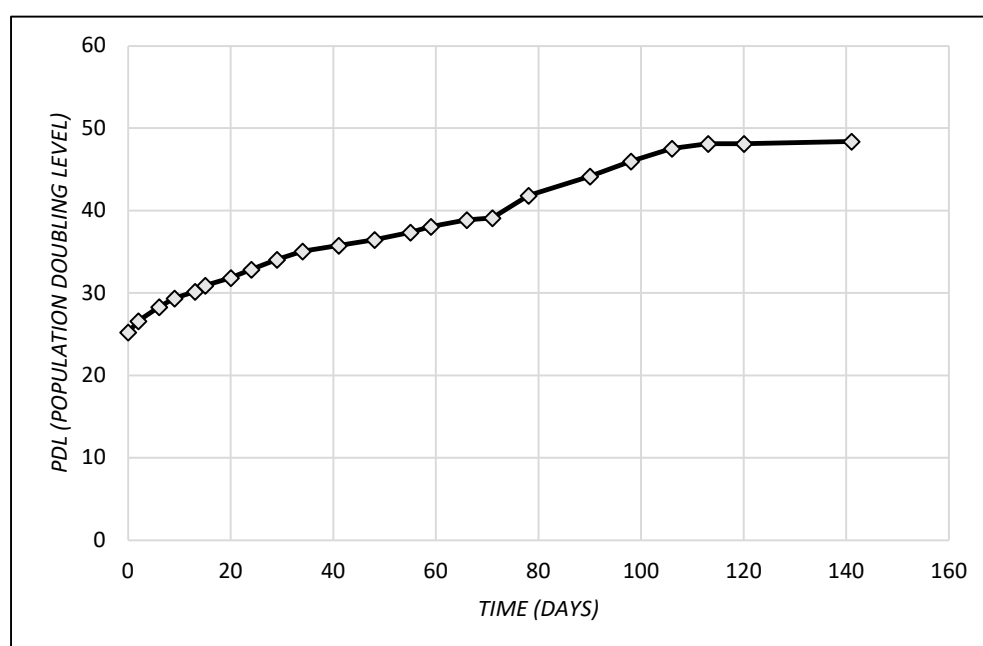
- Williams, G. C. (1957). Pleiotropy, Natural Selection, and the Evolution of Senescence. *Evolution*, *11*(4), 398–411. <https://doi.org/10.2307/2406060>
- Witkiewicz, A. K., Knudsen, K. E., Dicker, A. P., & Knudsen, E. S. (2011). The meaning of p16(ink4a) expression in tumors: functional significance, clinical associations and future developments. *Cell cycle (Georgetown, Tex.)*, *10*(15), 2497–2503. <https://doi.org/10.4161/cc.10.15.16776>
- Xia, X., Chen, W., McDermott, J., & Han, J. J. (2017). Molecular and phenotypic biomarkers of aging. *F1000Research*, *6*, 860. <https://doi.org/10.12688/f1000research.10692.1>
- Xie, Z., Bailey, A., Kuleshov, M. V., Clarke, D. J. B., Evangelista, J. E., Jenkins, S. L., Lachmann, A., Wojciechowicz, M. L., Kropiwnicki, E., Jagodnik, K. M., Jeon, M., & Ma'ayan, A. (2021). Gene Set Knowledge Discovery with Enrichr. *Current protocols*, *1*(3), e90. <https://doi.org/10.1002/cpz1.90>
- Xu, C., Wang, L., Fozouni, P., Evjen, G., Chandra, V., Jiang, J., Lu, C., Nicastri, M., Bretz, C., Winkler, J. D., Amaravadi, R., Garcia, B. A., Adams, P. D., Ott, M., Tong, W., Johansen, T., Dou, Z., & Berger, S. L. (2020). SIRT1 is downregulated by autophagy in senescence and ageing. *Nature cell biology*, *22*(10), 1170–1179. <https://doi.org/10.1038/s41556-020-00579-5>
- Yang, N. C., & Hu, M. L. (2005). The limitations and validities of senescence associated-beta-galactosidase activity as an aging marker for human foreskin fibroblast Hs68 cells. *Experimental gerontology*, *40*(10), 813–819. <https://doi.org/10.1016/j.exger.2005.07.011>
- Yang, Y., Gao, L., Chen, J., Xiao, W., Liu, R., & Kan, H. (2022). Lamin B1 is a potential therapeutic target and prognostic biomarker for hepatocellular carcinoma. *Bioengineered*, *13*(4), 9211–9231. <https://doi.org/10.1080/21655979.2022.2057896>
- Yap, K. L., Li, S., Muñoz-Cabello, A. M., Raguz, S., Zeng, L., Mujtaba, S., Gil, J., Walsh, M. J., & Zhou, M. M. (2010). Molecular interplay of the noncoding RNA ANRIL and methylated histone H3 lysine 27 by polycomb CBX7 in transcriptional silencing of INK4a. *Molecular cell*, *38*(5), 662–674. <https://doi.org/10.1016/j.molcel.2010.03.021>

- Yates, A., Akanni, W., Amode, M. R., Barrell, D., Billis, K., Carvalho-Silva, D., Cummins, C., Clapham, P., Fitzgerald, S., Gil, L., Girón, C. G., Gordon, L., Hourlier, T., Hunt, S. E., Janacek, S. H., Johnson, N., Juettemann, T., Keenan, S., Lavidas, I., Martin, F. J., et al., Flicek, P. (2016). Ensembl 2016. *Nucleic acids research*, *44*(D1), D710–D716. <https://doi.org/10.1093/nar/gkv1157>
- Yoon, J. H., Abdelmohsen, K., & Gorospe, M. (2013). Posttranscriptional gene regulation by long noncoding RNA. *Journal of molecular biology*, *425*(19), 3723–3730. <https://doi.org/10.1016/j.jmb.2012.11.024>
- Young, J. I., & Smith, J. R. (2001). DNA methyltransferase inhibition in normal human fibroblasts induces a p21-dependent cell cycle withdrawal. *The Journal of biological chemistry*, *276*(22), 19610–19616. <https://doi.org/10.1074/jbc.M009470200>
- Zasadil, L. M., Britigan, E. M., & Weaver, B. A. (2013). 2n or not 2n: Aneuploidy, polyploidy and chromosomal instability in primary and tumor cells. *Seminars in cell & developmental biology*, *24*(4), 370–379. <https://doi.org/10.1016/j.semcdb.2013.02.001>
- Zhang, M., Zeng, J., Zhao, Z., & Liu, Z. (2017). Loss of MiR-424-3p, not miR-424-5p, confers chemoresistance through targeting YAP1 in non-small cell lung cancer. *Molecular carcinogenesis*, *56*(3), 821–832. <https://doi.org/10.1002/mc.22536>
- Zhou, W., Karan, K. R., Gu, W., Klein, H. U., Sturm, G., De Jager, P. L., Bennett, D. A., Hirano, M., Picard, M., & Mills, R. E. (2023). Somatic nuclear mitochondrial DNA insertions are prevalent in the human brain and accumulate over time in fibroblasts. *bioRxiv: the preprint server for biology*, 2023.02.03.527065. <https://doi.org/10.1101/2023.02.03.527065>

## Supplement

**Supplementary Table 1** – provided clean read counts (clean tag count) by BGI for the sequenced RNA samples; SE50: single-end 50 nt in length.

Sample name	Sequence type	Clean tag count
IMR-90_Prolif_1	SE50	25,607,547
IMR-90_Prolif_2	SE50	23,769,239
IMR-90_Sen_1	SE50	29,804,305
IMR-90_Sen_2	SE50	22,446,258
IMR-90_Tetra_1	SE50	21,870,936
IMR-90_Tetra_2	SE50	25,276,786
Cja_Prolif	SE50	22,144,299
Cja_Sen	SE50	20,261,744



**Supplementary Figure 1** – assessment of cellular senescence in IMR-90 cells; diagram depicting population doubling level (y-axis) over a time span (x-axis: time in days); (A) negative SA-β-Gal assay of proliferating IMR-90 cells (control; 100x) (B) positive SA-β-Gal assay of senescent IMR-90 cells (100x).

**Supplementary Table 2** – Unitas annotation of small RNA sequencing data for proliferating IMR-90 cells (n=2).

<b>Unitas Annotation</b>	<b>Proliferating 1</b>	<b>Unitas Annotation</b>	<b>Proliferating 2</b>
low complexity	78773	low complexity	82366
miRNA	18516761	miRNA	20714389
miRNA:homo sapiens	18445076	miRNA:homo sapiens	20623982
miRNA:other	71685	miRNA:other	90407
rRNA	721131	rRNA	761057
genomic rRNA	697010	genomic rRNA	688339
Mt rRNA	24121	Mt rRNA	72718
tRNA	864842	tRNA	1405954
genomic tRNA	836416	genomic tRNA	1271694
5'tR-halves	50249	5'tR-halves	459728
5'tRFs	128506	5'tRFs	239831
3'tR-halves	2850	3'tR-halves	9044
3'tRFs	5866	3'tRFs	6726
3'CCA-tRFs	164932	3'CCA-tRFs	71306
tRF-1	69420	tRF-1	63218
tRNA-leader	1065	tRNA-leader	2188
misc-tRFs	413528	misc-tRFs	419652
Mt tRNA	28426	Mt tRNA	134260
5'tR-halves	980	5'tR-halves	6371
5'tRFs	8419	5'tRFs	40959
3'tR-halves	260	3'tR-halves	2403
3'tRFs	742	3'tRFs	3155
3'CCA-tRFs	4643	3'CCA-tRFs	16377
tRF-1	3291	tRF-1	12024
tRNA-leader	571	tRNA-leader	2451
misc-tRFs	9522	misc-tRFs	50521
scaRNA	315	scaRNA	728
protein coding	39858	protein coding	114062
misc RNA	92946	vault RNA	307
scRNA	12	ribozyme	107
snoRNA	38335	snRNA	15021
ribozyme	91	scRNA	19
lncRNA	155364	misc RNA	133656
vault RNA	132	snoRNA	57817
sRNA	33	lncRNA	246836
snRNA	6670	sRNA	36
no annotation	3253977	no annotation	2075194
mapped to piRNA producing loci	38116	mapped to piRNA producing loci	33697



**Supplementary Table 3 - Unitas annotation of small RNA sequencing data for senescent IMR-90 cells (n=2).**

<b>Unitas Annotation</b>	<b>Senescent 1</b>	<b>Unitas Annotation</b>	<b>Senescent 2</b>
low complexity	77840	low complexity	82553
miRNA	19347552	miRNA	20734974
miRNA:homo sapiens	19211883	miRNA:homo sapiens	20611818
miRNA:other	135669	miRNA:other	123156
rRNA	970895	rRNA	2585251
genomic rRNA	665200	genomic rRNA	2462635
Mt rRNA	305695	Mt rRNA	122616
tRNA	1196060	tRNA	1160308
genomic tRNA	789523	genomic tRNA	952098
5'tR-halves	12319	5'tR-halves	337716
5'tRFs	270847	5'tRFs	226300
3'tR-halves	2771	3'tR-halves	8403
3'tRFs	18539	3'tRFs	9908
3'CCA-tRFs	88768	3'CCA-tRFs	79856
tRF-1	135928	tRF-1	57568
tRNA-leader	3957	tRNA-leader	673
misc-tRFs	256394	misc-tRFs	231674
Mt tRNA	406536	Mt tRNA	208209
5'tR-halves	108	5'tR-halves	5551
5'tRFs	144531	5'tRFs	65761
3'tR-halves	77	3'tR-halves	1138
3'tRFs	8142	3'tRFs	5729
3'CCA-tRFs	56909	3'CCA-tRFs	34940
tRF-1	33755	tRF-1	24612
tRNA-leader	7290	tRNA-leader	3001
misc-tRFs	155724	misc-tRFs	67477
protein coding	109165	snoRNA	134596
scRNA	15	misc RNA	139615
scaRNA	1800	scaRNA	881
lncRNA	284101	vault RNA	544
ribozyme	357	scRNA	54
sRNA	13	sRNA	42
vault RNA	1063	protein coding	275437
snRNA	10740	snRNA	22483
snoRNA	114727	ribozyme	644
misc RNA	164464	lncRNA	406045
no annotation	1864322	no annotation	4260879
mapped to piRNA producing loci	45558	mapped to piRNA producing loci	49329

**Supplementary Table 4 - Unitas annotation of small RNA sequencing data for tetraploid IMR-90 cells (n=2).**

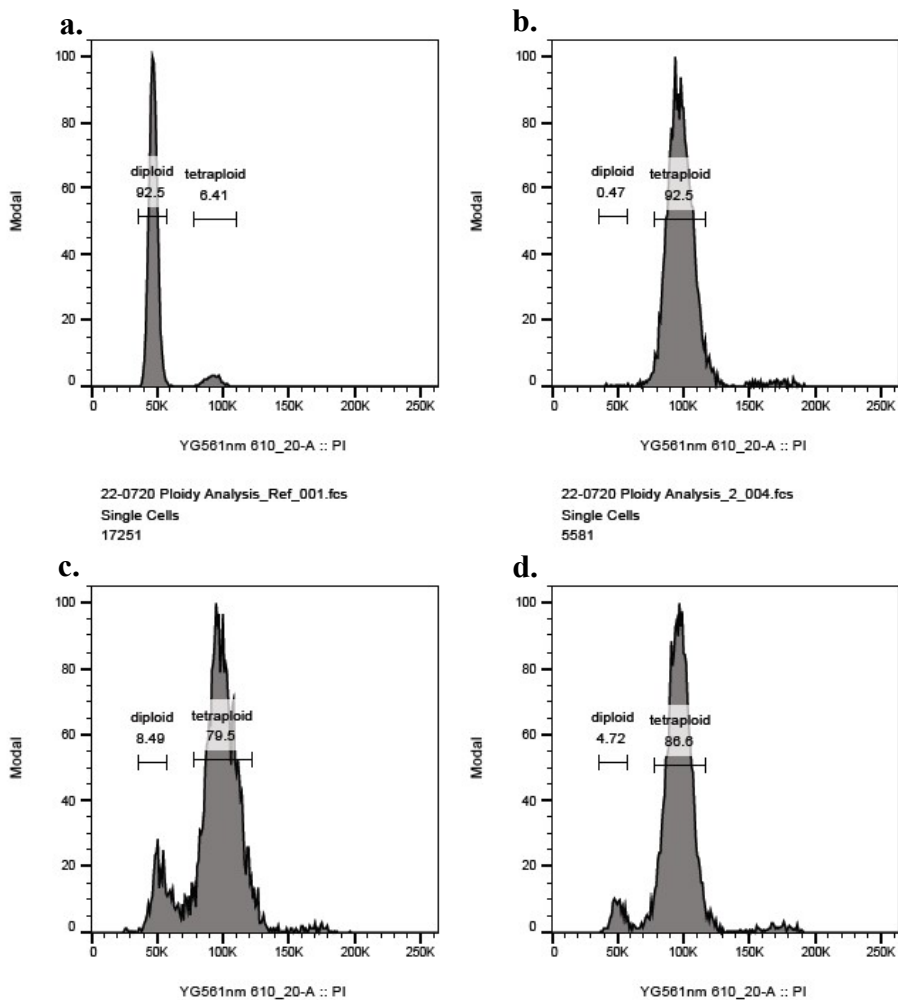
<b>Unitas Annotation</b>	<b>Tetraploid 1</b>	<b>Unitas Annotation</b>	<b>Tetraploid 2</b>
low complexity	91821	low complexity	55392
miRNA	17733302	miRNA	18905392
miRNA:homo sapiens	17621007	miRNA:homo sapiens	18826394
miRNA:other	112295	miRNA:other	78998
rRNA	424658	rRNA	337793
genomic rRNA	410760	genomic rRNA	304017
Mt rRNA	13898	Mt rRNA	33776
tRNA	1201912	tRNA	850019
genomic tRNA	1178048	genomic tRNA	797062
5'tR-halves	7068	5'tR-halves	14331
5'tRFs	538276	5'tRFs	240500
3'tR-halves	1231	3'tR-halves	759
3'tRFs	23384	3'tRFs	7502
3'CCA-tRFs	196959	3'CCA-tRFs	183589
tRF-1	140841	tRF-1	68857
tRNA-leader	1642	tRNA-leader	2037
misc-tRFs	268647	misc-tRFs	279488
Mt tRNA	23864	Mt tRNA	52957
5'tR-halves	58	5'tR-halves	397
5'tRFs	10683	5'tRFs	27096
3'tR-halves	89	3'tR-halves	86
3'tRFs	746	3'tRFs	939
3'CCA-tRFs	2964	3'CCA-tRFs	6484
tRF-1	2557	tRF-1	4025
tRNA-leader	311	tRNA-leader	758
misc-tRFs	6457	misc-tRFs	13173
scaRNA	662	snoRNA	28730
macro lncRNA	181	ribozyme	46
processed transcript	337924	scRNA	4
antisense	17826	lncRNA	133697
snRNA	5785	scaRNA	197
3prime overlapping	104	snRNA	2589
ncRNA		vault RNA	175
snoRNA	84330	sRNA	9
misc RNA	168976	misc RNA	70792
sense intronic	6202	protein coding	44429
scRNA	2	no annotation	1440835
protein coding	72771	mapped to piRNA	
sRNA	36	producing loci	27017
lincRNA	85522		
bidirectional promoter			
lncRNA	1787		
sense overlapping	394		
ribozyme	136		
vaultRNA	293		
no annotation	5042163		
mapped to piRNA			
producing loci	66501		

**Supplementary Table 5.1** – Differentially expressed miRNA in senescent IMR-90 cells (n=2); generated with sRNAde.

name	Young_2	Young_1	Old_1	Old_2	FoldChange	log2FoldChange	pvalue	padj
hsa-miR-4423-3p	0	7.64008497	28.7110717	37.0872505	7.03295898	3.117995469	0.00403948	0.03707521
hsa-miR-122-5p	105.917613	149.527377	922.343178	1655.01855	10.0190792	3.335116104	7.01E-12	1.62E-09
hsa-miR-432-5p	15653.7842	16721.9631	44264.3975	42234.0337	2.67160128	1.417762586	4.79E-09	3.42E-07
hsa-miR-27a-5p	2408.83917	1598.96064	907.090421	926.254082	0.45771475	-1.128380557	0.00331419	0.03366391
hsa-miR-302d-3p	46.1423262	37.1089841	279.035728	84.3734949	4.28625931	2.126003124	0.00223137	0.02419528
hsa-miR-429	69.2134894	63.3035612	224.305248	163.183902	2.89546305	1.547965666	0.00165744	0.02076283
hsa-miR-12136	770.786586	1358.84368	3106.17907	9070.61429	5.71337043	2.515498933	5.61E-06	0.00022624
hsa-miR-12135	108.014991	75.309409	229.688573	350.474517	3.14131917	1.661462029	0.00108521	0.01649166
hsa-miR-423-3p	138960.762	93672.8989	46162.0199	66349.0912	0.48364516	-1.047995562	0.00094649	0.01487112
hsa-miR-1228-3p	11.5355816	5.45720355	46.6554915	32.4513442	4.27040243	2.215490402	0.00428825	0.03897264
hsa-miR-3074-3p	38.8015016	32.7432213	9.86943089	1.85436253	0.18660473	-2.604054146	0.00370803	0.03519577
hsa-miR-874-3p	666.966352	1047.78308	209.052491	118.679202	0.19206745	-2.38705209	2.21E-06	9.30E-05
hsa-miR-138-5p	1246.8915	670.144596	348.121744	196.562428	0.28487436	-1.815295296	0.00056982	0.01056442
hsa-miR-34b-5p	195.056197	355.809671	97.7970879	66.7570509	0.30125596	-1.742567613	0.00141229	0.01870281
hsa-miR-503-3p	1278.35217	591.560865	237.763562	257.756391	0.26578155	-1.916081572	0.00018146	0.00421724
hsa-miR-20a-5p	4730.63713	7218.78886	1430.17026	1204.40846	0.22060788	-2.181258031	1.60E-09	1.24E-07
hsa-miR-383-5p	1449.28852	1879.4609	4957.14597	3314.67301	2.48407128	1.313274378	0.00044284	0.00855226
hsa-miR-302a-3p	48.2397047	36.0175434	204.566386	89.9365825	3.4374267	1.805189048	0.00375877	0.03519577
hsa-miR-4659a-3p	29.3632985	12.0058478	1.79444198	1.85436253	0.13024938	-3.504805925	0.00228181	0.02431305
hsa-miR-144-3p	0	2.18288142	64.5999113	13.9077189	19.246931	5.189424063	0.00021868	0.00482664
hsa-miR-15b-5p	26220.3769	19510.5941	6937.3127	7347.91151	0.31240534	-1.67865517	1.06E-08	7.04E-07
hsa-miR-942-5p	355.50565	234.659753	113.947066	97.3540326	0.36020527	-1.481874731	0.00213495	0.023571
hsa-miR-29c-3p	728.839017	1894.74107	7759.16712	3677.20089	4.3565108	2.124097235	0.00012939	0.00333177
hsa-miR-16-2-3p	892.434537	903.712908	139.069253	236.431222	0.20993855	-2.258312622	6.74E-07	3.29E-05
hsa-miR-15b-3p	2173.93278	3697.80113	722.262897	765.851723	0.2536912	-1.980277279	9.74E-07	4.51E-05
hsa-miR-21-5p	4875888.98	6484053.89	2724878.99	2725726.55	0.47980933	-1.059467384	4.78E-10	4.43E-08
hsa-miR-449c-5p	4.19475693	2.18288142	41.2721655	15.7620815	7.04664543	3.157058959	0.00206797	0.02337818
hsa-miR-362-5p	2839.85044	2377.15787	1165.49007	1004.13731	0.41609962	-1.265768179	0.00018197	0.00421724
hsa-miR-221-5p	15318.2036	10943.876	5670.43666	7248.70311	0.49197002	-1.023487158	0.00183695	0.02183139
hsa-miR-409-5p	1342.32222	1201.67622	2326.49403	3800.516	2.40731099	1.268042764	0.00114745	0.01688389
hsa-miR-132-3p	144.719114	305.603399	720.468455	732.473198	3.21660234	1.69033046	0.00089669	0.01433151
hsa-miR-548d-3p	7.34082463	14.1887292	0	0	0.08499949	-6.002519107	0.00157878	0.02032678
hsa-miR-212-5p	153.108628	130.972885	313.130126	452.464456	2.68313242	1.430010253	0.00194453	0.02225403
hsa-miR-485-3p	2962.54708	3839.68842	6519.20771	7732.69173	2.09485686	1.067091374	0.00077102	0.01276311
hsa-miR-26a-1-3p	140.524357	129.881444	43.9638285	49.1406069	0.34912779	-1.53849251	0.00192949	0.02225403
hsa-miR-19b-3p	9333.33417	8948.72238	3751.28096	1795.95011	0.30350109	-1.720557745	4.11E-05	0.00135908
hsa-miR-551b-5p	154.157317	158.258903	43.9638285	13.9077189	0.19042131	-2.430793587	0.00024137	0.00520352
hsa-miR-424-5p	37279.8535	54173.6596	19426.6289	24576.7937	0.48116752	-1.055423246	0.00073227	0.01234202
hsa-miR-1185-1-3p	423.67045	1003.03401	1595.25892	2911.34917	3.15573179	1.659456944	0.00224465	0.02419528
hsa-miR-424-3p	19259.1778	12787.3194	2490.68547	4380.93147	0.21447548	-2.221473195	2.94E-08	1.70E-06
hsa-miR-4707-3p	255.880173	76.4008497	36.7860606	12.9805377	0.15485952	-2.738185123	0.00051464	0.00973623
hsa-miR-129-2-3p	16.7790277	54.5720355	150.733126	126.096652	3.8013052	1.958043643	0.00374401	0.03519577
hsa-miR-665	53.4831509	216.105261	510.518743	478.425532	3.64869867	1.875754525	0.00553401	0.0479442
hsa-miR-34c-3p	507.565589	432.210521	231.483015	125.16947	0.38082564	-1.397543808	0.0050097	0.04381128
hsa-miR-197-5p	152.059939	65.4864426	30.5055137	21.325169	0.24519048	-2.06935328	0.00165259	0.02076283
hsa-miR-25-5p	763.445762	366.724079	160.602557	222.523503	0.34016633	-1.560921183	0.00352652	0.03496489
hsa-miR-302b-3p	61.8726647	65.4864426	425.282749	183.58189	4.72223914	2.257478468	0.00010696	0.00283302
hsa-miR-145-5p	51753.8623	115353.277	14335.797	6173.17285	0.12273996	-3.026438919	7.93E-10	6.69E-08
hsa-miR-412-5p	490.786561	439.850606	1506.43404	1145.99604	2.84615516	1.511004071	8.50E-05	0.00246272

**Supplementary Table 5.2** – Differentially expressed miRNA in senescent IMR-90 cells (n=2); generated with sRNAde.

name	Young_2	Young_1	Old_1	Old_2	FoldChange	log2FoldChange	pvalue	padj
hsa-miR-145-3p	2822.02273	4932.22057	610.110273	441.338281	0.13581943	-2.88250796	1.32E-11	2.45E-09
hsa-miR-935	49.2883939	46.9319505	82.5443311	311.532904	4.03253763	2.033730379	0.00442955	0.03948267
hsa-miR-3143	23.0711631	13.0972885	1.79444198	1.85436253	0.14799669	-3.310628762	0.00365557	0.03519577
hsa-miR-3138	128.988776	73.1265276	18.8416408	24.1067128	0.2202106	-2.235652956	0.00025143	0.00529719
hsa-miR-1299	16.7790277	4.36576284	55.6277014	49.1406069	4.61306003	2.303884701	0.00334097	0.03366391
hsa-miR-127-3p	256298.6	263446.501	567004.188	530106.615	2.11085892	1.077832991	1.78E-10	2.54E-08
hsa-miR-339-5p	479.250979	1307.54597	3156.42344	2675.84512	3.26155999	1.706805786	0.00108382	0.01649166
hsa-miR-451a	8866.66746	5172.33752	33631.4316	11468.305	3.21214448	1.683670665	0.00125658	0.01743401
hsa-miR-185-5p	7334.53249	6217.93772	19595.3064	14152.4948	2.48993879	1.31623329	2.55E-05	0.000909
hsa-miR-486-5p	177.22848	191.002124	798.526681	870.623206	4.51380806	2.180497534	2.70E-08	1.67E-06
hsa-let-7a-2-3p	2571.386	3383.4662	904.398758	1629.05748	0.42563692	-1.232999019	0.00385004	0.03568988
hsa-miR-29a-3p	266728.863	374091.303	700255.861	694982.623	2.17726626	1.122520439	3.83E-07	1.97E-05
hsa-miR-122b-5p	11.5355816	26.194577	96.8998669	50.0677882	3.74948554	1.964522279	0.00582038	0.04995822
hsa-miR-6529-5p	0	0	10.7666519	21.325169	17.0459105	6.348603916	0.000377	0.0074357
hsa-miR-486-3p	4.19475693	3.27432213	46.6554915	12.0533564	6.41127268	2.974104552	0.0044031	0.03948267
hsa-miR-26a-2-3p	299.925121	511.885693	121.124834	178.018802	0.37004133	-1.440361252	0.00493665	0.04358359
hsa-miR-151b	725.692949	773.831463	1671.5227	1902.57595	2.38164536	1.253082834	0.00027139	0.00559066
hsa-miR-182-5p	78.6516925	127.698563	440.535506	248.484578	3.31662701	1.740061111	0.00139423	0.01870281
hsa-miR-210-5p	98.5767879	152.801699	17.0471988	24.1067128	0.17031403	-2.611383427	8.74E-06	0.00033771
hsa-miR-431-5p	24086.2943	20845.4261	41303.5683	57303.5108	2.19454517	1.133951975	9.48E-05	0.00258388
hsa-miR-18a-5p	1166.14243	1840.16904	362.47728	310.605723	0.22440595	-2.159027403	3.29E-07	1.79E-05
hsa-miR-92a-3p	138254.994	111069.372	44577.5277	38899.8899	0.33481985	-1.578566103	1.92E-10	2.54E-08
hsa-miR-155-5p	100586.076	119349.042	22761.5993	24285.6588	0.21392141	-2.224895932	8.78E-21	8.14E-18
hsa-let-7a-3p	5101.87312	6565.01587	2603.73531	3087.51361	0.48789983	-1.035602827	0.00126006	0.01743401
hsa-miR-664a-3p	491.83525	1108.90376	3001.20421	2499.68068	3.43342544	1.781064603	0.00020023	0.00452715
hsa-miR-155-3p	12.5842708	49.1148319	3.58888396	2.78154379	0.13140574	-3.272963904	0.00169071	0.02089716
hsa-miR-17-5p	4517.75322	6765.84096	1244.44551	1162.6853	0.21346956	-2.228812071	2.52E-10	2.92E-08
hsa-miR-449a	76.554314	62.2121205	1419.40361	491.406069	13.5885354	3.783264405	3.87E-10	3.99E-08
hsa-miR-17-3p	459.325884	562.091966	134.583149	106.625845	0.23764388	-2.081930391	1.94E-06	8.57E-05
hsa-miR-7-1-3p	2038.65187	1761.58531	743.796201	745.453735	0.39220329	-1.351525709	7.79E-05	0.00232798
hsa-miR-33b-3p	209.737847	261.94577	38.5805026	94.5724888	0.28532334	-1.825430921	0.00213588	0.023571
hsa-miR-668-3p	225.468185	215.01382	446.816053	991.15677	3.25430821	1.706768627	0.00120076	0.01739227
hsa-miR-1197	143.670425	263.037211	1370.95367	408.886937	4.35969493	2.129956022	0.00122349	0.01743401
hsa-miR-6842-3p	0	0	28.7110717	2.78154379	16.7463077	6.323413995	0.00146799	0.01916662
hsa-miR-7705	17.827717	13.0972885	171.369209	57.4852383	7.01152343	2.886943238	8.85E-05	0.00248694
hsa-miR-10395-3p	67.1161109	40.3833063	697.140709	95.4996701	7.25702839	2.882055062	0.00071285	0.01223721
hsa-miR-152-3p	5289.58849	4482.547	10556.7022	15208.5543	2.63626962	1.398664241	1.86E-05	0.00069068
hsa-miR-143-5p	48.2397047	113.509834	22.4305248	16.6892627	0.25111391	-2.046389191	0.00286022	0.02979129
hsa-miR-143-3p	473200.043	669353.301	98586.6424	50243.9526	0.13026292	-2.940517241	7.40E-18	3.43E-15
hsa-miR-92a-1-5p	525.393306	243.391278	93.310983	42.6503381	0.17898817	-2.4989355	6.93E-05	0.00214006
hsa-miR-410-3p	10897.9785	14349.171	32166.2697	21470.7365	2.12438863	1.087116471	0.00114508	0.01688389
hsa-miR-1304-3p	449.887681	295.780432	121.124834	124.242289	0.33085151	-1.603778856	0.00061269	0.01082594
hsa-miR-4741	70.2621786	17.4630514	4.48610495	4.63590631	0.12395634	-3.266923909	0.00061575	0.01082594
hsa-miR-585-3p	2.09737847	0	39.4777236	40.7959756	20.0795947	5.235067077	2.75E-05	0.00094329
hsa-miR-29b-3p	10091.5365	23976.7695	53068.8271	49375.1838	3.00690023	1.588340652	0.00016696	0.0041601
hsa-miR-205-5p	2.09737847	12.0058478	219.819143	18.5436253	14.9263734	4.083777086	0.00033165	0.00668357
hsa-miR-3615	1829.96271	1179.84741	326.58844	716.711116	0.34706689	-1.528673093	0.00325766	0.03355386
hsa-miR-106a-5p	31.460677	22.9202549	4.48610495	4.63590631	0.19726547	-2.576503548	0.00271459	0.02859576
hsa-miR-4423-5p	307.265945	324.157891	803.910007	760.288635	2.47259189	1.308790004	0.00061896	0.01082594
hsa-miR-449b-5p	0	2.18288142	31.4027347	17.616444	12.1971372	4.511120844	0.00078829	0.0128201
hsa-miR-3943	8.38951386	7.64008497	226.09969	312.460086	29.9817972	5.069462658	2.48E-16	7.68E-14



**Supplementary Figure 2** – FACS diagrams of proliferating, tetraploid IMR-90 cells; **(a)** proliferating, diploid DNA control; **(b)-(d)** proliferating, tetraploid IMR-90 DNA samples.

**Supplementary Table 6.1** – differentially expressed SenMayo data set genes in senescent IMR-90 cells (RNA-seq; n=2).

<b>Gene</b>	<b>Sen FC</b>	<b>Sen P-Value</b>
ANGPT1	1.85792947	0.004132692
ANGPTL4	4.09724853	0.005117579
PTGER2	-1.0154703	0.007892847
HMGB1	-1.3887867	0.018896144
IL15	0.76159526	0.022526004
FGF2	1.71201642	0.032463231
CXCL12	-2.1922496	0.041886037
CXCL1	-1.2875766	0.04543442
WNT16	5.85178983	0.050828667
JUN	-1.2317853	0.060167785
IGFBP2	-1.5888405	0.062329376
MIF	-0.9652524	0.071444511
CXCL10	-1.6438562	0.081491005
RPS6KA5	1.52426658	0.084721943
CXCL8	-1.7786436	0.093823597
ITPKA	-1.3519854	0.117237176
SERPINE1	1.6435669	0.122975237
TUBGCP2	-1.4656738	0.126724241
IGFBP5	0.29933534	0.142885768
TNFRSF11B	1.98248604	0.143158859
ICAM1	-0.8974636	0.150547709
INHA	4.4918531	0.151957891
BEX3	-0.5717805	0.166443573
KITLG	1.50828866	0.194117251
EGFR	2.04906631	0.208328646
MMP3	1.42164022	0.209936171
ACVR1B	1.63626373	0.212691803
FGF7	0.88791215	0.213184172
PTGES	-0.8663216	0.219396403
IGFBP7	-1.2417333	0.221962369
CD9	1.67020975	0.223256316
ESM1	3.33985	0.231664077
GDF15	-0.6698288	0.253293985
HGF	0.87432758	0.257486621
CD55	-0.9712635	0.258697545
PLAU	-0.8365378	0.271314563
CTSB	-0.6886896	0.286886282
FAS	1.66774555	0.292958119
CSF1	1.38204321	0.297425735
MMP1	1.4128865	0.298347746
TNFRSF1B	-0.7633137	0.310363654
IGFBP6	-0.7107917	0.316478192
IGFBP3	1.66769705	0.320272887
SCAMP4	0.95109036	0.322570038

**Supplementary Table 6.2** - differentially expressed SenMayo data set genes in senescent IMR-90 cells (RNA-seq; n=2).

<b>Gene</b>	<b>Sen FC</b>	<b>Sen P-Value</b>
ITGA2	1.25477952	0.329632708
SEMA3F	-0.6872126	0.333084451
SERPINE2	0.48837342	0.341576533
PAPPA	2.0177093	0.347021357
IGFBP4	-0.4262901	0.351273044
DKK1	1.15051848	0.352886122
CTNNB1	0.71402085	0.359240202
NRG1	2.22055103	0.364337647
GMFG	-0.7104934	0.368831256
PLAUR	-0.620278	0.372477291
CXCL3	-0.6166713	0.375304952
BMP2	3.75097976	0.387542273
VEGFC	0.96036419	0.388590262
EDN1	1.90968922	0.40178038
CXCL16	1.2895066	0.410308025
PIGF	0.51836477	0.428151572
VEGFA	0.95794195	0.442446751
MMP14	0.76282118	0.527353809
C3	-0.6866339	0.563320469
SPX	-0.6520767	0.56356422
ANG	0.43462823	0.599410055
NAP1L4	0.1365334	0.619786469
IQGAP2	0.3325753	0.619812187
TIMP2	0.27937041	0.636197352
AREG	-0.6021036	0.67174229
PGF	0.53886609	0.68562249
PLAT	0.34400191	0.70920547
MMP10	0.63742995	0.718281915
GEM	0.40776307	0.725341996
FGF1	-0.146625	0.752373034
ICAM3	0.39231742	0.767070636
EREG	0.29003756	0.792774227
CXCL2	-0.1154772	0.830969149
MMP2	0.18571782	0.833097137
BMP6	-0.1850319	0.833864967
ETS2	-0.072711	0.872043343
VGF	0.2115041	0.89824787
SELPLG	-0.0420913	0.900288867
WNT2	-0.1138985	0.902239749
CCL2	-0.0934192	0.932809874
AXL	-0.0457778	0.943211804
PTBP1	-0.0183277	0.968791221
CCL5	0.03747473	0.969835151
TNFRSF1A	0.00411826	0.990160104

**Supplementary Table 7.1** - differentially expressed SenMayo data set genes in tetraploid IMR-90 cells (RNA-seq; n=2).

<b>Gene</b>	<b>FC Tetra</b>	<b>P-Value Tetra</b>
ANGPT1	1.38825383	0.010410426
ANGPTL4	1.71049337	0.074923158
PTGER2	-0.139168	0.756004015
HMGB1	-0.5716033	0.228209661
IL15	0.13663462	0.492907447
FGF2	1.04547289	0.043084262
CXCL12	-1.5292845	0.072935536
CXCL1	-0.5936798	0.654399991
WNT16	4.6982621	0.25857215
JUN	-0.4754573	0.214942089
IGFBP2	-0.70929	0.273982948
MIF	-0.6674998	0.399801695
CXCL10	0.8901224	0.490778876
RPS6KA5	0.89930603	0.475242536
CXCL8	0.14473509	0.917219481
ITPKA	0.63370678	0.677328589
SERPINE1	1.4117794	0.017832035
TUBGCP2	-1.268548	0.164390609
IGFBP5	0.55742549	0.484601538
TNFRSF11B	0.87436436	0.053832198
ICAMI	-0.4796574	0.58254556
INHA	3.24792751	0.003442351
BEX3	-0.4452482	0.106499097
KITLG	0.97854394	0.154189686
EGFR	1.42309962	0.044506809
MMP3	-1.6389013	0.361879246
ACVR1B	0.64776768	0.017932085
FGF7	0.62315756	0.134971129
PTGES	-1.101538	0.048358872
IGFBP7	1.07146776	0.506919064
CD9	0.9834671	0.128284033
ESM1	2.83289001	0.102238807
GDF15	-0.2512305	0.770109887
HGF	0.99818315	0.05494795
CD55	0.25590295	0.826881277
PLAU	-0.6302617	0.164472341
CTSB	-0.2403193	0.769696462
FAS	0.96934981	0.089933651
CSF1	0.66278864	0.407440726
MMP1	-0.077716	0.945459297
TNFRSF1B	-0.8276073	0.241487804
IGFBP6	-0.8508435	0.056827646
IGFBP3	1.38613641	0.350411393
SCAMP4	0.05435243	0.869091246



**Supplementary Table 7.2** - differentially expressed SenMayo data set genes in tetraploid IMR-90 cells (RNA-seq; n=2).

<b>Gene</b>	<b>Tetra FC</b>	<b>Tetra P-Value</b>
<i>ITGA2</i>	1.02072991	0.410775432
<i>SEMA3F</i>	-0.0054775	0.993606837
<i>SERPINE2</i>	0.83835827	0.347431118
<i>PAPPA</i>	1.01447873	0.211813243
<i>IGFBP4</i>	-0.736969	0.041631517
<i>DKK1</i>	0.8611262	0.40083223
<i>CTNNB1</i>	0.35777709	0.507138962
<i>NRG1</i>	1.06916209	0.005018482
<i>GMFG</i>	-3.169925	0.116547791
<i>PLAUR</i>	-0.4208638	0.487680751
<i>CXCL3</i>	-1.7162071	0.111111111
<i>BMP2</i>	1.89386392	0.13259378
<i>VEGFC</i>	-0.0312698	0.956733894
<i>EDN1</i>	1.48842515	0.082485011
<i>CXCL16</i>	0.47393113	0.157299028
<i>PIGF</i>	0.32986092	0.454174953
<i>VEGFA</i>	0.59604083	0.4613718
<i>MMP14</i>	0.15311579	0.685223257
<i>C3</i>	-0.2819384	0.725474481
<i>SPX</i>	-1.6520767	0.274099122
<i>ANG</i>	-0.142019	0.648876558
<i>NAP1L4</i>	0.24033658	0.434361848
<i>IQGAP2</i>	-0.3625701	0.485504245
<i>TIMP2</i>	0.19932413	0.67081739
<i>AREG</i>	-1.2517191	0.383774438
<i>PGF</i>	-0.2684888	0.368323834
<i>PLAT</i>	-1.2346133	0.069625924
<i>MMP10</i>	-0.169925	0.884529946
<i>GEM</i>	0.29260754	0.677337033
<i>FGF1</i>	0.43609909	0.61332589
<i>ICAM3</i>	0.2976805	0.820871611
<i>EREG</i>	0.06286007	0.964768735
<i>CXCL2</i>	0.6214884	0.667419963
<i>MMP2</i>	-0.2473013	0.507372389
<i>BMP6</i>	-0.3798481	0.574925818
<i>ETS2</i>	0.31138455	0.575304385
<i>VGF</i>	-1.5849625	0.539212428
<i>SELPLG</i>	-0.1301475	0.897345823
<i>WNT2</i>	-1.1253394	0.368663124
<i>CCL2</i>	-0.1579703	0.869129713
<i>AXL</i>	0.29846355	0.696451459
<i>PTBP1</i>	-0.3019461	0.285779622
<i>CCL5</i>	0.98089116	0.221526903
<i>TNFRSF1A</i>	-0.1205184	0.787300477

**Supplementary Table 8** – RT-qPCR quantification table for assessment of miR-29a-3p and let-7a expression in miR-29a-3p inhibited IMR-90 cells (cDNA), with mock control, negative control, wildtype (WT).

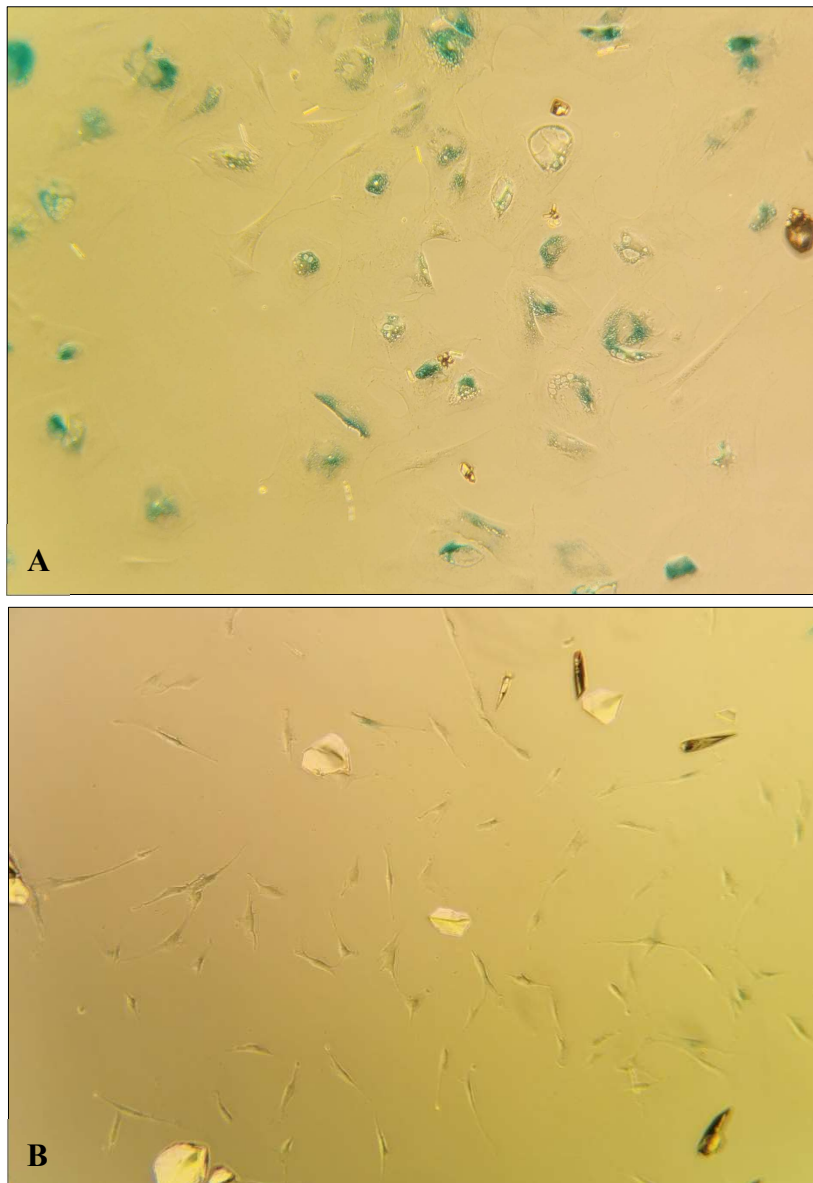
Name	Ct	Mean	MOI - Reference	Treated - Wildtype	Relative Quantity	Fold Change
miR1 1 29a	23	23	5	4.5	0.044194174	-4.5
miR1 2 29a	23					
miR2 1 29a	23	23	5			
miR2 2 29a	23					
Mock1 1 29a	21	21	1	0.25	0.840896415	-0.25
Mock1 2 29a	21					
Mock2 1 29a	18	18.5	0.5			
Mock2 2 29a	19					
Negativ1 1 29a	17	17	0.5	0	0	0
Negativ1 2 29a	17					
Negativ2 1 29a	21	20.5	0.5			
Negativ2 2 29a	20					
miRI 1 29a	19	18.5	0.5	0.25	0.840896415	-0.25
miRI 2 29a	18					
miRII 1 29a	19	19	1			
miRII 2 29a	19					
WT1 1 29a	19	19	0			
WT1 2 29a	19			0	0	0
WT2 1 29a	22	21.5	1			
WT2 2 29a	21					
LK 29a	33	31				
Lk 29a	29					

**Supplementary Table 9** - RT-qPCR quantification table for assessment of LMNB1 and Beta Actin (BETA) expression in miR-29a-3p inhibited IMR-90 cells 0- and 7-days post inhibition (cDNA).

Name	Ct	Mean	Name	Ct	Mean	GOI - Reference	Treated - Wildtype	Relative Quantity	Fold Change
miR1 BETA	22.9	22.84	miR1 LMNB1	29.91	29.805	6.97	0.485	0.71449707	-0.485
miR1 BETA	22.7		miR1 LMNB1	29.7					
miR2 BETA	27.2	27.22	miR2 LMNB1	31.51	32.85	5.63	-0.855	1.808758755	0.855
miR2 BETA	27.3		miR2 LMNB1	34.19					
miRI BETA	19.4	19.47	miRI LMNB1	26.28	26.48	7.015	0.53	0.692554734	-0.53
miRI BETA	19.5		miRI LMNB1	26.68					
miRII BETA	24.7	24.73	miRII LMNB1	30.62	30.855	6.13	-0.355	1.278985581	0.355
miRII BETA	24.7		miRII LMNB1	31.09					
WT1 BETA	23.6	23.64	WT1 LMNB1	30.06	30.12	6.485			
WT1 BETA	23.7		WT1 LMNB1	30.18					
PDL52 BETA	16.8	17.16	PDL52 LMNB1	27.88	28.255	11.095	4.61	0.040949794	-4.61
PDL52 BETA	17.5		PDL52 LMNB1	28.63					
PDL51 BETA	16.1	16.65	PDL51 LMNB1	27.86	27.935	11.285	4.8	0.035896824	-4.8
PDL51 BETA	17.2		PDL51 LMNB1	28.01					
LK BETA	32.4		LK LMNB1						
LK BETA	32.2		LK LMNB1	34.8	34.8				

**Supplementary Table 10** RT-qPCR quantification table for assessment of SIRT1 and Beta Actin (BETA) expression in miR-29a-3p inhibited IMR-90 cells 0- and 7-days post inhibition (cDNA).

Name	Ct	Mean	Name	Ct	Mean	GOI - Reference	Treated - Wildtype	Relative Quantity	Fold Change
miR1 SIRT1	29.9	29.565	miR1 BETA	22.71	22.63	6.935	-0.31	1.2397077	0.31
miR1 SIRT1	29.3		miR1 BETA	22.55					
miR2 SIRT1	31.3	31.045	miR2 BETA	27.2	27.1	3.95	-3.295	9.815079818	3.295
miR2 SIRT1	30.8		miR2 BETA	26.99					
miRI SIRT1	25.8	25.64	miRI BETA	19.01	19.07	6.57	-0.675	1.596596773	0.675
miRI SIRT1	25.5		miRI BETA	19.13					
miRII SIRT1	30	29.495	miRII BETA	24.45	24.61	4.885	-2.36	5.13370359	2.36
miRII SIRT1	29		miRII BETA	24.77					
WT1 SIRT1	30.4	30.695	WT1 BETA	23.49	23.45	7.245	0	1	0
WT1 SIRT1	31		WT1 BETA	23.41					
PDL52 SIRT1	25.9	25.945	PDL52 BETA	17.29	17.26	8.69	1.445	0.367292158	-1.445
PDL52 SIRT1	26		PDL52 BETA	17.22					
PDL51 SIRT1	25.9	26.12	PDL51 BETA	17.2	17.48	8.645	1.4	0.378929142	-1.4
PDL51 SIRT1	26.3		PDL51 BETA	17.75					
Lk SIRT1			LK BETA	30.92					
Lk SIRT1			LK BETA	32.45					



**Supplementary Figure 3** – photo documentation of SA- $\beta$ -Gal assay (100x) **(A)** positive SA- $\beta$ -Gal assay of senescent *Callithrix jacchus* lung fibroblasts; **(B)** negative SA- $\beta$ -Gal assay of proliferating *Callithrix jacchus* lung fibroblasts.

## **Danksagung**

Ich möchte mich herzlich bei all jenen bedanken, die mich auf dem Weg zur Erfassung dieser Dissertation unterstützt haben. Ein besonderer Dank gebührt Prof. Dr. Hans Zischler, der mich mit seiner fachlichen Kompetenz, seiner inspirierenden Anleitung und seinem unermüdlichen Engagement durch meine Forschungsarbeit begleitet hat. Sein Rat und seine Unterstützung waren für mich von unschätzbarem Wert. Darüber hinaus möchte ich mich sehr für die Betreuung der Dissertation durch meinen Zweitgutachter Prof. Dr. Thomas Hankeln bedanken. Ein herzliches Dankeschön geht auch an die Mitglieder der AG Zischler, insbesondere Mirjam Weisser, Jonas Möhner und Maurice Scheuren, die mich stets ermutigt und unterstützt haben. Die kollegiale Atmosphäre und die fachliche Expertise in der Gruppe haben meine Forschung bereichert und meinen Horizont erweitert. Ein großer Dank gebührt auch meiner Familie, meinen Freunden und insbesondere Samira Asgari, die mich in allen Phasen meines Promotionsprojekts unterstützt haben. Ihre moralische Unterstützung und ermutigenden Worte haben mir Kraft gegeben, auch in anspruchsvollen Momenten durchzuhalten. Vielen Dank für euer Mitwirken und Vertrauen.

## **Eidesstattliche Versicherung**

Hiermit erkläre ich, Valentina Woronzow, dass die vorliegende Dissertation mit dem Titel: „*Generation of genetic and epigenetic variation during cellular senescence and early tumorigenesis in a human and nonhuman primate lung fibroblast model*“ von mir selbstständig und ohne unerlaubte Hilfsmittel angefertigt wurde und ich mich dabei nur der ausdrücklich bezeichneten Quellen und Hilfsmittel bedient habe. Diese Dissertation wurde weder in der jetzigen noch in einer abgewandelten Form einer anderen Prüfungskommission vorgelegt.

Mainz, der 17.11.2023

---

(Valentina Woronzow)

## Lebenslauf

Valentina Woronzow

Albert-Schweitzer Straße 10-12

55128 Mainz

E-Mail: vaworonz@uni-mainz.de

Staatsangehörigkeit: Deutsch

## Bildungsgang

**Johannes Gutenberg-Universität Mainz | Oktober 2020 – November 2023**

Doktorandin, Biologie (Dr. rer. nat.)

Institut für Organismische und Molekulare Evolutionsbiologie, Anthropologie

**Johannes Gutenberg-Universität Mainz | Oktober 2018 – September 2020**

M. Sc. Anthropologie

**Johannes Gutenberg-Universität Mainz | Oktober 2014 – September 2018**

B. Sc. Biologie

**Gymnasium an der Stadtmauer, Bad Kreuznach | 2005 – 2014**

Allgemeine Hochschulreife

## Berufserfahrung

**Johannes Gutenberg-Universität Mainz | Oktober 2020 – September 2023**

Wissenschaftliche Mitarbeiterin

Institut für Organismische und Molekulare Evolutionsbiologie, Anthropologie

**Johannes Gutenberg-Universität Mainz | August 2018 – September 2020**

Wissenschaftliche Hilfskraft

Institut für Organismische und Molekulare Evolutionsbiologie, Anthropologie

## Publikationsliste

- Möhner, J., Scheuren, M., **Woronzow, V.**, Schumann, S., & Zischler, H. (2023). RDA coupled with deep sequencing detects somatic SVA-retrotranspositions and mosaicism in the human brain. *Frontiers in cell and developmental biology*, 11,1201258. <https://doi.org/10.3389/fcell.2023.1201258>